THE BEHAVIOUR OF NEUROLOGIC WATER DURING AXONAL AND SYNAPTIC NEUROTRANSMISSION: AN IN SILICO STUDY

by

Erin Martin

Submitted in partial fulfillment of the requirements
for the degree of Master of Science

at

Dalhousie University
Halifax, Nova Scotia
July 2011

DALHOUSIE UNIVERSITY

DEPARTMENT OF CHEMISTRY

The undersigned hereby certify that they have read and recommend to the Faculty of Graduate Studies for acceptance a thesis entitled "THE BEHAVIOUR OF NEUROLOGIC WATER DURING AXONAL AND SYNAPTIC NEUROTRANSMISSION: AN IN SILICO STUDY" by Erin Martin in partial fulfilment of the requirements for the degree of Master of Science.

Dated: July 27, 2011

Supervisor: _____

Readers: _____

_____

_____

Departmental Representative: _____

DALHOUSIE UNIVERSITY

DATE: July 27, 2011

AUTHOR: Erin Martin

TITLE: THE BEHAVIOUR OF NEUROLOGIC WATER DURING AXONAL AND SYNAPTIC NEUROTRANSMISSION: AN IN SILICO STUDY

DEPARTMENT OR SCHOOL: Department of Chemistry

DEGREE: MSc CONVOCATION: October YEAR: 2011

_____

Signature of Author

DEDICATION PAGE

"*The best is yet to come.*"

TABLE OF CONTENTS

LIST OF TABLES

LIST OF FIGURES

ABSTRACT

Water is known to take on highly organized structures to influence the reactivity of chemical and biological systems; despite this, water is often only implicitly or approximately included in theoretical studies of biochemical systems, if not omitted entirely. Many of the current models for biological processes predate an understanding of the complex behaviour of water, yet these models have not been updated. This thesis presents an exploration of how a better of water might affect the models used to describe neurotransmission. Two classes of systems are investigated, representing the two main categories of neurotransmission: that which occurs along the length of a neuron, and that which occurs between one neuron and another cell. Lipid bilayers are studied using molecular dynamics, and neurotransmitters are studied using Car-Parrinello molecular dynamics. The results indicate that water structures may play a more specific role in neurotransmission than was previously thought.

LIST OF ABBREVIATIONS USED

ACEnet	Atlantic Computational Excellence network
ACh	Acetylcholine
AP	Action potential
B1	Tertiary lipid bilayer of SM, DOPC and cholesterol
B2	Tertiary lipid bilayer of SM, DOPC and 25% cholesterol
B3	Unary lipid bilayer of SM
B4	Unary lipid bilayer of DOPC
BLYP	The Becke-Lee-Yang-Parr exchange-correlation functional
BER	Berendsen thermostat
Ca^{2+}	Calcium cation
CNS	Central nervous system
CPMD	Car-Parrinello Molecular Dynamics
DFT	Density Functional Theory
DOPC	Dioleylphosphatidylcholine
EKINC	Electron kinetic energy
H^+	Proton
$H_5O_2^+$	Zundel cation
$H_9O_4^+$	Eigen cation
GA	Anionic gamma-aminobutyric acid (COO^- and NH_2)
GABA or GN	Gamma-aminobutyric acid (neutral: COOH and NH_2)
GC	Cationic gamma-aminobutyric acid (COOH and NH_3^+)
GZ	Zwitterionic gamma-aminobutyric acid (COO^- and NH_3^+)
K^+	Potassium ion
LDA	Local spin density approximation
l_o	Liquid-ordered lipid domains
l_d	Liquid-disordered lipid domains
MM	Molecular mechanics
MD	Molecular dynamics
MOE	Molecular Operating Environment
Na^+	Sodium cation
NOR	Node of Ranvier
NHA	Nosé-Hoover-Andersen thermostat
NPA	Nosé-Poincaré-Andersen thermostat
NPT	Isobaric-isothermal ensemble
NVE	Microcanonical ensemble
NVT	Canonical ensemble
PBC	Periodic boundary conditions
PME	Particle mesh Ewald
QM	Quantum mechanics
RMSD	Root-mean-square deviation
RPDF	Radial pair distribution function
SM	Sphingomyelin
μVT	Grand canonical ensemble

ACKNOWLEDGEMENTS

First and foremost, I wish to express my deepest gratitude to Dr. Donald Weaver for welcoming me to his research group and for supporting my project. His advice, guidance, patience and sense of humour have been invaluable.

I would like to acknowledge Dr. Russ Boyd and Dr. Axel Becke for sitting on my supervisory committee, and express additional thanks to Dr. Russ Boyd, for sharing his computational resources with me, and for his consistent support and encouragement.

I would like to thank all the members of both Dr. Weaver's and Dr. Boyd's research groups, for their support and friendship. This project would not have been possible without the help of Dr. Christopher Barden (Weaver Research Group), Dr. Ross Dickson (ACEnet), Autumn Meek (PhD candidate), Laura Albrecht (PhD candidate) and Gavin Heverly-Coulson (PhD candidate). In the face of countless technological glitches and many theoretical questions, your knowledge and assistance was greatly appreciated.

Lastly, I would like to thank the ACEnet team for their technical support and for providing a platform for research with advanced computational methods in Atlantic Canada, and the Department of Chemistry and the Faculty of Graduate Studies at Dalhousie University, for their financial and academic support of my graduate studies.

CHAPTER 1 INTRODUCTION

1.1 CONCEPTUALIZING WATER

Water is the most crucial molecule in the composition and functioning of living organisms. While some organisms portray a unique ability to thrive on the fringes of hospitable conditions, and still others do so in utterly inhospitable environments, all known life exists at temperatures and pressures where liquid water can as well. No other solvent can compete with the macromolecular complexity that water achieves from such micromolecular simplicity. With a mere three atoms, each water molecule has the combined ability to form up to four simultaneous hydrogen-bonds, with solutes and other water molecules. The properties of this richly inter-connected solvent – a complex balance between molecular organization and random motion, the ability to auto-dissociate, and to act together in chains to transmit protons and electrical currents at "anomalously high" rates – make this molecule one of the most versatile and most difficult to model mathematically [1–4]. The challenges of modelling water encompass many of the significant issues facing the developers and users of computational chemistry. These are challenges such as: incorporating the Brownian randomness observed in biological processes into inherently rigid mathematical equations, navigating complex potential energy surfaces with multiple closely-spaced minima, modelling the energies related to the solvation process and solvent-solvent potentials, accurately describing diffuse densities of electrons and small free-moving nuclei in a bulk environment, and reaching a true definition the strength and nature of hydrogen-bonds and other intermolecular forces; all while maximizing computational outcomes and minimizing computational costs [1–6].

The growing ability to model large and complex water-containing systems influences numerous scientific disciplines. Biomedical research and drug discovery, catalyst technology, and atmospheric chemistry; these and other fields use computational chemistry to optimize efficacy and efficiency and to better-understand the elemental

processes that govern both. Meanwhile, the general understanding of the properties of water from experimental observations has also expanded and matured, challenging the perception of water as an observer which merely regulates temperature, or provides the occasional proton or hydroxyl group in chemical pathways. As knowledge of the subject increases, and the models for describing it are improved, it becomes necessary to incorporate these advances into existing models for many systems which contain water. To address this goal two questions must be asked: what properties of water are altogether new, have been redefined, or have new ways of being modelled mathematically, and to what systems could these discoveries bring heightened understanding? This introduction will address both of those questions, and provide a general outline of the work presented in this thesis.

1.1.1 Structures Made of Water

Most scientists tend to think of water in terms that any undergraduate in a first-year chemistry course would understand. Phrases such as "universal solvent" and "poor conductor" encourage the viewpoint that water is the spectator, or the stage, and that true chemistry is played out by much more interesting molecules and compounds. While there is some obvious truth to that position – there are organic, inorganic, analytical, physical, computational and other types of chemists, but not so many "water" chemists – a second-year student in physical chemistry might go on to tell you about how the viscosity, density, isothermal compressibility, and the "peculiar" temperature dependence of water's molar heat capacity, all defy the trends observed for most other compounds [7]. New research indicates that some misconceptions about water, particularly in the realm of electrical and thermal conductivity are – at best – over-simplifications or – at worst – altogether inaccurate [2, 8]. A good deal of research has been conducted on the organization of water, including how solvent-solvent effects shape the conformations of enzymatic proteins and drive biological catalysis, and there is a much more developed understanding of how the size, polarity and charge of a solute can either organize or disrupt dozens of solvent molecules at once [9–11]. It is what water can do *if* organized that inspires the need to know *when* water is organized.

Some of the most frequently discussed water-structures are Zundel and Eigen cations, water clathrates, water wires and networks surrounding kosmotropes and chaotropes [4, 10, 13–16]. The smallest of these classes of structures consists of only two or three water molecules with a hydronium cation suspended between them, and are referred to as the Zundel and Eigen cations, respectively [6, 14–18]. These structures have been explored extensively using experimental techniques such as photodissociation dynamics, neutron diffraction, and X-ray absorption [18]. The interest in these molecules stems from the desire to understand how solutions stabilize excess acidic protons. Differing experimental results have engendered a debate as to which of the acidic structures – H_3O^+, $H_5O_2^+$ or $H_9O_4^+$ – is the dominant structure in solution [6, 17]. Simulation methods have been used to clarify the process, but due to the variety of computational techniques available they have actually added to the debate. Simulations based on classical mechanics indicate that either a lone H_3O^+ cation or the complex Eigen cation ($H_9O_4^+$) should be most prevalent in solution [6]. In contrast, the more fully developed *ab initio* methods, used to study the timing and the energetics involved in the proton-transfer between the possible structures, have shown that the Zundel cation ($H_5O_2^+$) is the more stable and most prevalent of the two structures [17, 6]. The key contributions from the *ab initio* based research are an appreciation for the quantum effects on the proton transfer within these structures, and clarification of the equilibrium that exists between the cations [6]. The overall dynamic relationship between Zundel and Eigen cations demonstrates the way in which water is constantly responding to minute changes in its local environment. The average position of an acidic proton between two water molecules also shows how, over a longer time-period, two water molecules appear as though they are two parts of one larger molecule. Generally, computational methods provide a way to explore the organization of water in any system with non-neutral pH conditions or with small charged solutes.

The next level of organization in water involves slightly larger clusters known as water clathrates. A clathrate is a term used to describe any cage-like molecule, or group of molecules, which is stable enough to trap other small compounds. Water clathrates have been known for decades [16], but have acquired new significance in the last ten years.

Methane-containing water-clathrates are estimated to be the gatekeepers for an astounding two million megatonnes of carbon, trapped in methane bubbles in the deeper regions of the oceans [19]. In 2007, Canada produced 747 megatonnes of emissions [20], making the ongoing retention by the water-clathrates worth nearly 2700 years of Canada's current annual greenhouse gas emissions. Unlike the Zundel and Eigen cations, dynamic dissociation would seriously undermine the strength of these structures. The driving forces behind the long-term stability of clathrates are high pressures and low temperatures [19]. While the chemistry of these structures is more relevant to climate scientists, marine scientists, and some materials chemists, their existence does indicate how important it is to properly understand and describe the strength of the hydrogen-bond network. Are there other systems in which clathrates could exist, or are there other systems whose water structures could be equally surprising or significant?

One organized water structure in particular has received a great deal of attention from physicists, and from those who study proteins embedded in lipid membranes and the pathways of cellular processes. "Water wires" are quasi-one-dimensional strings or chains of water molecules linked together by a series of hydrogen bonds [4]. Their hydrogen bonding geometry is very specific, and is maintained by restrictive interactions with a variety of hydrophobic regions [21]. They are called water wires for their ability to rapidly conduct acidic protons and, therefore, electrical current. Under the right conditions water wires take in a proton at one end of the chain, re-align according to their dipoles in domino succession, and release a free proton on the far side [22].

Water wires have been found inside "free" proteins – those not associated with a lipid membrane – and spanning the inner cavities of membrane-associated proteins [4, 22, 23, 24]. Their conductivity is central to the operation of proton-pump proteins which take-up extracellular protons (H^+) to regulate intracellular pH, maintain the transmembrane electrochemical potential gradient, and facilitate synthesis of the adenosine triphosphate that is essential to cell function [4, 22, 24]. Effecting these same processes, water wires are being investigated for their potential ability to fill occasional defects in lipid bilayers,

causing a leak of protons across cellular membranes [25]. They have also been suggested, via results from infrared spectroscopy and molecular dynamics simulations, to play a role in the formation and stabilization of β-amyloid fibrils, and their toxic β-sheet conformers [23]. This discovery has medicinal implications for humans; misfolded β-amyloid proteins are believed to play a major role in the pathogenesis of Alzheimer's disease, the predominant cause of elderly dementia. Water wires may provide more than clarification of the way in which living cells operate or how Alzheimer's progresses, but they are also "expected to play a central role in future nanoscale devices" as they have been described, both experimentally and computationally, to exist within carbon nanotubes [21]. Any system that has substantially non-polar regions in close contact with water may have such wires forming, and perhaps there are other structures that exist at the boundary between hydrophobic and hydrophilic regions which possess similar or additional properties to water wires.

The final type of water organization that will be explored here is the effect on water by different solutes. Ions and solutes are well-known to be crucial to the three-dimensional conformational geometry of proteins, but they also play a major role in the position and motion of solvent molecules themselves [10, 11]. A solute which induces order in its surrounding solvent is said to be a kosmotrope, while one which creates disorder is a chaotrope [10, 26]. Given that water exhibits an ongoing balance of order and disorder, even without dissolved ions or molecules, the labelling of a solute as a kosmotrope or chaotrope is inherently relative, and there are a number of ways one may examine this property. Experimentally, one can measure the change in a solution's viscosity when solute is added, and the entropy change associated with this process [10]. An increase in viscosity, or a decrease in entropy, would indicate that the motions of molecules are more restricted when solute is present. The inferred logic is that the reduced mobility is due to stronger intermolecular bonding and organization. Computationally, one can look at the water density and geometry – the average number of hydrogen bonds in the shells of water around a solute, and the temperature dependence of this value – to examine the effect of the solute on individual solvent atoms [10, 11]. Solvation is driven by ion-

dipole, dipole-dipole and hydrophobic interactions, and so the likelihood of a given solute being either kosmotropic or chaotropic depends heavily on its size, charge, charge distribution and polarity [10, 26]. Monte Carlo dynamics simulations have been used to determine which types of ions and molecules perform which role in solution [10, 26]. The results do not tend to provide a simple rubric for labelling any solute. Instead, due to the variety and subtlety of the properties of solutes, their water-ordering abilities are less like polar distinctions and more like a spectrum of qualifications.

In general, ion-water behaviour is a balance between the intermolecular forces of hydrogen bonding and ion-dipole interactions. The most deterministic property of the kosmotrope/chaotrope behaviour of a solute is its charge density, which depends on the magnitude and localization of charge. A plot of the atomic radius of ions, versus average number of hydrogen bonds in the surrounding solvent, shows a fairly linear relationship between charge density and the ability to induce or reduce the order of water [10].

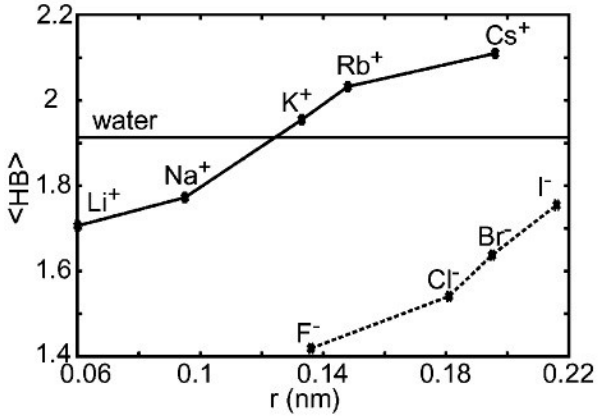

Figure 1.1: The average number of water-water hydrogen bonds per water molecule in the first shell around various ions [10].

On this graph the average number of hydrogen bonds is compared to that which is observed for water under the same temperature and pressure conditions. Small ions such as fluoride (F^-) and lithium (Li^+) which have low charge distribution – high charge density – interrupt hydrogen bonds between solvent molecules and induce order via electrostatic interactions [10]. These smaller solutes are labelled as kosmotropes because they create order in the solution which would not exist in pure water, and the electrostatic

network they establish is stronger and more stable than a dynamic hydrogen bond network [10]. Larger ions such as iodide (I^-) and cesium (Cs^+) with higher charge distribution – lower charge density – do not tend to re-orient water molecules according to their dipoles. The larger the solute ion, the less influence that the electrostatic force has on the dipoles of the water molecules, and the greater influence afforded to hydrogen bonding on the activity of the solvent [10]. In other words, the larger the ion the smaller its kosmotropic influence; instead, the surrounding water molecules hydrogen-bond to one another and encircle the ion [10]. The process of water forming a cage around solutes with more diffuse or delocalized charge – those which are more non-polar – has been observed in Monte Carlo dynamics simulations [26]. These induced cage structures are much more dynamic and disordered than the water-clathrates found in the ocean deep, or the tight network which exists around smaller ions, therefore larger ions are said to be chaotropic [10].

Related to the charge density of an ion is the sign of its charge, but both anions and cations have demonstrated the ability to act as kosmotropes [10, 27]. The main difference between anions and cations is the relationship between ionic radius and the degree of kosmotropic character observed. This relationship influences the kosmotrope/chaotrope trends seen in Figure 1.1. This graph shows that a large anion such as I^- has the same effect on water ordering as a much smaller cation such as Li^+ [10]. This trend is a consequence of charge density, but also the geometry of water molecules, and there being a significant difference between the spatial demands of the positive and negative ends of the water dipole [10]. For simple ionic solutes this trend is simple enough to explain and observe; however, the majority of solutes are significantly more complex and chemically diverse, and their behaviour less straightforward to predict. For a zwitterionic molecule the solution's pH may have a significant impact on the strength of its kosmotropic influence, but depending on its other chemical properties – size, polarity and charge density – it may have very little effect. Each solute in a real system should be investigated individually in order to fully understand where it fits in the kosmotrope/chaotrope spectrum.

From the preceding discussion, some important things to consider when studying water organization in a new system are: the description of intermolecular forces (especially hydrogen bonding), the constraints placed on water by hydrophobic regions, the temperature and pressure of the system, the presence of acidic protons (the pH), and the charge, size and polarity of molecular and ionic solutes. Any given biological system will require consideration of most if not all of these issues, though simplifications must often be made due to the scale of the system and limitations of the computational models available.

1.1.2 Where Water Matters

Given the prevalence of the molecule, the properties of water involving organization and conductivity are relevant to a vast number and variety of systems. If the investigation is limited to water in biological systems at or below the cellular level, there is still a staggering list of potential targets for research. The water in one particular biological region has received a greater amount of attention than others: the nervous system.

Neurologic water has already been explored on a variety of levels. Macroscopically, a deprivation of water in the central nervous system (CNS) has been linked to poor cognitive skills and decreased memory storage and retrieval [28, 29]. Conversely, an excess accumulation of fluid in the CNS – due to injury, infection, and as part of the inflammatory process – may involve dangerous swelling in a confined space, reduced neurological function, and even death [30, 31]. Such intense sensitivity of the CNS to the concentration of water has been a factor in the fascination with the movement and regulation of neurologic water. The amount of water inside and outside nerve tissues is controlled by a class of integrated membrane proteins known as aquaporins, and by certain co-transporter proteins which move solutes and water molecules simultaneously [32, 33]. Recognizing the significance of water in the brain led, in part, to the discovery of these vital proteins, and this research now provides a means of targeting and treating diseases which affect these crucial proteins [34]. The importance of neurologic water

may seem quite obvious – a concept that anyone who has had a headache and cured it with a glass of water can appreciate – but identification and quantification of the chemical mechanisms which underlie this importance remains a fairly underdeveloped field. What research has been done to this effect seems to indicate the involvement of organized water structures in the global functioning of the CNS.

It is now understood that interstitial fluid near the myelin sheath is acidic, as is the fluid which fills the synaptic cleft between two communicating neurons [35, 36]. The implications of this finding are the potential presence of Zundel and Eigen cations and water wires in the CNS, in addition to the water wires involved in proton-pump proteins and the (mis)folding of amyloid fibrils discussed previously [9, 23]. The crucial role of ions (especially Na^+, K^+ and Ca^+) and solutes in neurotransmission raises the question of how these solutes affect their surrounding solvent, and how this relationship might affect the function of these same ions and solutes. The nervous system encapsulates many of the defining characteristics of systems with water structures: boundaries between hydrophobic and hydrophilic regions, acidity, and even electrical conductivity. The CNS is, in many ways, a mystery. A greater understanding of how water influences essential processes in the nervous system holds inherent value and potential benefits to biology, biochemistry, pharmacy and medicine.

1.1.3 Water: a Neuromodulator?

Neurotransmission is a process which involves innumerable moving parts: ions to regulate transmembrane potentials, proteins to regulate the ion concentrations, ions to cause the release of neurotransmitters into the synaptic cleft, neurotransmitters to cause depolarization of the nerve cell across the synapse, and a host of other molecules (such as peptides and hormones) which modify and participate in these processes. Energetically speaking, neurotransmission is the most demanding process in the human body, and all of this energy comes from dietary glucose [37]. A close link between glucose metabolism in the brain and neuronal activity was proposed over a century ago and, although it is very logical, this relationship has proven difficult to measure [37]. There is some debate as to

how much glucose the brain requires, and how this energy is divided amongst the various aspects of neurotransmission [37–39]. Nerve activity levels, determined by positron emission tomography and functional magnetic resonance imaging, have been compared to the amount of ^{13}C-labelled glucose taken-up by nerve tissue [37]. This comparison found that one neurotransmitter pathway, the glutamatergic system, appears to require between 80 and 90% of the total cortical glucose available, leaving very little energy for the numerous other excitatory and inhibitory neurotransmission pathways and cellular processes [37]. It is important to note that this research makes several assumptions – that the model for glucose uptake and use are perfectly accurate, that the glutamatergic system is isolated from other neurotransmission systems and does not share its glucose-derived energy, and that there is no other way that energy in the brain can be accounted for [38, 39]. Despite the assumptions and debate surrounding this research, the findings do leave one wondering how the brain manages its high energy demands. The last assumption, that energy cannot be accounted for by any other means, is particularly troubling because there is already a class of molecules which are known to aid in the neurotransmission process by either heightening or dampening nerve conduction: neuromodulators.

The definition of a neuromodulator varies greatly between sources. In the most general sense, a neuromodulator is "a substance that alters nerve impulse transmission" [40]. This definition is so general that it could include the lipids which make up the myelin sheath, or even the DNA which codes for the proteins that synthesize these lipids. Clearly this definition strays too far from a logical level of precision. A much more specific definition states that a neuromodulator is "a substance, other than a neurotransmitter, released by a neuron [which transmits] information to other neurons, altering their activities" [40]. This definition is so specific that it excludes substances which are clearly relevant to neurotransmission, such as Na^+, K^+ and Ca^+ cations. As the concept of neuromodulation is both complex and fairly new, with a wealth of data yet to be collected, it may be better to speak of neuromodulation in slightly more general terms (but not so general as to be misleading). The act of modifying neurotransmission implies some active role, rather than passive or secondary, and so the most sensible definition of a neuromodulator is: "a

substance…that potentiates or inhibits the transmission of a nerve impulse but is not the actual means of transmission itself" [41]. This definition is precise enough to explain the fundamental role of the neuromodulator, but is broad enough to account for gaps in our understanding of the full integration of the nervous system, and allows for incorporation of new research.

Hormones and small peptides are the typical examples of neuromodulators, but other molecules such as pregabalin, an analog of the inhibitory neurotransmitter γ-aminobutyric acid (GABA), adenosine, hydrogen sulphide and even zinc ions, have all been qualified as being neuromodulators. [42–45]. One molecule that has not been labelled as such – due to its ubiquity, lack of specificity, and unfortunate track record of being over-looked – is, of course, water. The activity of neuromodulators is usually characterized by interaction with a receptor, and while water may not have specific interactions with a receptor, there is potential for the specific influence of water on neurotransmitters and on neurotransmission [46]. If the prevalence of water structures and micro-organization are included in the overall analysis of neuronal activity, it may be found that water is intimately involved in both saltatory and synaptic neurotransmission. (Further discussion of both of these arguments will be presented in Chapters 2 and 3, respectively.) The goal of this thesis is to explore the properties of water in two regions which are central to neurotransmission and, more specifically, to assess whether or not water could modulate neural conductivity to such an extent as to be called a neuromodulator.

1.2 OUTLINE OF RESEARCH AND THESIS

The general approach adopted in this thesis has been to identify biological regions where the presence of water structures is possible and may possibly play a role in biochemical functions, to choose one or more molecular targets from within those regions, to develop a solvated model of the molecules and to perform molecular dynamics (MD) or Car-Parrinello Molecular Dynamics (CPMD) simulations on the systems to observe any trends in behaviour. The two systems chosen were the raft and non-raft lipid domains found in the myelin sheath which surrounds the axons of nerves (to be discussed in Chapter 2), and two of the neurotransmitters which are found in the synapse (Chapter 3).

1.2.1 Large Systems and Statistical Models

The first molecular targets which will be discussed in this thesis are two of the lipids which constitute the myelin sheath: sphingomyelin (SM) and dioleylphosphatidylcholine (DOPC). The biological significance of these molecules is not their individual chemistry, but rather the job they perform together, in the hundreds and thousands. Their analysis is comprised of MD simulations done on several tertiary and unary bilayers that were constructed from each lipid type. The reasoning for these systems will be discussed, with pertinent biological background information. The method used to build, solvate and prepare these systems will be described, in addition to the computational theory and the algorithm used to simulate their behaviour. Finally, the MD simulations will be analyzed using the root-mean-square deviation (RMSD), radial pair distribution functions (RPDFs), the g_{max}/g_{min} ratio for the first solvent peak, and the number of hydrogen bonds present in the systems during their simulations.

1.2.2 Small Systems and Quantum Models

The second group of molecular targets consists of the neurotransmitters GABA and acetylcholine (ACh). These molecules do act individually, and the majority of their time is spent in the interstitial fluid which fills the synaptic gap. For the most part, their analysis and discussion follows the template of the calculations performed on lipid

bilayers. Beginning with the essential biological and theoretical background information the choice of systems and computational methods will be explained. Like the lipid bilayer study, the analysis will focus on the RMSD, the RPDFs, the g_{max}/g_{min} ratios and the number of hydrogen bonds present during each frame of the simulations.

1.3 SUMMARY OF RESULTS

The g_{max}/g_{min} ratio for the SM bilayer indicates that liquid-ordered (l_o) domains have a kosmotropic effect on their first solvation sphere, and the average number of hydrogen bonds during the trajectory show that the bulk solvent has a reduced connectivity as compared to the water-water interactions when no solute bilayer is present. The g_{max}/g_{min} ratio and the average number of hydrogen bonds observed during the trajectory of the DOPC bilayer indicate that the liquid-disordered (l_d) domains may also be kosmotropic. From these results it appears there is a certain possibility that water structures can exist near the myelin sheath, given that both the l_o-type and l_d-type lipids exhibited a kosmotropic influence on their solvent, but it cannot be stated conclusively whether or not these water structures plays a role in axonal neurotransmission, but this research is the first step to deeper and more definitive investigations.

The g_{max}/g_{min} ratios and the average number of hydrogen bonds calculated for ACh indicate that this excitatory neurotransmitter is strongly kosmotropic. The inhibitory GABA neurotransmitter is also shown to be a kosmotrope, but not quite as strongly as ACh. Also, the degree to which GABA re-orders its solvent varies with changes in the pH; under acidic conditions GABA is the least kosmotropic, under basic conditions it is more kosmotropic, and the zwitterionic GABA at neutral pH is the most kosmotropic.

It appears that solvated synaptic neurotransmitters create order which would not otherwise exist. This re-ordering of the solvent directly influences the ability of these molecules to diffuse through the synapse and interact with receptors on the post-synaptic membrane, and so water should be considered a neuromodulator of synaptic neurotransmission.

CHAPTER 2 SALTATORY CONDUCTION, LIPID RAFTS AND THE LIPID-WATER INTERFACE

2.1 WATER AND THE MYELIN SHEATH

When water contributes to conductivity it is due to constrained geometries that allow for the orientation shift in one water molecule to rapidly change that of any surrounding waters. The requisite constrained geometry arises from hydrophobic-hydrophilic repulsions and the dipole-dipole orientation of these restricted waters [21, 22, 24]. A possible region for such an influence to exist can be found at the border between extracellular fluids and the fatty membranes of neurons, where conductivity is known to be crucial. The current model for conductivity along neurons involves local-circuit currents and the discharge of capacitance – but like any theory there is room for further investigation and new ideas. This chapter will focus on the existing concepts of neuron structure and function, the theoretical methods used to study a new hypothesis, and the outcomes of such a study. The goal of this project is the development of simple models to test the hypothesis that micro-structures in the membranes of neurons may create an environment around which water structures can exist, and can contribute to neurotransmission.

2.1.1 The Anatomy and Physiology of Saltatory Nerve Conduction

The cells which constitute the human body are constantly communicating with one another. Glycoproteins in cellular membranes allow for signalling and recognition between neighbouring cells; immune cells communicate with one another to coordinate a response to foreign molecules, infectious organisms and dead or dying host cells; and hormones coordinate multiple organ systems to up-regulate and down-regulate processes such as cardiovascular and respiratory output, digestion, sensory alertness and the growth and division of cells [47, 48]. Perhaps the most obvious category of cellular communication is neurotransmission. Neurotransmission is a generalized term for the various processes which allow information and commands to be relayed between sensory

organs, neurons and certain tissues. The two main categories of neurotransmission are synaptic (to be discussed in Chapter 3) and axonal.

In axonal neurotransmission an impulse is conducted over large distances within the body, at rapid speeds, down an axon to the synaptic bulb (see Figure 2.1). Rather than the small chemical messengers used in many other cell-to-cell communication pathways, axonal neurotransmission relies on an electrochemical gradient and a series of transmembrane proteins.

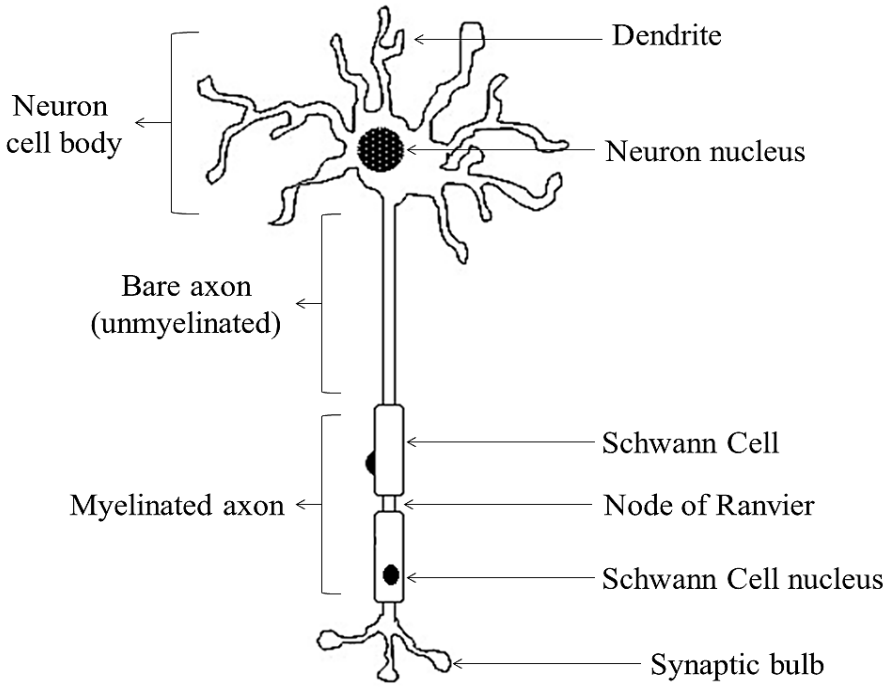

Figure 2.1: The main features of a neuron (not to scale) [47, 48].

Embedded all along the cellular membrane of a neuron are protein pumps which regulate the sodium (Na^+) and potassium (K^+) cation concentrations in the cell [47]. When a nerve cell sits idle, the K^+ cations present in the cytosol leak out into the extracellular fluid through K^+ channel proteins, by travelling down their concentration gradient [47]. To prepare a nerve for firing, Na^+/K^+ protein pumps force Na^+ ions out of the cell, while they bring the K^+ ions back into the axon [47]. A greater number of Na^+ ions leave the cell than K^+ ions are brought in, and this causes a build-up of positive charge on the outside of the cell. At the same time there is a predominance of negatively charged ions, amino

acids and phosphate groups inside the cell [47]. The action of the protein pumps and the components of the cytosol result in a resting transmembrane potential of approximately -70 mV relative to the extracellular fluid [47]. When the membrane is polarized in this way it can be stimulated to transmit an impulse from one end of the axon to the other.

Axonal neurotransmission consists of the rapid and successive depolarization of the transmembrane potential, known as an action potential (AP) [47, 49]. An AP is generated by the coordinated movement of large numbers of Na^+ ions. In addition to the Na^+/K^+ pumps which maintain the transmembrane potential, there are voltage-gated Na^+ channels in the membranes of axons [47, 49]. When stimulus (a electrochemical messenger or external stimulus such as heat or pressure) depolarizes a small region of the membrane to a threshold of -55 mV, nearby voltage-gated Na^+ channels adopt an open conformation and Na^+ ions from the extracellular fluid rush into the cell, along their electrochemical gradient [47, 49]. The influx raises the potential to approximately +30 mV [47, 49]. As the region of the cell nearest to the stimulus becomes increasingly positive, the voltage-gated Na^+ channels in nearby regions of the cell membrane open, depolarizing that region, and so on [47, 49]. In this way the process continues in domino succession down the length of the axon. Charge carriers diffuse passively, within the axoplasm and in the extracellular fluid, according to their electrochemical gradients. This creates a current loop (see Figure 2.2) around the membrane of the axon and discharges the adjacent membrane segments [47–49].

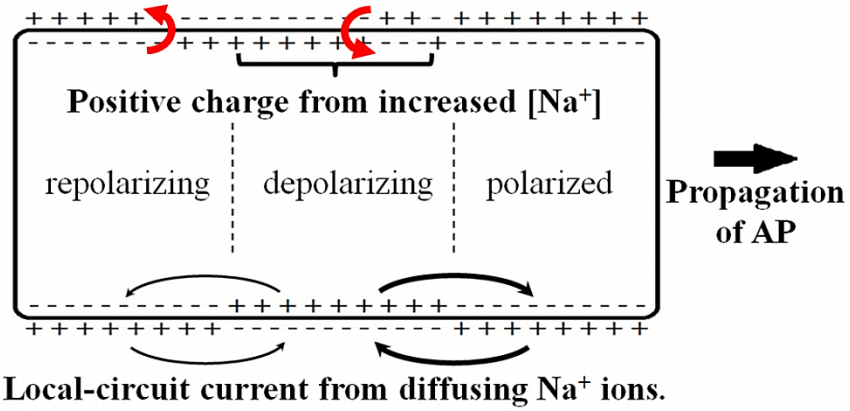

Figure 2.2: Active and inactive regions of a membrane during an AP, and the local-circuit current caused by the passive flow of Na^+ ions [49].

The passive diffusion shown in Figure 2.2 indicates that there is some backflow of Na^+ ions into the region surrounding the recently repolarized axon. The repolarization carried out by Na^+/K^+ pumps requires a significant amount of energy, and any backflow with the potential to send an AP in the opposite direction of the original signal would be highly inefficient. It is fortunate, then, that voltage-gated Na^+ channels experience a refractory period after depolarization, during which time they cannot be stimulated [48]. Directionality in the transmission of nerve impulses helps simplify the summation of excitatory and inhibitory messages, and it also helps maintain high transmission speeds.

High velocity neurotransmission is an unmistakeable advantage; faster delivery and processing of stimulus and faster execution of response to stimulus are desirable attributes for any organism. The velocity of axonal neurotransmission is affected largely by two factors: the diameter of the axon and the presence of myelin [47, 49]. A larger axon diameter creates faster neurotransmission because it presents a greater number of charge-carriers to participate in the flow of current, a larger cross-sectional area through which current can flow and lower resistance to that current [47, 49]. The electrical local-circuit current generated along an axon can be compared to the restricted pathway of electric field lines, known as electric flux, Φ_F [50]:

$$\Phi_{\boldsymbol{F}} = \int \boldsymbol{E} \bullet \boldsymbol{dA} \tag{2.1}$$

where E is the electric field and dA is a small cross-section of the path of the field lines. From this equation it can be seen that when we increase the cross-sectional area the electric flux also increases. From Gauss's law [51]:

$$\int \boldsymbol{E} \bullet \boldsymbol{dA} = \frac{\boldsymbol{Q}}{\boldsymbol{\varepsilon_0}} \tag{2.2}$$

it can be seen that electric flux is directly proportional to charge, Q. Since electrical current is simply the movement of charge it follows that increasing the cross-sectional area of the axon will increase the current. This increase must be due to a drop in resistance because the transmembrane potential required to initiate an AP depends on the channel proteins, which have not changed, and from Ohm's Law [49]:

$$\boldsymbol{I} = \frac{\boldsymbol{V}}{\boldsymbol{R}} \tag{2.3}$$

it is known that the current can only be increased by increasing the transmembrane voltage (V) or by decreasing the resistance (R). Increasing axon diameter to 1.5 μm can bring the velocity of an AP up to 2 m/s; however, axonal neurotransmission can reach speeds of 130 m/s [47]. This 128 m/s increase in velocity is not achieved by thicker axons, as width quickly becomes a burden on the size and structure of the organism. Instead, the axons of some high velocity neurons are ensheathed with myelin.

Myelin is created by the closest neighbours of neurons, a type of oligodendrocyte known as Schwann cells [47–49]. Their chief role is to wrap around a small segment of a single axon 20 to 300 times [48]. Each Schwann cell constitutes an intermodal region which is up to 2 mm in length, and between adjacent myelin segments is the Node of Ranvier (NOR) which is typically 2 μm in length [47, 49]. The dense, fatty lobes which the Schwann cells form around axons boost the velocity of neurotransmission, without drastically increasing the space requirements of the neuron. The same mechanisms which cause and propagate an AP in unmyelinated axons – electrochemical gradients and huge movements of charge carriers – hold for those which are myelinated, but they are carried out in a slightly different manner. The current of any AP travels through one of two mediums: across the axolemma (the membrane of the axon) or within the axoplasm. (The extracellular fluid will be omitted from this discussion because it is generally consistent, whereas the anatomy of axons can vary substantially.) Compared to the cell membrane, the cytosol is a "low-resistance pathway" [49]. Myelination increases transmission velocity by decreasing the amount of current which has to travel through the high-resistance membrane.

Instead of being spread out along the full length of the axon, the Na^+ and K^+ protein pumps and channels which are so vital to the continuous conduction of an AP are concentrated in the NOR (see Figure 2.1) [47, 49]. The influx of Na^+ ions, which depolarizes the membrane and opens other voltage-gated Na^+ channels, occurs principally in the NOR, and instead of the local-circuit current seen in unmyelinated axons (Figure 2.2) a current loop exists surrounding an entire segment of myelin

extending to the next NOR (Figure 2.3). The name "saltatory conduction" comes from the fact that on a graph of time versus distance along an axon the current "appears to jump" from one NOR to the next [47, 49]. Figure 2.3 below shows the entrance of depolarizing Na^+ ions, the subsequent current circuits, and the relative speed of transmission for both unmyelinated and myelinated axons.

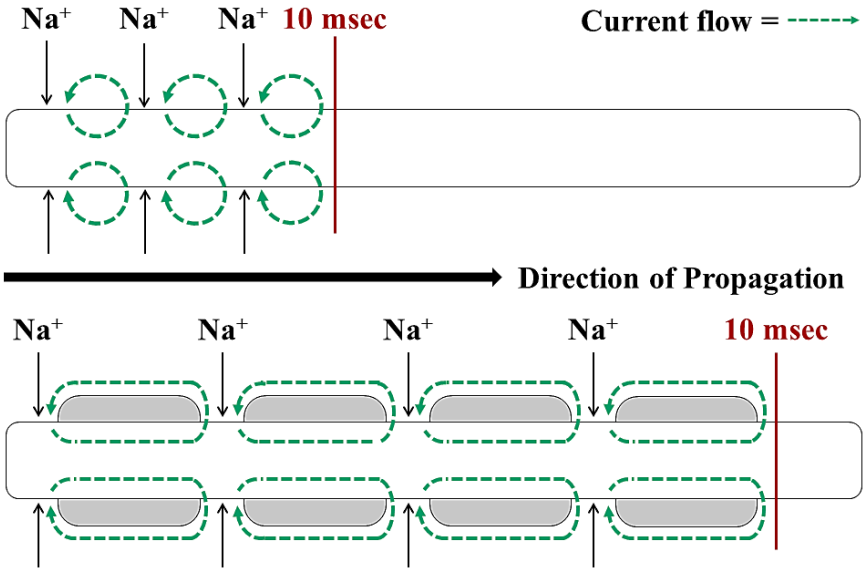

Figure 2.3: The velocity and circuit pathway of an AP for unmyelinated (top) and myelinated (bottom) nerves (not to scale) [47, 48].

Another important effect of myelination on transmission velocity is the lowering of capacitance. Capacitance per unit length of axon (r_c) decreases as the thickness of the insulating material increases [49]. The concentric layers of myelin between the NORs are significantly insulating, and so this decreases the capacitance between two sequential NORs. The rate of passive spread of current driving an AP is given by [49]:

$$\frac{dI_{passive}}{dt} = \frac{l}{r_a \cdot r_c} \tag{2.4}$$

Thus, the increased rate of current transmission for myelinated over unmyelinated neurons results from lower axial resistance (r_a) and lower capacitance. Much more is known and can be said about the anatomy and physiology of myelination and saltatory conduction, but (at least) one significant question remains. How does one depolarized NOR elicit an open conformation from the voltage-gated Na^+ channels in an NOR up to 2 mm away? Once depolarization of a subsequent NOR has started, the loops around

adjacent myelin segments are completed, but the driving force for that second depolarization is only ever explained via comparison to electrical circuits [47- 49]. These models are not at all inaccurate, but the myelinated neuron *in situ* is not as simple or isolated as current flowing through wires, capacitors and resistors. Just as in standard electronics charge carriers must be involved, but it appears that at 130 m/s that something else is contributing to the discharge of successive NORs.

2.1.2 Lipid Rafts in the Myelin Sheath

The prevailing conceptual model of the cell membrane is the fluid-mosaic model, which describes a cell membrane as an ever-evolving blend of lipids and proteins with little short- or long-range order [47, 52]. In this model, the lateral movement of a given molecule and the identity of its neighbours are essentially random. More than a decade ago this model was challenged, and the presence of certain microstructures now known as lipid rafts was proposed [52, 53]. Lipid rafts, appropriately named, are groups of lipids which behave as a single unit, moving through the surrounding membrane without dissociating and while maintaining a higher level of order than non-raft lipids. This preference for certain lipids to group into raft domains, leaving behind the non-raft domain, creates a spectrum of membrane phases from solid-ordered (s_o) to liquid-ordered (l_o) to liquid-disordered (l_d), in order of increasing fluidity [52]. In general, the mobility of molecules in a raft domain is lower than those in non-raft domains.

The original concept for lipid rafts "originated from studies on epithelial cell polarity," and the distinct characteristics of cell membranes which face outwards (apical membranes) and those which face into the epithelial tissue (basolateral membranes) [52]. The presence of proteins in one membrane and not the other, as well as differences in lipid distribution, lead to more in-depth explorations of lipid membrane structure. The plausibility of lipid domains is most commonly supported by the observation of partitioning of cell membranes, when in the presence of non-ionic detergents, into a detergent-soluble fraction and a detergent-resistant fraction [52, 54]. The detergent-soluble fraction is comprised of non-raft lipids and proteins, and the detergent-resistant

fraction, made up of raft lipids and proteins, is evidence that some lipids congregate naturally based on certain chemical properties. The lipid raft theory has also been confirmed and explored by numerous techniques including (but not limited to): electron, photonic force and atomic force microscopy; fluorescence microscopy, spectroscopy, and resonance energy transfer; infrared and spin-label electron resonance spectroscopy; immunoglobulin E signalling; flotation of detergent-resistant membranes; differential scanning calorimetry; the chemical cross-linking of proteins to rafts; ^{2}D-NMR; and a variety of MD simulations [52–65]. This wealth of research provides an excellent starting point for computational chemists to investigate the more subtle aspects of lipid-ordering, and their influence on cellular processes.

The compositions of non-raft and raft domains have been analyzed for both their protein and their lipid composition. The lipids in the l_d domain are more likely to have unsaturated acyl chains, such as those found in DOPC (see Figure 2.4) [52]. The double-bonds in unsaturated lipids increase the average amount of space required for each molecule, and therefore the space between neighbouring molecules.

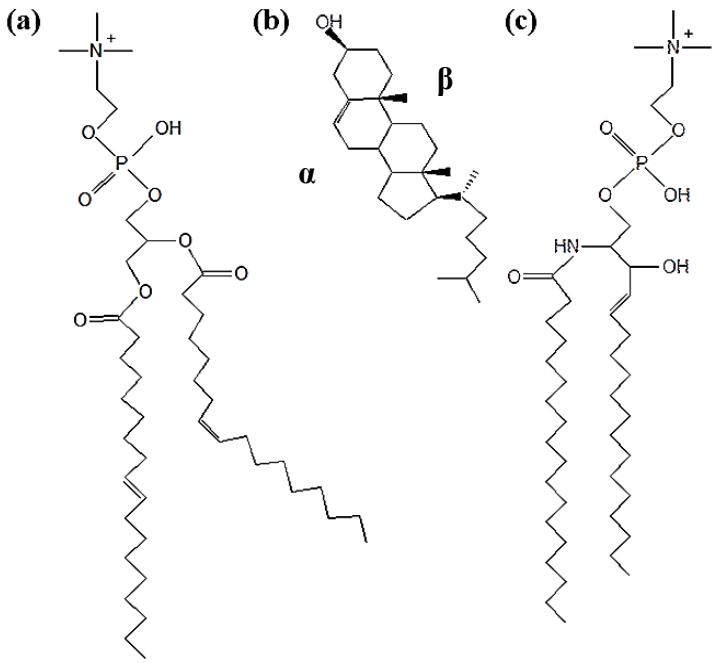

Figure 2.4: The structures of a) DOPC, b) cholesterol and c) SM.

This, is turn, creates more opportunity for lipids to move past one another as it contributes to the disorder in l_d domains. Conversely, l_o domains are comprised of more saturated and close-packing lipids such as SM, a sphingolipid (see Figure 2.4) [52–54, 63]. Lacking double-bond character allows the l_o molecules to adopt a more efficient conformation and brings groups of such lipids closer together. The preferential interactions which occur between the headgroups of sphingolipids, and other raft lipids, also reinforce the stability of the l_o domain [53, 54, 65]. The reason for lipid-rafts, however, is not merely a matter of differences between phospholipids – the formation of lipid rafts is driven by the presence of sterols, especially cholesterol (see Figure 2.4) [58].

Cholesterol is the most ubiquitous molecule in any cell membrane, existing in both raft and non-raft domains; its presence creates both stability and fluidity [52, 54–58, 64]. Cholesterol has been observed playing exactly opposite roles in the two domains. While it induces order in the l_d regions of a membrane, it enhances fluidity in the l_o regions [57]. Cholesterol molecules fill the gaps between l_d lipids and (especially) l_o saturated sphingolipids, when their headgroup interactions leave space between their acyl chains [52, 53, 54]. Figure 2.5 below shows the packing observed in the l_o and l_d phases of lipid membrane dynamics, and the relative behaviour of lipids in each region.

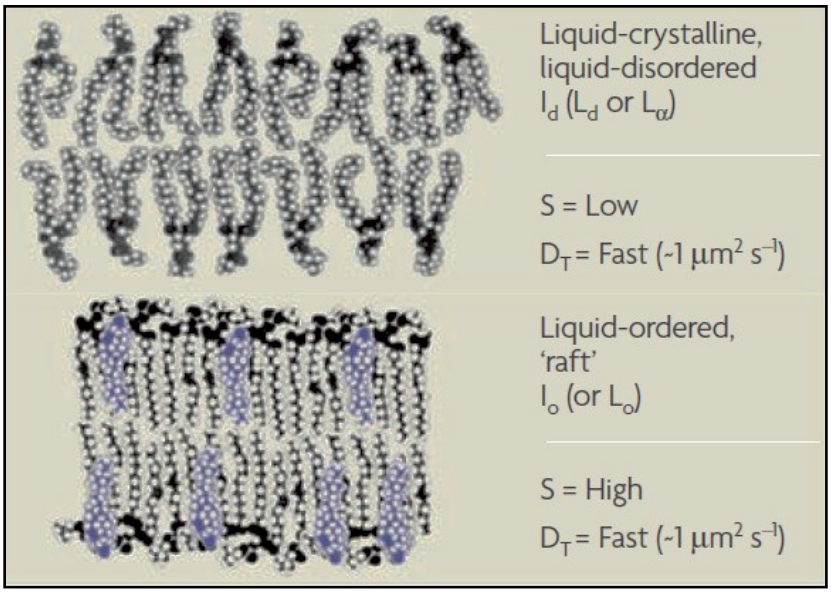

Figure 2.5: The l_d and l_o domains of the lipid membrane [64].

The liquid-disordered region is represented by phosphatidylcholine, and the liquid-ordered region is shown using SM and cholesterol (blue) [64]. Van Meer notes that the "order parameter of a segment of acyl chain" is represented by S, and D_T describes "the translational diffusion coefficient" of a lipid in that membrane [64].

The geometry of the cholesterol molecule also appears to play a role in forming the raft and non-raft domains. Cholesterol has two faces: the "smooth" β-face of the sterol rings, and the "rough" α-face with a methyl substituent [66]. The β-face participates in ordering unsaturated lipids in the l_d domain, while the α-face prefers to face towards the alkyl chains of the l_o domain [66]. It has been suggested that due to the two-faced nature of cholesterol, that it forms a border between raft and non-raft domains. Regardless, cholesterol has been shown to be the controlling force in the persistence of lipid rafts over long time-scales, and even in their size [57]. Experimentally, when the concentration of cholesterol in a lipid membrane gets near 30%, the membrane begins to look more like a sea of l_o domains, dotted with small rafts of l_d domains, reversing the definitions of what constitutes a raft or a non-raft domain [57]. When the amount of cholesterol reaches 30% the lipid bilayer is also closer to the composition of the myelin sheath [67]. This may indicate that the myelin sheath is more likely to be a sea of l_o-type lipids (for example SM) with pockets of l_d-type lipids (for example DOPC). The most crucial l_o-type lipid in myelin is SM, in fact it is the most abundant sphingolipid in mammalian cells and is, in some cases, the most abundant non-sterol lipid altogether [58]. Some experimental results have suggested that sphingolipid rafts can only exist in an external membrane leaflet [54]. This suggests that SM-based rafts in myelin membranes point in anatomically correct directions to be able to play a role in water-ordering and neuromodulation.

The idea that the lipid membrane plays a more active role in saltatory neurotransmission is not a new one. In recent years a theory has been proposed in which successive NORs are depolarized by a soliton, a single and self-sustaining sound wave which travels through the lipid membrane of a neuron at approximately the same speed as a nerve

impulse [68–71]. The concept is rooted in thermodynamics; relationships between volume, lipid area, compressibility, enthalpy, heat capacity, specific heat, and correlations to phase transition temperatures during an AP, all point towards something more than just proteins, ions and electricity [68–71]. This theory recognizes and addresses the gross over-simplification of the Hodgkin and Huxley circuit-based model for APs. Most importantly, research into the theory of soliton-lipid propagation has encouraged researchers to consider and perhaps adopt "a revised view of the action potential," one in which "membrane lipids play a fundamental role in the propagation of nerve pulses" [68]. What might an investigation of the role of lipid rafts and water structures contribute to this discussion?

Raft and non-raft domains have inherently different mobility and order characteristics. While there is no experimental reason to believe this may be the case, it stands to reason that the behaviour of lipid in the myelin sheath could affect the water molecules directly above it. This is demonstrated by the steric restraints which allow water wires to form inside proteins and nanotubes; and by the controlled environments which allow clathrates to persist; but the best example of this reality is the description of molecular and ionic kosmotropes and chaotropes (Chapter 1). If the myelin sheath is thought of as existing in two possible phases (l_o or l_d), and each has one of two effects on neighbouring water molecules, then there are four possible scenarios for the influence of lipid rafts on peri-cellular water. The first case is the non-case, where neither raft-type lipids nor their counterparts induce order in water. The opposite of this case would be an observable relationship between both lipid types and their waters. The best likelihood that water structures exist above the myelin sheath is that both l_o and l_d domains induce a certain level of order in their solvent waters, but even just the observation of kosmotrope behaviour in l_o domains allows for the possibility of organized water structures on the surface of the myelin sheath. Keeping in mind that the high concentration of cholesterol in the myelin sheath likely means that most of the myelin sheath is l_o, and that rafts are of l_d type, the four possibilities are conceptualized in Figure 2.6 below.

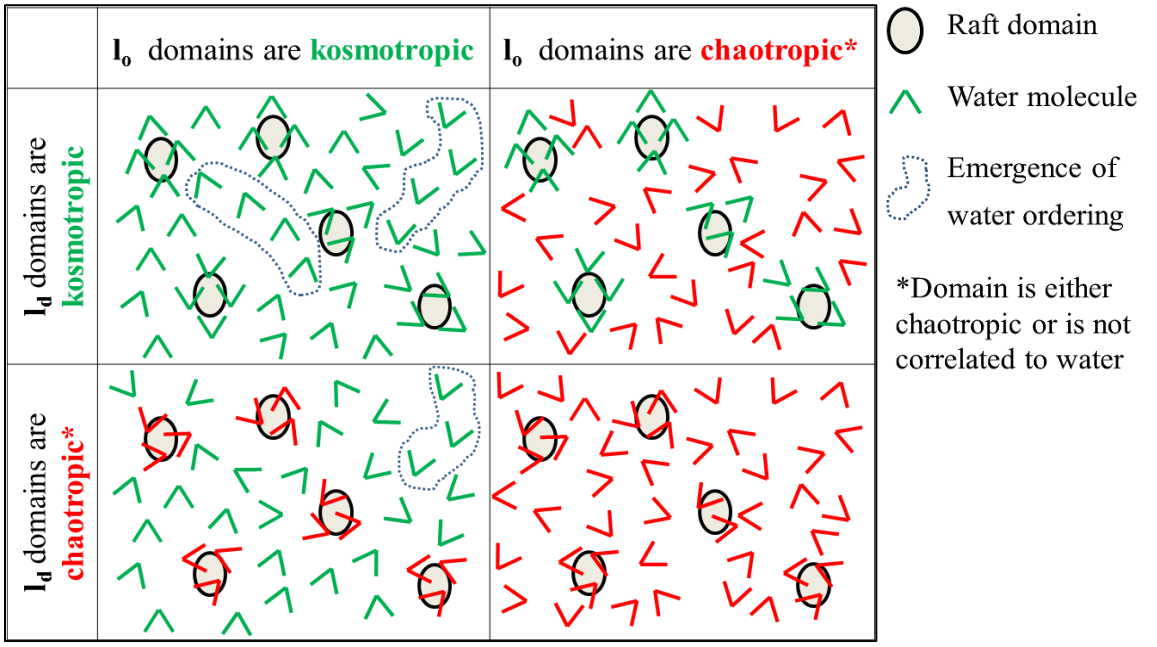

Figure 2.6: The possible influences of l_d and l_o domains on axonal water.

Throughout the research done on the composition, size, stability, dynamics, protein-inclusion and signal transduction of lipid rafts, very little attention has been paid to the effect of these lipid microstructures on water. Usually the opposite is the case. Generally, when water is included in computational models it is for the sole purpose of better replicating physiological conditions, and in most cases it is represented by single-point charges instead of explicit molecules [72, 73]. Such simplifications help keep the time-cost of already lengthy simulations down. By now it is understood that raft and non-raft domains have significantly different properties, enough so that they can be studied independently. This allows for more simplified models of each type of membrane region, using similar modelling techniques, but this time including more information about the water molecules. At this point, a picture begins to emerge of what type of model system one might use to examine the behaviour of molecular water near the myelin sheath, using computational methods. Some of the most common lipids used to model and test raft behaviour are DOPC, SM, and cholesterol [52–58, 60, 64, 65]. It has been suggested that 1-palmitoyl,2-oleyl-*sn*-glycerophosphocholine (POPC) is a more biologically relevant l_d-type lipid than DOPC, but the typical mammalian cell is known to be well represented by

a tertiary system comprised of cholesterol, SM and some form of an unsaturated phosphatidylcholine [56–58]. As a means of ensuring the algorithms were appropriate for the systems being tested, and to remain consistent with the field of lipid membrane research, the eventual bilayers used to generate results were based on this commonly accepted model.

2.2 Modelling Lipid Bilayers With Molecular Dynamics

Any model that aims to represent the complexity of a chemical system uses best-fit formulas and approximations for the many interactions which can occur. Computational chemistry has always been developed alongside experimental data, but different research groups use different training sets for developing their methods, and some of these are designed to fit only a very specific type of system. The result is a long list of choices of mathematical models, parameters, approximations and even various modelling software. Often there is no singular best way to undertake a theoretical study, only certain ways that are more advisable, or more common, than others. As the size and complexity of the system of interest in a theoretical study increases, the technicality of the available computational modelling technique decreases. The typical lipid bilayer model, with anywhere between fifty and several hundred lipid molecules (in addition to several hundred or several thousand water molecules), cannot reasonably be modelled using the most detailed or advanced methods. Instead, it is acceptable to use "simpler" mathematics based on a Newtonian and statistical world, and not necessarily a quantum mechanical one. The most popular method used in the study of lipid bilayers is MD simulation.

Molecular dynamics is a time-dependent statistical form of molecular mechanics (MM). The central aspects of MM, molecular force fields and the various minimization algorithms, are crucial to MD as well, but MD is also concerned with concepts such as statistical ensembles, thermostats and periodic boundary conditions. The issues faced when attempting to create a description of a system for an MD simulation include: properly representing the non-bonded interactions – dealing with Van der Waals and

long-range electrostatic interactions – dealing with solvents and establishing appropriate timesteps, cut-offs, and constraints. Since the first MD simulation of hard spheres undergoing perfectly elastic collisions, in 1957, the technique has been greatly improved to provide meaningful information about real systems [74]. This section outlines the theory which gives rise to this technique, as well as some specifics on how to implement this technique for lipid bilayer systems.

2.2.1 Molecular Mechanics and Molecular Force Fields

Molecular mechanics is a method of modelling that is based on the principles of classical mechanics; on Newtonian physics. Newton's three laws of motion – the conservation of momentum, the relationship between momentum and force, and the balance between action and reaction – are all reflected in the construction of a molecular force field [74, 75]. Like the wavefunction used to describe a quantum mechanical system, a molecular force field is the central mathematical representation of a system in MM. Contrary to quantum mechanics (QM), it describes the potential energy, **V**, of a system based (principally) on the coordinates of the nuclei, N, in a given system, while it omits the explicit interactions of electrons. The standard force field is a sum of the terms for bond lengths, bond angles, bond torsions, and the various non-bonded interactions [74]:

$$\mathbf{V}(\boldsymbol{r}^N) = \sum_{bonds} \frac{k_i}{2}\left(l_i - l_{i,0}\right)^2 + \sum_{angles} \frac{k_i}{2}\left(\theta_i - \theta_{i,0}\right)^2 + \sum_{torsions} \frac{V_n}{2}(1 + cos(n\omega - \gamma))^2 + \sum_{non-bonded*} \quad \textbf{(2.5)}$$

In the first term the bond lengths are compared to a harmonic oscillator, deviating from an ideal internuclear distance [74]. The second term uses the same structure, but describes the angle of a bond relative to the optimal low-energy angle [74]. The third term describes the effect of rotation around a single bond on the potential energy [74]. The last term, the sum of all non-bonded interactions, is the more complicated and computationally demanding contribution to the potential energy. Non-bonded interactions take place between any two atoms which are not bound to one another, whether they are in separate molecules, on opposite ends of the same molecule, or are on opposite ends of the system of interest. The interactions covered in this term are repulsion, dispersion and

electrostatics. The most common form of the non-bonded term uses Coulombic repulsion and the "Lennard-Jones 6-12 potential" for interactions between two atoms, *i* and *j* [74]:

$$\sum_{non-bonded} = \sum_{i=1}^{N} \sum_{j=i+1}^{N} \left(4\varepsilon_{ij} \left[\left(\frac{\sigma_{ij}}{r_{ij}} \right)^{12} - \left(\frac{\sigma_{ij}}{r_{ij}} \right)^{6} \right] + \frac{q_i q_j}{4\pi\varepsilon_0 r_{ij}} \right) \quad \textbf{(2.6)}$$

The 6-12 potential is employed in many of the most popular force fields, such as the CHARMM (Chemistry at HARvard, Macromolecular Mechanics) force fields [76, 77]. The CHARMM force fields are commonly used with a variety of different systems, ranging from small molecules to large proteins. One of the main goals a good force field is to choose parameters that are transferable, so that it can produce sufficiently accurate results for a wide variety of systems [74]. Like many others, the CHARMM force fields were built by, after establishing the main form of the equation, slowly changing the parameters until the force field produced results for a set of systems which agree with experimental results [74, 77]. In contrast to this, some of the more recent force fields are being developed using *ab initio* methods, and are only then compared to experimental data [78, 85]. The best example of this is the MMFF94 force field by Halgren et al., and perhaps the most peculiar aspect of this particular force field is that it does not use the 6-12 potential [78–84]. Instead, it uses a "buffered 14-7 potential" to describe the dispersion and exchange components of van der Waals interactions [78-84]:

$$\sum_{non-bonded} = \varepsilon_{ij} \left[\left(\frac{1.07 R_{ij}}{r + 0.07 R_{ij}} \right)^{7} \left(\frac{1.12 {R_{ij}}^{7}}{r^7 - 0.12 {R_{ij}}^{7}} - 2 \right) \right] + \frac{q_i q_j}{D\left(R_{ij} + \delta\right)^{n}} \quad \textbf{(2.7)}$$

in which R_{ij} is a buffering constant for polarization. The main accomplishment of 14-7 potential is that it better replicates dispersion interactions [74]. Due to the *ab initio* method used to build MMFF94, it has been shown to reproduce experimental results, even on types of systems which were not used in the development of the force field [86]. The first form of MMFF94 has encountered difficulties in its description of water [87], but a later version, MMFF94x, has been used to replicate X-ray diffraction results of liquid systems which are heavily-influenced by the proper description of long-range electrostatics [87, 88]. It has also been successfully compared to other force fields in its description of sugar, amino acids and protein-binding [89]. The best algorithm produced in this study used MMFF94 force field types, and so it will be discussed in slightly greater detail.

2.2.2 The MMFF94 Force Field

Like any force field, MMFF94 consists of the expressions used to approximate how internal (or bonded) and external (or non-bonded) interactions affect the potential energy of a system. As discussed previously, in MMFF94 the non-bonded Coulomb and van der Waals interactions are described by the buffered 14-7 potential (shown in Equation 2.7). The electrostatics component of this potential was parameterized using the Hartree-Fock level of theory and a 6-31G* basis set [78–84]. The van der Waals component is generally considered one of the more difficult aspects of a system to model and so the expression for it was created with a higher level of theory. The 14-7 potential was created by comparison to results obtained by fourth order Møller-Plesset (MP4) calculations, using a basis set which is contracted to *5s,3p,2d/3s2p* orbital space [78–84]. The remaining internal components of the potential energy are calculated as follows. The energy for a bond between any atoms *i* and *j* is given by:

$$E_{bond} = K_{bond}\left(r_{ij} - r_{ij}^{\circ}\right)^2 \bullet \left(1 + cs\left(r_{ij} - r_{ij}^{\circ}\right) + \frac{7}{12}\left(cs^2\left(r_{ij} - r_{ij}^{\circ}\right)^2\right)\right) \qquad \textbf{(2.8)}$$

in which r_{ij} is the bond length, K_{bond} is the force constant for the bond, and *cs* is a cubic stretch constant [78–84]. Similarly, for any three atoms *i*, *j* and *k* (where *j* is the attached to both *i* and *k*) the energy association with the angle between them Θ_{ijk} is given by:

$$E_{angle} = K_{\theta}\left(\theta_{ijk} - \theta_{ijk}^{\circ}\right)^2 \bullet \left(1 + cb\left(\theta_{ijk} - \theta_{ijk}^{\circ}\right)\right) \qquad \textbf{(2.9)}$$

in which K_{Θ} is the force constant and *cb* is a cubic-bend constant of $-0.007^{\circ-1}$ [78–84]. For a linear or near-linear angle the energy is given by [78–84]:

$$E_{angle,linear} = K_{ijk,linear}\left(1 + cos\theta_{ijk}\right) \qquad \textbf{(2.10)}$$

The energy of a combined mode of stretching and bending is given by [78–84]:

$$E_{stretch-bend} = \left(K_{ijk}\left(r_{ij} - r_{ij}^{\circ}\right) + K_{kji}\left(r_{kj} - r_{kj}^{\circ}\right)\right) \bullet \left(\theta_{ijk} - \theta_{ijk}^{\circ}\right) \qquad \textbf{(2.11)}$$

The energy for out-of plane bending at sp^2-hybridized centers, for example in a benzene ring, is given by:

$$E_{oop} = K_{oop}\left(\chi_{ijk;l}\right)^2 \qquad \textbf{(2.12)}$$

in which $\boldsymbol{\chi}_{ijk;l}$ is the Wilson angle between the *ij* bond and the plane created by *i*, *j* and *k* [78–84].

The final component of the internal energy, dihedral and torsional strains on a molecule, is given by:

$$E_{torsion} = 0.5\big(V_1(1 + cos\Phi) + V_2(1 + cos2\Phi) + V_3(1 + cos3\Phi)\big) \quad \textbf{(2.13)}$$

in which V_1, V_2 and V_3 are force constants and Φ is the dihedral angle of interest [78–84]. The potential energy of internal forces were parameterized using the geometries, vibrational spectra and conformational energetics of 360 compounds, as predicted by second order Møller-Plesset (MP2) calculations with a 6-31G* basis set [78–84].

2.2.3 Finding Minima on a Potential Energy Surface

Minimization is, for most purposes, the first step in a theoretical study of a chemical system. Just as every conformation of a molecule corresponds to a certain level of energy – some being more restricted and therefore energetic, others being low energy and therefore more favourable – a large system containing thousands of atoms has higher energy and lower energy configurations. Collectively, a plot of all the possible configurations for the atomic coordinates versus their potential energy creates a topographical map; this is called the potential energy surface. Depending on the available energy a system may move all over the potential energy surface, experiencing a wide variety of configurations. It is preferable to begin a simulation in an energy well, an area which corresponds to a more stable configuration, so that your the represents a more probable situation in the lifetime of the system. Finding the global minimum, or even a good local minimum, by mathematical means has proven a difficult task. In fact, no minimization algorithm has ever been proven to find the global minimum [74]. Nonetheless, preparing the system for a long simulation is an essential way to prevent a good portion of the computational time from being wasted on settling out so-called "hot-spots" in the initial configuration, or relieving areas of high strain and unlikely positioning [74]. There are a number of different methods available, and while some are more preferred than others, no one method is known to be better than the others [74]. The minimization employed in this study by the MOE 2010.10 software package follows a non-linear optimization algorithm [90].

The goal of non-linear optimization is to adjust the atomic coordinates of the system until the forces acting on them are approximately zero [92]. The optimization ends when either the number of specified iterations is completed, when the root-mean-square gradient satisfies the stated criteria, or when the level of accuracy requested for the energy being calculated has been met [92]. In the 2010.10 version of MOE the optimization algorithm is a combination of the Steepest Descent method and the Conjugate Gradient-Truncated Newton method [90]. In the steepest descent method the direction in which the system should shift on the potential energy surface is calculated from the current position and the direction of net force [?]. The direction vector is defined as parallel to the net force, and generally this points toward deeper points in an energy well. This is a popular method due to its speed and efficiency, however it does encounter difficulty with steep and narrow energy wells, and so after a while the MOE software switches to a more accurate (though slightly more time consuming) method [74]. The Truncated Newton method uses tangential approximations to approach the minimum point on a curve, and it is a recursive method in that it uses a different algorithm within its calculations to define the direction vectors; in this case those vectors are obtained using the Conjugate Gradient method [74]. Conjugate Gradient is similar to Steepest Descent, with the main exception being it defines vectors based on the current position as well as the previous direction vector [74]. This prevents the unpredictable behaviours seen in some Steepest Descent calculations, and increases the ability of the algorithm to find a very accurate minimum point. The combination of Steepest Descent with Conjugate Gradient-Truncated Newton is an effective way to balance efficiency with accuracy, for a good overall minimization algorithm. Once the force field model has been chosen and the atomic positions of a system have been approximately optimized, the system is ready to undergo an MD simulation.

2.2.4 Molecular Dynamics Simulations

Molecular dynamics is the study of the time-dependent trajectories of all the particles in a given system [74, 93]. An MD simulation begins with the energy minimized coordinates for all atoms in the system. The user defines the length of the simulation, and the timestep

between calculations. At the beginning, all of the forces acting on all of the particles are calculated, based on the force field selected, the circumstances specified (such as temperature, pressure, boundaries and how water and certain forces are handled) and any constraints imposed [74]. These forces are applied to the particles for the duration of the user-specified timestep, and it is assumed that the forces are constant during this interval [74]. The resulting coordinates for all particles are calculated according to Newton's second law [74]:

$$\frac{d^2x_i}{dt^2} = \frac{F_{x_i}}{m_i} \tag{2.14}$$

Once the trajectories – the calculated positions and velocities – of all particles are determined for that timestep, the particles are then moved and the process starts over [74]. At the beginning of the next timestep the incoming trajectories are combined with the calculation of all forces acting on all particles, to find the new trajectories for the next timestep [74]. MD is often called a "deterministic method" because the state of the system depends on the states which precede it, and also because "the state of the system at any future time can be predicted from its current state" [74]. MD is also a deterministic method because the simulation is heavily influenced by the user's choice of parameters such as timestep, ensemble and thermostat. Thus the next step in running an MD simulation – after minimization is complete – is to set-up an algorithm which will represent the system in a realistic manner, and to establish a way to manage the physical variables of temperature, pressure and volume.

In MD the macroscopic properties described above are controlled by the choice of statistical ensemble and the thermostat. Statistical ensembles were suggested by Gibbs as a replacement for the time average of a system with many particles [93]. Any "experimentally observable property is just the time average" of that property, but when the system being simulated is very large the time to find this average by computational means is also large [93]. Statistical ensembles simplify the math by holding certain parameters to a constant, and allowing others to evolve with time in order to find their statistical average. There are four widely-recognized ensembles: the canonical ensemble

(NVT) in which the number of particles, N, the volume, V, and the temperature, T, are held constant; the microcanonical (NVE) in which the particles, volume and energy, E, are held constant; the grand canonical (μVT) in which the chemical potential, μ, volume and temperature are held constant; and the isobaric-isothermal (NPT) ensemble in which the number of particles, the pressure, P, and the temperature are held constant [74, 93]. The most popular ensemble for use in biological systems, especially for lipid bilayer systems, is the isobaric-isothermal ensemble, because its predictions are most directly relevant to experimental data [74].

Controlling the pressure of the simulation system is usually done by simply allowing the volume to fluctuate, but controlling the temperature is a slightly more complicated task; for this, MD simulations use thermostats [74]. Some of the most popular thermostats - the Berendsen (BER) and Nosé-Hoover-Andersen (NHA) – control the temperature by coupling the system to a bath, considered to be external or internal, respectively [96]. The bath helps to maintain the temperature at a constant by "supplying or removing heat from the system as appropriate" [74]. The BER thermostat is regarded as a weaker approach to temperature control [94, 95]. The NHA thermostat is an accepted algorithm for use with the canonical ensemble, but more recently it has been found deficient and problematic [96]. One of the main criticisms of NHA is that it is an "*ad hoc*" method, and not Hamiltonian [96]. The Hamiltonian is a function which is "of immense importance in classical mechanics" as it represents the sum of all kinetic and potential energy in a system [93]. The relationship between temperature and kinetic energy is unmistakeable, so it is favourable to use a thorough definition of kinetic energy to aid in the control of temperature. Thus, the recommended thermostat for constant temperature molecular dynamics is the Nosé-Poincaré-Andersen (NPA) thermostat, which is built from the Nosé Hamiltonian for kinetic and potential energy [92, 94–96].

After the macroscopic concerns are addressed, the user may choose to make use of microscopic constraints or restraints during an MD simulation. Restraints are an imposed guideline for atomic motion which is usually, but not always, followed [74]. An example

of a restraint is requiring that heavy atoms stay within a certain distance (in angstroms) of their original coordinates. An energy penalty would be imposed if this guideline were not followed, and so the simulation only strays from restraint conditions if the alternative is fairly energetically favourable. Constraints, on the other hand, are a firm rule which the simulation must abide by [74]. In a complex many-body system there are innumerable vibrational modes, many of which may not be of interest and may simply increase the time required to perform the simulation. Constraints allow the lower frequency modes associated with conformational changes and significant interactions to be the focus of the simulation [74].

A variety of constraints exist, as well as methods to employ them, but they all function to control certain internal coordinates or bond lengths, "without affecting the other internal degrees of freedom" [74]. For example, in a lipid bilayer a significant amount of time is spent calculating the motion of hydrogen substituents on the aliphatic chains – motion which is not necessarily relevant to the water molecules above and below the bilayer. In this situation it is beneficial to constrain carbon-hydrogen bonds to the optimized length and angle for the duration of the simulation, although the carbons they are attached to may themselves move. Another common means of controlling the location and flow of particles in the simulation system is by imposing periodic boundary conditions.

2.2.5 Periodic Boundary Conditions

Periodic boundary conditions (PBC) are a relatively straight-forward concept that enables a large number of molecules to be represented and modelled by a much smaller sample. They are mostly used in systems which need to be solvated. The computational cost of modelling large numbers of explicit water molecules quickly makes many simulations unrealistic. Some methods of solvation deal with this cost by using implied water, simply hinting that water surrounds the solute, but with PBC the water that is actively engaged with the solute and with other water molecules, and still keep the simulation time to reasonable lengths.

Periodic boundary conditions are constructed by repeat units of the simulation cell. All the molecules in the system are contained in a cell of a specific size, and this cell is repeated on all sides and corners of the original cell [74]. During a simulation, whenever a particle exits one side of the central cell a mirror particle enters from the cell on the opposite side, so that the number and type of particles in the main simulation cell always remains constant [74]. For example, imagine a simulation cell which contains one simple solute in the middle, and approximately fifty water molecules around it. A water molecule in the corner of the simulation cell "feels" the presence of the water nearest to it in the same cell, as well those in the seven cells which surround it. Effectively, the solute in the middle of the simulation cell is infinitely solvated. More importantly, the PBC ensure that all the particles in a simulation "experience forces as if they were in a bulk fluid" [74]. PBC allow for bulk properties of water and large systems to be more accurately determined from much smaller and computationally more efficient systems.

The main challenge associated with PBC is establishing proper treatment of long-range interactions so that the boundary between two cells is smooth and there is no artificial barrier to particles, and so that long-range electrostatic interactions are present and are in realistic amounts. Two of the most common methods for treating electrostatics in PBC are particle mesh Ewald (PME) summation and the reaction field method [74, 75]. In PME summation every particle interacts with all other particles, and with all of their replicated images in the repeated cells [74]. While PME produces accurate results, it converges very slowly and greatly increases the time it takes to run a simulation [74].

The reaction field method aims to be a more efficient and generally applicable method. It uses a functional cut-off and an approximate background to describe long-range electrostatics. When using the reaction field method the user defines the radius, r_c, for a sphere surrounding any given molecule; anything which falls inside that sphere reacts with the original particle explicitly, and anything outside r_c is described by a dielectric constant [74]. The electrostatic interactions for any given particle are given by [74]:

$$E_i = \frac{2(\varepsilon_s - 1)}{\varepsilon_s - 1}\left(\frac{1}{r_c^3}\right)\sum_{j;r_{ij}\leq r_c}\mu_j \qquad \textbf{(2.15)}$$

in which "μ_j are the dipoles of neighbouring molecules that are within the cut-off distance (r_c) of the molecule i". In this equation everything preceding the summation corresponds to things outside the reaction sphere, and the summation represents the dipoles of the molecules within the reaction sphere. Thus, under PBC every particle experiences the true electrostatics of its closest neighbours, but only experiences an approximation of how the further particles in bulk are behaving. The goal is to choose the cut-off such that significant interactions are explicitly included, but the relatively minor and effectively time-consuming interactions are covered by the average dielectric field. Establishing a proper cut-off has been shown to be problematic, especially for lipid bilayers, but despite these issues the reaction field method "performs rather well" and is recommended when using time-demanding smei-explicit water solvation [73, 92].

2.2.6 Molecular Dynamics and Lipid Bilayers

The first fully explicit simulation of a (32 molecule) lipid bilayer, in 1982, used periodic boundary conditions to extend the size of the system, and restraints on the motion of polar head groups to "reproduce the interactions between the head groups and the water layer" [74]. Since then major improvements have been made to increase the size and length of simulations possible, and the accuracy of the methods used [74]. As well, MD algorithms "have been greatly refined…to include realistic ensembles of…water in bilayer configuration" [63]. Fortunately, the accuracy of these methods has advanced enough that "studies of lipid–water systems…provide a strong theoretical basis upon which the results of experiments may be tested" [63]. Fully-solvated lipid bilayers are readily simulated and commonly used to understand process such as domain formation, transmembrane diffusion, transmembrane protein activity and the interaction of other molecules with the lipid bilayer [62, 72, 97–99].

Typical MD simulations of lipid bilayers involve a complex process of minimizations and short MD simulations, before a final multi-phase simulation [62, 72, 74, 97, 99–101]. The rigorous preparation of lipid bilayers for an MD simulation helps to confirm that the algorithm is accurate, and that the simulation will produce meaningful results. For

example, the preparation for a “handmade” tertiary bilayer of SM, DOPC and cholesterol involved a preliminary energy minimization, a 200 ps MD run at 500 K, 4 consecutive 200 ps runs (ramping down the temperate by 50 K each time), a 2 ns MD simulation at 300K with regenerated velocities every 200 ps, a 3 ns continuous MD simulation, and finally a 200 ns production run [62]. In stark contrast to this is the preparation of a protein-containing lipid bilayer which only required one minimization step, and a 0.5 ns MD simulation, before the final production run [97].

In the MOE 2010.10 software package an MD simulation can be set-up to include a heating, equilibration, and production phase [92]. This does not remove the need to minimize and prepare a bilayer properly beforehand, but it does streamline the final simulation process. During the heating phase the temperature increases over a user-defined range. Once the target temperature is reached, the equilibration phase is used to remove any lingering hot spots. During the production phase the temperature is maintained, and the dynamics data are collected. In some cases a cooling phase is also run, the main goal of which is to see if the simulation has brought the system over an energy barrier and down into a new energy well on the PES [74].

An acceptable algorithm for MD simulations of a lipid bilayer consists of: an all-atom forcefield (in which all atoms are explicitly described), the NPT ensemble, the NHA or NPA thermostat, the PME or reaction field model for long-range electrostatics, some constraints on light bonds (for example carbon-hydrogen bonds), some restraints on heavy atoms and periodic boundary conditions [62, 72–74, 97–101].

2.3 Building and Simulating Lipid Bilayer Models

2.3.1 Simplified Hydrophobic Surfaces as Lipid Bilayer Models

The development of this project has seen much trial and error, even from the very first stages of building the models. The eventual systems used in the MD simulations were based on the structure of lipid rafts in the myelin sheath, but before these were built other

models were created and tested. In an effort to minimize computational costs the first systems were designed to be very simple. In saltatory neurotransmission the current, or AP, travels alongside manifold layers of dense lipid tissue, and so the basic concept to be modelled was the conductivity of water alongside a hydrophobic surface. This effect has been demonstrated in previous simulations: the conduction of protons by water wires through carbon nanotubes. Thus, the first models were based on carbon nanotubes. All systems discussed in Chapter 2 were built with the SYBYL 7.2 software package [102].

Two models were made, based on the idea of a network of benzene rings that are separated by small aliphatic moieties. The aliphatic spacers were placed to reduce rigidity and represent the fluidity and motion present in a lipid membrane, as well as to ensure that any observed conductivity would be the result of water structures, and not long-range conductivity of conjugated benzenes. The first system used ethyl spacers between linked benzene rings (see Figure 2.7). Starting from a single benzene ring, ethyl substituents were added and benzene rings attached to them, until a small 5x5 benzene ring grid was built. This grid was copied into empty molecule spaces in the SYBYL 7.2 software, the grids were arranged side-by-side, the molecule spaces were merged, and the grids were joined by establishing covalent bonds between them. In this way a large system with long-range order is created fairly quickly, and the process was repeated until a large grid containing 300 benzene rings was established.

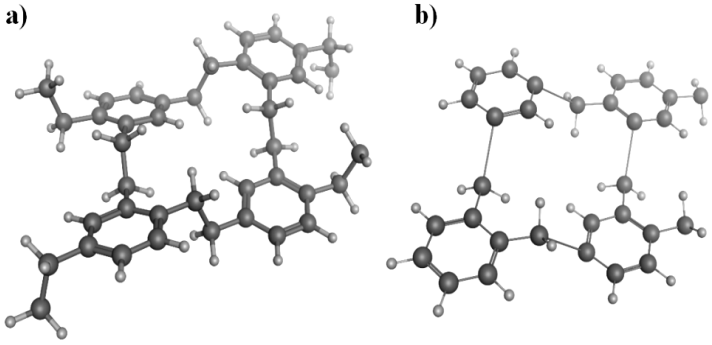

Figure 2.7: The two benzene-based systems with a) ethyl and b) methyl spacers.

The system was then prepared for simulations, and studied, using the MOE 2009.10 software package [91]. After minimization, the grid was subjected to a short MD simulation, and during this simulation the grid folded over on itself. The two sides of the grid were covalently joined to make the tube shaped model shown in Figure 2.8. The tube was prepared for simulations using MOE: it was solvated and energy minimized. During a 5000 fs MD simulation the tube with the ethyl spacers was shown to be too flexible, demonstrating wave-like motion throughout the simulation. So, a new system was built using the smaller methyl moiety in-between benzene rings (see Figure 2.7). The second tube displayed the same wave-like instability as the first, and the tube-shaped model was discarded.

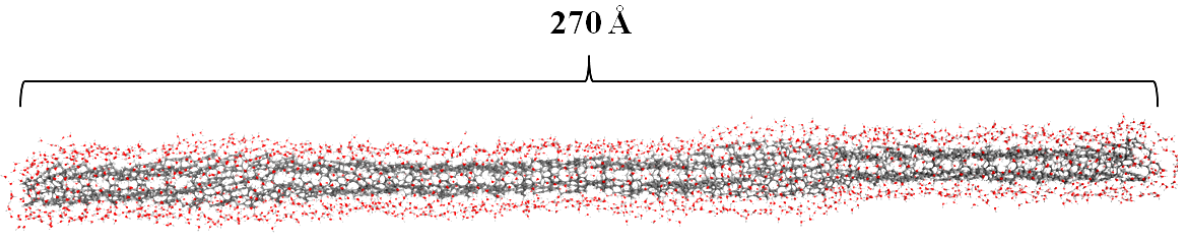

Figure 2.8: The benzyl/ethyl system, solvated by 5 layers of water and minimized.

Another system was briefly explored which attempted to utilize π-π stacking between benzene rings as a source of stability. Grids of benzene rings and ethyl spacers, from the previous model, were stacked four high. In the starting geometry there was an average distance of 3.09 Å between benzene rings in adjacent grids. This system fell apart during its energy minimization in MOE 2009.10, and was never brought to the MD simulation level. In light of the three failed attempts with simplified models a more stable and biologically representative model was sought. After further research into membrane structure and lipid rafts, a series of bilayers comprised of phospholipids were prepared and tested.

2.3.2 The Full Lipid Bilayer Models

The chief failure of the simplified models was a lack of long-scale stability. In light of this a new strategy was developed based on more realistic models, but still with the mindset of modelling the movement of current along a lipid surface. Initially, a series of established .pdb files (.pdb stands for program database, most commonly used in the protein databank) of unary bilayers (containing only one type of lipid) were downloaded for a preliminary study. These bilayers were studied in order to get a better handle on the modelling software and technique as it applies to realistic lipid bilayers, so that future calculations could be made quickly, and to establish a functional algorithm for future calculations. For a few months the MOE software was unavailable for this project, and so some of the following simulations were completed with the SYBYL 7.2 package [102].

The first membrane taken from a .pdb file consisted of 128 1-palmitoyl-2-linoleoyl-*sn*-glycero-3-phosphatidylcholine molecules, and the second was made of 64 dipalmitoylphosphatidylcholine molecules [103, 104]. The 128 lipid bilayer was minimized with a wall restraint of 5 and minimum PBC, and this produced no change to the estimated potential energy or the visual appearance. The boundary conditions created by the system were much larger than required, but could not be adjusted manually. The bilayer was then fully solvated and 2 dummy atoms of charge +1 were inserted on one side of the top leaflet of the membrane. The dummy charges were intended to represent excess Na^+ ions at the polarized end of an internodal segment of the myelin sheath. This system was re-minimized and an MD simulation was run for 200 ps at 300 K, with the all-atom CHARMM27 force field [76, 77]. The simulation used no specific constraints on atomic positions, bond lengths or bond angles. The algorithm used for this simulation returned a stable bilayer, but the solvent water molecules readily dispersed due to the generous boundary conditions, and no significant migration of the dummy atoms was observed.

The 64 lipid bilayer was minimized for 500 iterations using a wall restraint of 5 and minimum PBC, a non-bonded cut-off of 8.0 Å and the built-in Tripos 5.2 force field

[105]. Again the boundary conditions created by the system were much larger than required. Following the treatment used on the 128 lipid membrane, the second membrane was prepared for a dynamics simulation of dummy atom migration. An MD simulation was run at 300 K using an NVT ensemble, the Tripos 5.2 force field and an 8.0 Å non-bonded cut-off. In this case the bilayer was less stable, becoming entangled and appearing like a micelle, and again the solvent waters spontaneously dispersed. At this point several decisions were made: 1) the bilayers were too small and their periodic boundary conditions were too big and 2) the SYBYL 7.2 program was not the preferred platform for running the MD simulations. It also became apparent that it would not be feasible, with the current models, to simulate any water-guided migration of point charges across a lipid membrane. Again, after further research into the structure of the myelin sheath and the unique properties of water, the model was restructured. Instead of trying to model the movement of charge along the lipid membrane the focus was shifted to the balance between the lipid membrane and its solvent, and the motion of the water itself.

Following the test runs done on lipid bilayer .pdb files, four original bilayers were constructed. The new bilayers were based on the SM, DOPC and cholesterol lipids – crucial molecules in the myelin sheath, and in the description and study of lipid rafts. The first (B1) and second (B2) systems were tertiary bilayers of SM, DOPC and cholesterol. The third bilayer (B3) was a unary bilayer of SM, and the fourth (B4) was a unary bilayer of DOPC. The compositions of these systems are summarized in Table 2.1 below.

Table 2.1: The compositions of the original bilayer systems: B1, B2, B3 and B4.

System	Composition	Total Lipids	Total Waters	Total Atoms
B1	SM/DOPC/cholesterol	129	0	15,840
B2	SM/DOPC/cholesterol	240	5,521	29,904
B3	SM	354	5,392	65,028
B4	DOPC	346	7,318	71,086

The B1 system was built with a 1:1 ratio of SM and DOPC. The lipids were arranged in small clusters (approximately five lipids per cluster), and the clusters were distributed randomly. This structure was minimized for 500 iterations using the Tripos 5.2 force field, a non-bonded cut-off of 8.0 Å and no boundary conditions. Afterwards the cholesterol was inserted into natural gaps between the clusters, and the system was re-minimized for 1000 iterations. The construction of this bilayer was an attempt to create a a low level of pre-set order that may demonstrate the formation of raft and non-raft domains during an MD simulation. The final MD simulation (run in SYBYL) of B1 was 5000 fs long, used MMFF94, the NTP ensemble at 310 K and 1 atm, a cut-off of 8.0 Å and no specific constraints or periodic boundary conditions. Throughout the simulation B1 held together well, if expanding slightly, but there was no observation of more distinct domain formation. It was decided that the relative amount of cholesterol in B1 was too low, as compared to the make-up of real membranes. After a review of the literature it was also decided to use the NPT ensemble, not the NVT ensemble, in future calculations.

The second model used twelve each of SM and DOPC, for every six cholesterol molecules; this model had a cholesterol concentration of 25% – a better approximation of the composition of human myelin tissue. It also attempted to utilize the stabilizing interactions of the rough α-face of the cholesterol molecule with saturated aliphatic chains (such as those on SM), and the interactions of the smooth β-face with the unsaturated acyl chains (such as those on DOPC). Instead of placing small clusters at random, like with B1, the construction of the B2 system was intentionally organized. A clustered row of six cholesterol molecules was constructed, then the twelve SM were placed in a cluster on the α-face, and the twelve DOPC were placed in a cluster on the β-face. This was scaled-up, in both length and width, until there was an elongated leaflet containing 120 molecules. This leaflet was then duplicated and placed underneath with the aliphatic SM chains pointing towards those of SM in the top leaflet (likewise for the DOPC and the cholesterol). The result was an elongated bilayer with a strip of cholesterol molecules down the middle, SM on one side and DOPC on the other. The goal of building such a bilayer – which does not necessarily exist in the natural lipid membrane –

was to look for a difference between the behaviour of water above raft and non-raft domains when they are distinct regions, but are in close proximity.

Each SM, DOPC and cholesterol cluster was pre-minimized for a short run of 200 iterations using the MMFF94 force field, before being combined into the bilayer described above [78–84]. This was done to reduce the minimization time for the larger bilayer. Afterwards, an MD simulation was carried-out using MMFF94 and the NPT ensemble at 310 K and 1 atm. The output of this simulation was re-minimized, and at this point the system was transferred into the updated SYBYL-X software package [106]. A second MD simulation was completed using the MMFF94 force field and the NPT ensemble, at 310 K and 1 atm. The system was repetitively minimized and simulated before solvation to prevent the loss of the bilayer structure when water was added (for example, becoming a micelle). After the second successful MD simulation the system was solvated using a five-layer box-soak, with no periodicity. Then, the completed B2 system was minimized using the MMFF94x force field (which was the only built-in force field that could fully characterize both the bilayer and the water molecules) and a tether of 10 on the coordinates of heavy atoms [88, 92]. This minimization was repeated, with the heavy atom tether increased to 100. Finally, the 5000 ps MD simulation was started. Unfortunately, this simulation failed due to memory allocation after 1854 calculation steps. After two mixed bilayers, of mixed success, a third and fourth system with only one lipid type each were made. The B3 system represents the l_o domains, while the B4 system represents the l_d domains. The idea was to isolate each system for ease of calculation, and compare the movement seen in these systems with each other, and any useful information from the mixed B2 system.

The third system was constructed by simply repeating the SM molecule until there was a grid containing 192 lipids. The grid was duplicated, flipped, and the bilayer was lined up. Due to the chemical simplicity of this bilayer, as compared to B1 and B2, less effort was spent preparing the system with minimizations and MD simulations, before solvation. Only one minimization was completed before a five-layer box-soak was applied. The

minimization of this system crashed and the calculations were moved over to the MOE 2009.10 software, which was now available. The system was minimized, using the same parameters, and an MD simulation using the NPT ensemble was initiated. This, and four successive attempts, failed because the bilayers were falling apart. It did not seem to matter what tethers, constraints or wall weights were used. Also, switching from NPA to NHA, and adding more water for repulsive stability, did not improve the outcome. Eventually an algorithm did emerge which maintained a stable bilayer, without imposing unrealistic constraints.

The first MD simulation which appeared to work well used rigid water molecules. While constraining the geometry of the water molecules may sacrifice some of the more exotic interactions which lead to water structures, it does not interfere with translational motion of the bulk water or the ability for hydrogen bonding to occur. This simulation ran for 28 days and simulated approximately 12.5% of the desired length, but was cut short by an unexpected power outage, so the simulation was restarted using similar parameters. This ran for 45 days and reached just over 16% of the desired simulation length, when the connection to the licence server was lost and the job was again terminated. Unfortunately, due to the size of the system and the length of the simulation, attempts to restart from the last trajectory were unsuccessful because of the size limitations of the program's database files. For the same reason it was not possible to begin a new simulation from the last position of the failed simulation and to merge the two, for analysis. It was decided that the systems were too complex, and were proving to be too computationally demanding. The system was pared down, the solvation was simplified and periodic boundaries were employed to reduce the computational load.

After a few complications with the cell parameters, the B3 system was prepared using the improved MOE 2010.10 software [92]. The previous solvation algorithm placed water molecules on all sides of the lipid bilayer. The new algorithm allowed for solvation of only the top and bottom of the bilayer, while leaving the aliphatic chains exposed. This allowed for closer and more accurate boundary conditions, and increased the stability of

the bilayer by extending the hydrophobic network. It also prevented the use of strict constraints which would create artificially rigid bilayers. The eventual 354 lipid B3 system was minimized with the MMFF94x force field. The MD simulation was done in three stages: a 100 ps heating phase from 0 K to 310 K, a 100 ps equilibration phase, and a 1000 ps production phase. The successful B3 simulation used: the MMFF94x force field; the NPT ensemble; the NPA thermostat; reaction field electrostatics for the solvent, with a dielectric constant of 1 inside the reaction field, and a dielectric constant of 80 for the exterior field; a non-bonded cut-off which tapers to zero between 6 and 8 Å from the atom of interest; a triclinic (P1) periodic cell with dimensions of 115 x 105 x 75 Å; and rigid water molecules. This MD simulation finished in 15 days.

The time to prepare the B4 system was greatly reduced by the trial and error of the previous three systems. A few attempts, similar to those in B3, were made with the full solvation of the MOE 2009.10 algorithm, before the MOE 2010.10 update was released. Once the new solvation method was available and the successful algorithm was established, the system was prepared and simulated using the same variable parameters as were used for the B3 system. The P1 periodic cell had dimensions of 112 x 110 x 75 Å. The MD simulation for B4 was completed in 18 days. These original bilayers are larger than those typically found in databanks, and were constructed this way because of the sensitivity of lipid bilayers to long-range electrostatics. A larger simulation cell reduces the additional errors due to incorrect long-range electrostatics when using PBC, and it provides a better value for the correlation of water motion to the surface of the bilayer.

2.4 Results from the Lipid Bilayer Study

The trajectory files produced by MOE 2010.10 were prepared for analysis with the Open Babel GUI software [107]. The B3 and B4 bilayers were analyzed using the VMD (Visual Molecular Dynamics) software [108]. VMD was used to study the RMSD, the RPDF and the number of hydrogen bonds per frame of the MD simulation trajectory.

The RMSD provides a measure of how much each atom moves compared to the reference position during an MD simulation. The reference position may be an X-ray structure, or an optimized structure, or the average position during a trajectory. For the B3 and B4 systems, the RMSDTT (Trajectory Tool) in VMD was used to establish the general success of the simulation algorithm employed, and the overall stability of the system. For each system a separate RMSD was calculated for all atom types, as well as a general calculation of all atom types at once. The reference for all RMSD calculations was the average position from the corresponding MD trajectory. Each RMSD calculation produced a value for all frames of the trajectory, and an average value for the entire simulation. These values have been plotted, by system, for comparison.

An RPDF is used to track particles when Brownian motion is known to be an influence [74, 109].The RPDF, g(r), describes the probability of there being a particle (such as an atom or a molecule) at any distance, r, from another particle [74, 109]. The g(r) is calculated as the number of particles in a spherical shell (see Figure 2.9) surrounding the origin particle, with thickness δr and a volume of [109]:

$$V = \frac{4}{3}\pi(r + \delta r)^3 - \frac{4}{3}\pi r^3 \approx 4\pi r^2 \delta r \qquad \textbf{(2.16)}$$

The typical RPDF for a liquid, shown in Figure 2.9, shows a large initial peak rising from a very low value, followed by steadily decaying peaks [109].

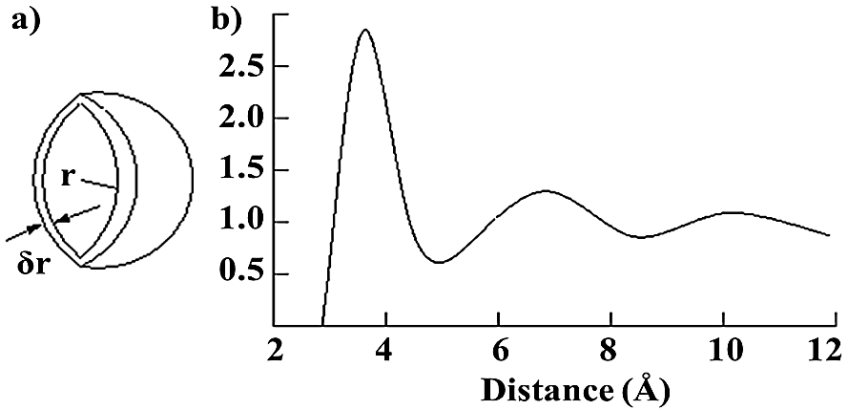

Figure 2.9: a) The RPD sphere and b) the standard shape for the RPDF of a liquid (in this case, liquid argon at 100 K) [109].

Radial distribution can be measured by X-ray diffraction, but it is most commonly used to study liquids in molecular dynamics simulations [74, 109]. The radial pair distribution analysis tool in VMD was used to understand how much more spread out the water molecules in the lipid bilayer simulations were when the various solutes were present. The RPDF for the lipid bilayer was performed for oxygen (the dominant component of water molecules with imposed rigidity) surrounding the carbon, nitrogen and phosphorous individually, and then simultaneously, and the RPDF was calculated up to 10 Å away from these origin atoms. Each calculation produced a normalized value for all atoms in the system during all frames of the trajectory, based on the distance from the origin atom, defined by the function g(r). The final RPDF is for all of the atom types in the solute at the same time, and is not a sum of the RPDF for each atom type individually. Radial distribution functions can also be used to study the hydration shell of a solute, and infer the strength of hydrogen bonds in the solvation sphere [10, 11]. This is done by calculating the ratio of the maximum and minimum values of g(r) for water-water interactions, and comparing it to that of the water-solute interaction [11]. When the g_{max}/g_{min} ratio is larger for water-water interactions than for solute-water interactions, the water is not strongly influenced by the solute. If, on the other hand, the solute-water ratio is higher, then the water is preferentially interacting with, and being re-ordered by, the solute. For this comparison the g_{max} was considered to be the second largest peak in the RPDF (because the first peak corresponds to the phosphate moiety), and the minimum was the bottom of this peak. The solute-water ratio was based on the RPDF for oxygen surrounding the normalized positions of carbon, nitrogen and phosphorous, and the water-water ratio was based on the RPDF calculated for oxygen surrounding oxygen.

Lastly, the hydrogen bond analysis tool was used to establish whether there were, on average, more or less hydrogen bonds between water molecules when the various solutes were present, as compared to normal bulk water. For both bilayers a search was performed for the number of hydrogen bonds containing oxygen and hydrogen, or nitrogen and hydrogen, for every frame of the trajectory. A hydrogen bond was defined as having a maximum length of 3.0 Å, and a maximum of 20° displacement from the axis

of the X-H bond (of the hydrogen bond donor). On average, the number of water-water hydrogen bonds per water molecule in a pure sample is just below two [10]. That is to say that for every water molecule, N, there should be a minimum of just below 2N hydrogen bonds observed at any time in a given solvated system. Any more or less than this value and the solute(s) within are behaving as a chaotrope or kosmotrope, respectively [10].

2.4.1 B3: The SM Bilayer

The results of the RMSD analysis of the B3 bilayer are shown in Figure 2.10 below.

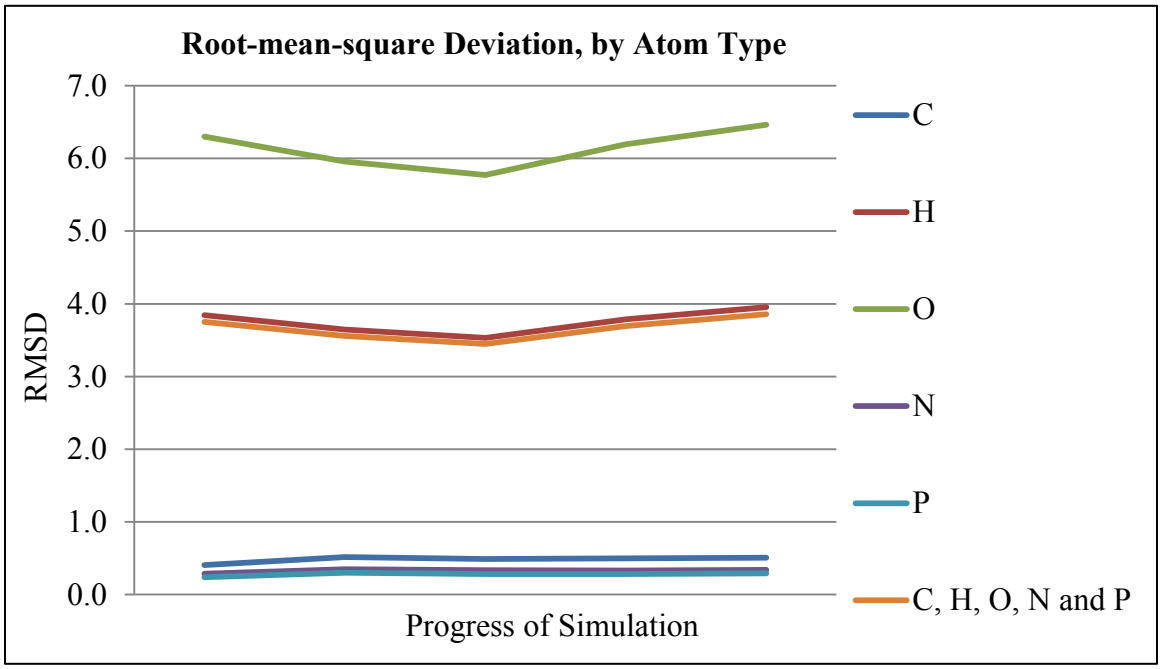

Figure 2.10: The calculated RMSD values for the B3 lipid bilayer.

The average RMSD values for each atom type are shown in Table 2.2 below.

Table 2.2: The averages of the calculated RMSD values, by atom type, for the MD simulation of the B3 bilayer.

System	C	H	O	N	P	C, H, O, N and P
B3	0.484	3.753	6.136	0.328	0.279	3.663

The high mobility of the oxygen indicates that the water was significantly more mobile than the lipid bilayer, which is to be expected. The mid-range value for the average RMSD observed for hydrogen makes sense, given that some of the hydrogen is tied up in the very stable bilayer, while some of it exists in the much more mobile solvent phase. The overall RMSD should be – as it is – a normalized value between these two extremes. Their low degree of deviation from average positions indicates that the main atoms which constitute in the lipid molecules – carbon, phosphorous, and nitrogen – were the most stable. This can be explained by the favourable van der Waals interactions between the aliphatic chains, and the hydrogen bonding which often occurs between the polar headgroups and contributes to the lipid ordering phenomenon discussed previously. Finally, the RMSD values are consistent throughout the trajectory, and can be explained by observed and anticipated behaviours. These factors indicate that the algorithm used to perform the MD simulation was successful in maintaining an appropriate balance between restraint and mobility, throughout the length of the trajectory.

The RPDF can give an indication of the degree of solvation surrounding selected groups or atom types. The results of the RPDF analysis for B3 are shown in Figure 2.11 below.

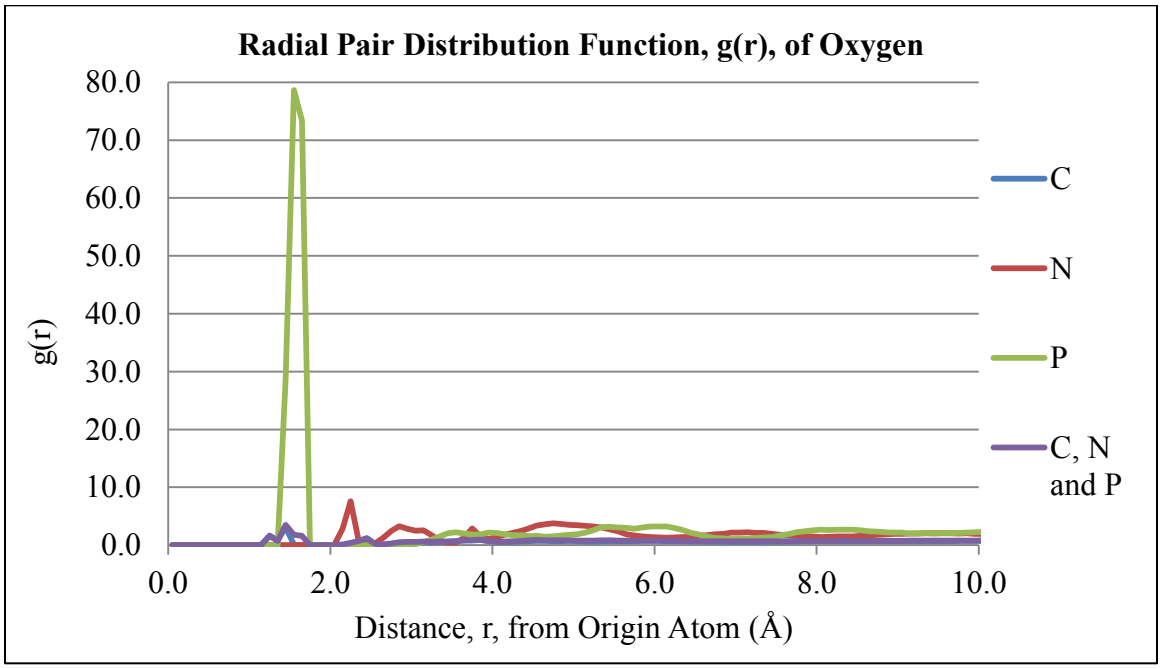

Figure 2.11: The calculated RPDF values for the B3 lipid bilayer.

The carbon, nitrogen and phosphorous represent the lipid bilayer, and the oxygen represents the functionalities on the lipid bilayer when r is less than 2.0 Å, and the presence of water molecules when r is larger, in this case between 2.0 and 10.0 Å. The RPDF for oxygen surrounding phosphorous shows a large spike at approximately 1.8 Å, which corresponds to the 4 oxygen atoms in the phosphate moiety. The size of this peak in the RPDF for phosphate does hinder analysis of the other RPDFs, and so a closer view of the smaller peaks of the RPDFs is shown in Figure 2.12 below.

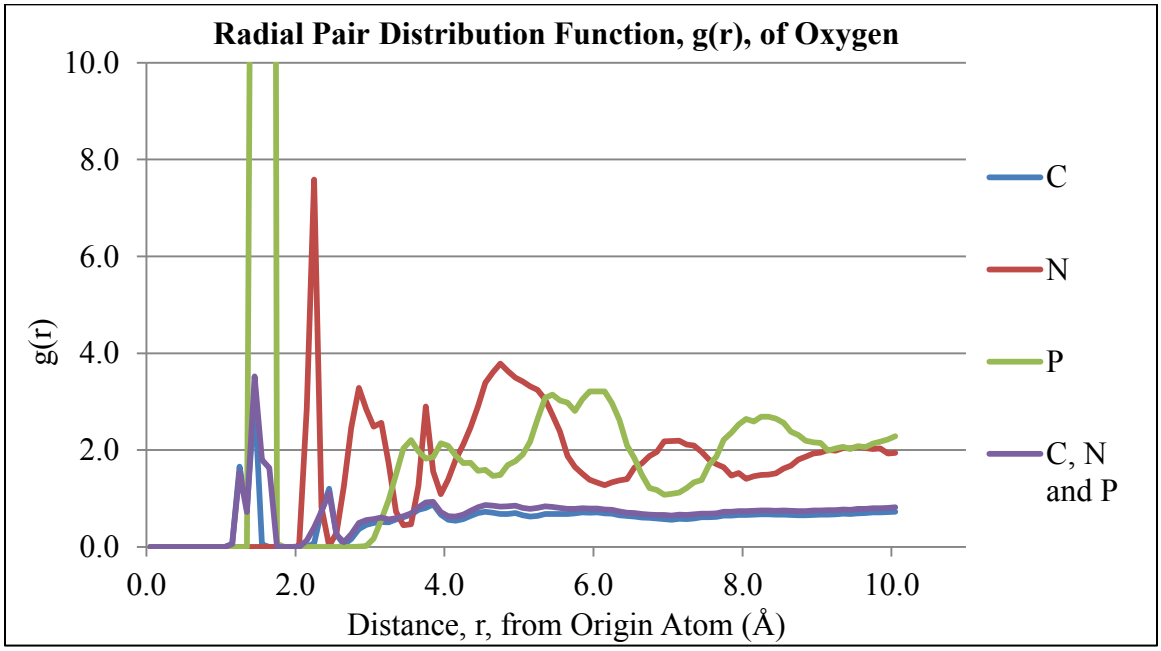

Figure 2.12: The calculated RPDF values for the B3 bilayer showing the details of the smaller peaks.

Overall, the four RPDFs calculated follow the expected trend for solvation (shown in Figure 2.9): a high first peak, followed by increasingly smaller peaks. The trends show that there is significantly less oxygen surrounding carbon atoms (which agrees with their general location deep within the lipid bilayer), than there is surrounding phosphorous and nitrogen. One aspect that stands out as unusual is that for both phosphorous and nitrogen the third solvation peak is higher than the second. This seems to indicate that the phosphate and amine groups tend to disperse the water molecules in their second solvation sphere, so that a denser ring of water forms at a slightly greater distance. The g_{max}/g_{min} was calculated to be 0.2718 for water-water interactions, and 4.4470 for solute-

water interaction. From this comparison we can see that the hydrogen bonds between the lipid bilayer and the water are stronger than those between waters in the bulk, a key trait of kosmotropes [10]. The number of hydrogen bonds in a system also demonstrates the kosmotrope/chaotrope behaviour of solutes. In Figure 2.13 below are shown the number of hydrogen bonds counted per frame, and the overall average number of hydrogen bonds containing oxygen during the trajectory produced by the MD simulation.

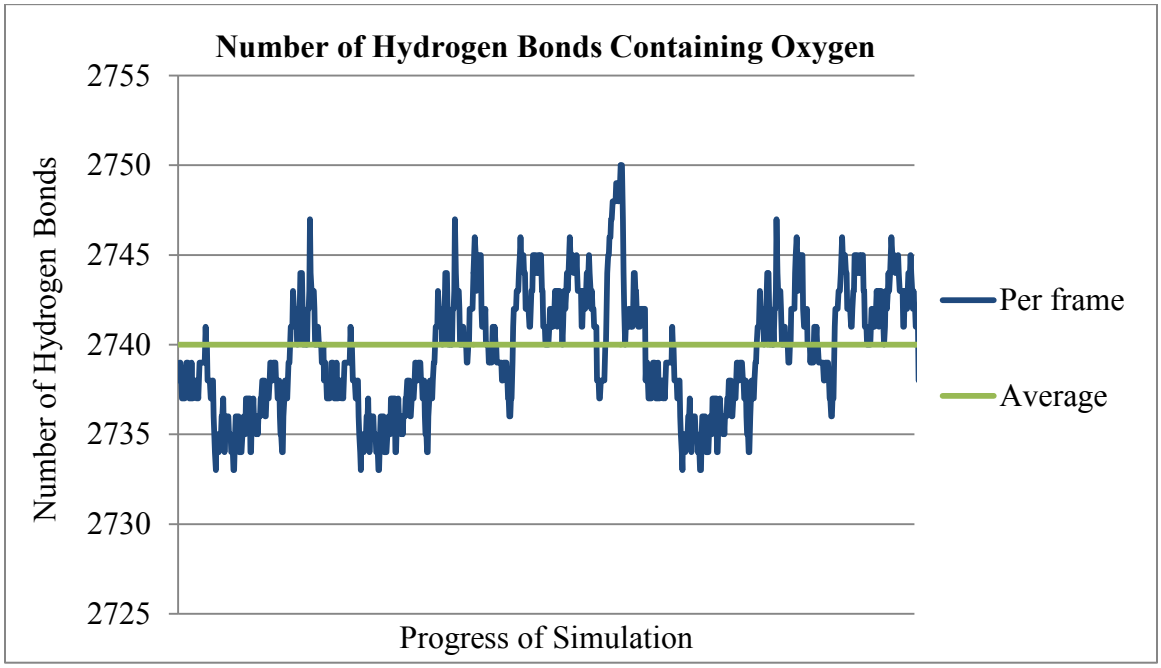

Figure 2.13: The number of hydrogen bonds observed during the MD simulation of the B3 bilayer.

The curve of the per-frame hydrogen bond count appears to be unstable, and seems to indicate that the bilayer and/or the solvation network may not have reached equilibrium before the production run started; however, the RMSD values were consistent throughout the trajectory, and dynamic association and dissociation are especially expected to occur in a solvated system. Also, the difference between the highest and lowest number of hydrogen bonds is only 177, which represents a mere 6.5% deviation from the average of 2740 hydrogen bonds. Compared to the 5392 water molecules in the system this average value is quite low, at a ratio of only 0.51 hydrogen bonds per water molecule, again indicating kosmotropic behaviour [10].

2.4.2 B4: The DOPC Bilayer

The results of the RMSD analysis of the B3 bilayer are shown in Figure 2.10 below.

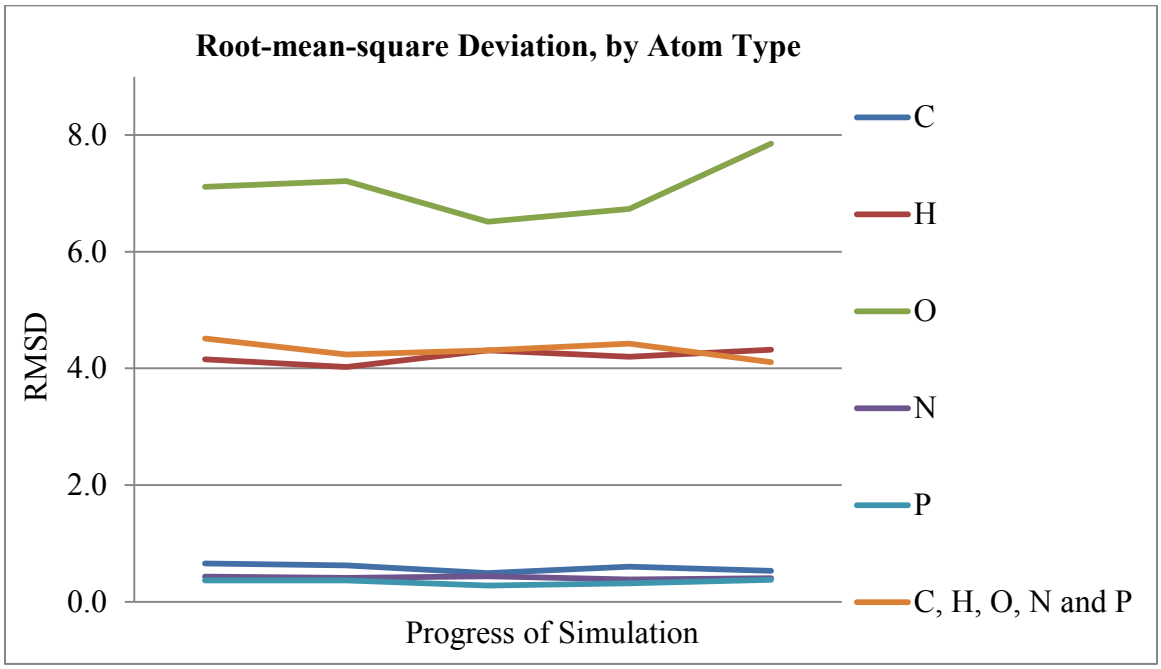

Figure 2.14: The calculated RMSD values for the B4 lipid bilayer.

The average RMSD values for each atom type are shown in Table 2.3 below.

Table 2.3: The averages of the calculated RMSD values, by atom type, for the MD simulation of the B4 bilayer.

System	C	H	O	N	P	C, H, O, N and P
B4	0.582	4.201	7.084	0.416	0.342	4.318

The RMSD B4 bilayer demonstrates similar behaviour to the B3 bilayer – the oxygen molecules are the most mobile; the carbon, nitrogen and phosphorous of the bilayer are the least mobile; and the hydrogen and average of all atoms have an average degree of mobility. The RMSD values for the B4 systems are also fairly consistent throughout the trajectory, though the oxygen does appear to increase in mobility near the end of the simulation. This may indicate that a longer simulation would have demonstrated an even higher degree of water motion.

The results of the RPDF analysis for B4 are shown in Figure 2.15 below.

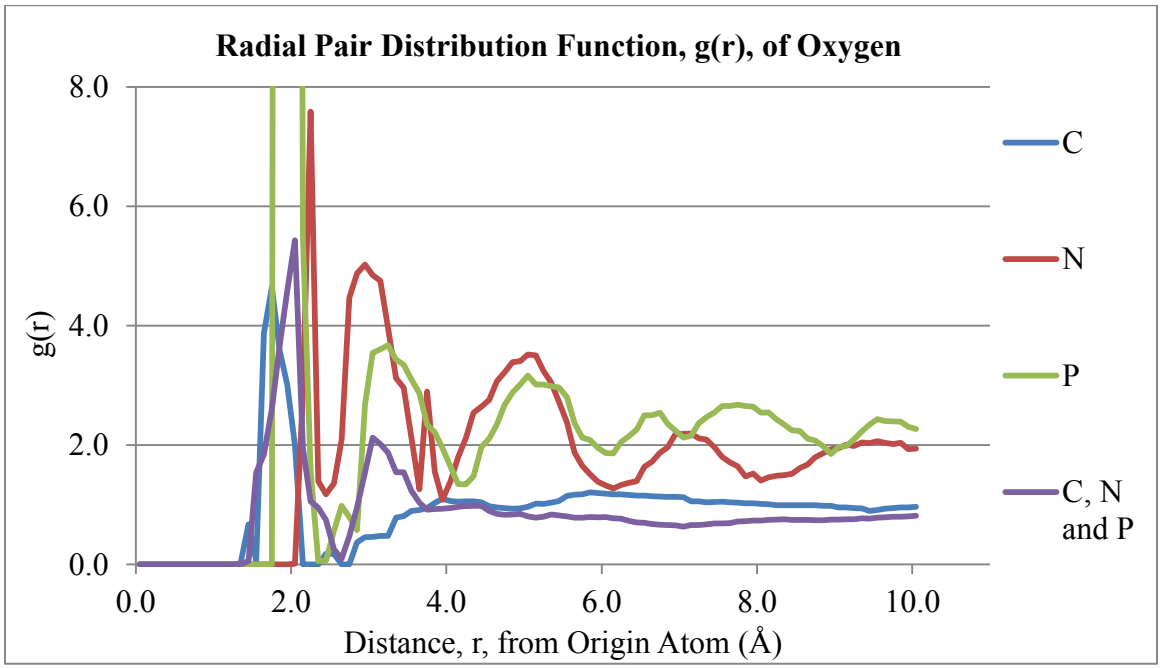

Figure 2.15: The calculated RPDF values for the B4 lipid bilayer showing the details of smaller peaks.

The RPDFs for the B4 bilayer are similar to the expected trend for liquids (a large first peak followed by decaying peaks), and show similar characteristics to the RPDFs of the B3 bilayer. The carbon has the least solvation because it is mostly hidden inside the bilayer, while the nitrogen and phosphorous have significant first and second solvation peaks. Unlike the B3 bilayer, the second solvation peak for these atoms is not larger than the third. This indicates that water may be able to come in closer to the l_d-type bilayer domains, than to the l_o-type domains.

Similar to the B3 bilayer, the g_{max}/g_{min} ratio for solute-water interaction was found to be larger than that of the water-water interactions, with values of 3.330 and 3.2108, respectively, just barely indicating a kosmotropic effect for l_d domains. These two values are quite close, and a longer simulation may have brought them even closer. This tends to indicate that l_d domains have less influence on the hydrogen bonding of their solvent waters than the l_o domains. The number of hydrogen bonds observed per frame of the B3 lipid bilayer simulation are shown in Figure 2.16 below.

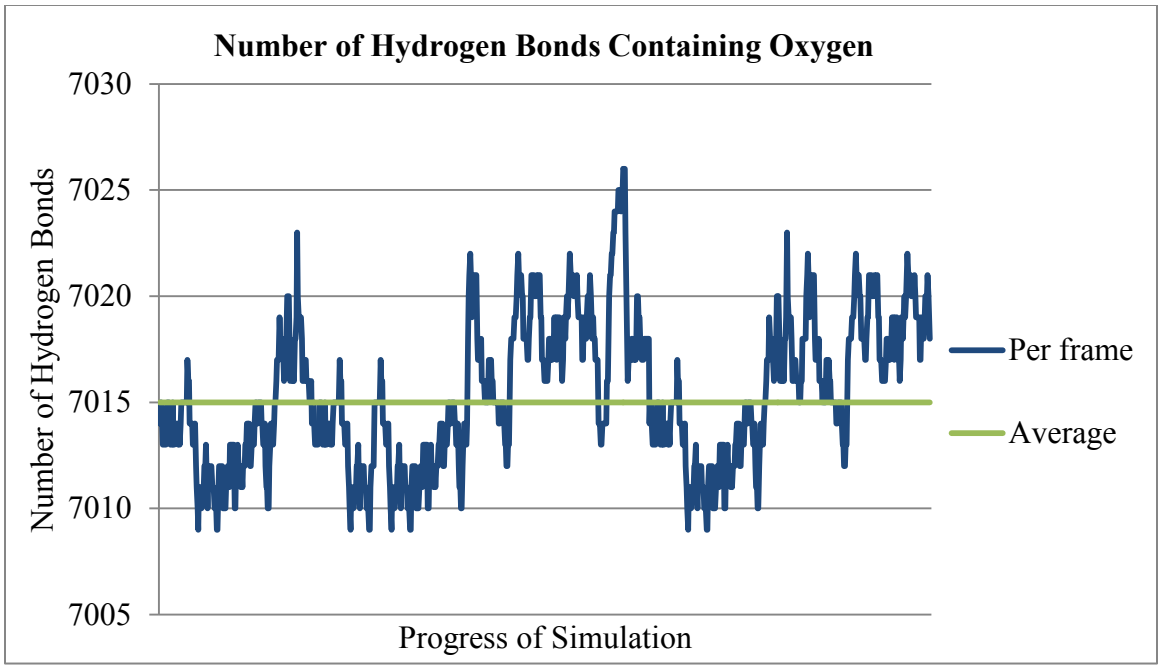

Figure 2.16: The number of hydrogen bonds observed during the MD simulation of the B4 lipid bilayer.

The average number of hydrogen bonds for the simulation of the B4 bilayer was approximately 7015. The variation between the highest and lowest number of hydrogen bonds present is only 17, or 0.24% of the average number of hydrogen bonds. Given that there were 7318 water molecules in this system, the ratio of hydrogen bonds to solvent molecules of 0.96, higher than the value for the B3 system, but still below the value of 2 for normal bulk water. Again, the l_d domain appears less kosmotropic than the l_o domain, but it is still demonstrating kosmotropic properties.

2.5 Discussion of the Results from the Lipid Bilayer Study

At the surface, the B3 and the B4 bilayer are nearly identical. Both lipid molecules have prominent phosphate and amine functional groups extending into the extracellular fluid. Any difference between their influences on the solvent seems unlikely and unreasonable, but it can be explained by the relative packing of the two bilayers. Whatever effect the polar headgroup has on the bilayer will be intensified when the lipids are packed more closely – as in the sphingomyelin-containing l_o domains – and will be reduced when the

lipids are more dispersed – as in the l_d domains made of DOPC-type molecules. In both cases, the stability of the bilayer is a key part of the influence it may have on the behaviour of the solvent. The RMSD trends for both the B3 and the B4 bilayers confirm that the bilayers are much less mobile than the solvent phase, and that the systems are fairly stable through the MD simulations.

The RPDF of the B3 lipid bilayer demonstrates a degree of dispersion of the second solvation sphere. This contributes to a slightly denser third solvation sphere, and a more distinct first solvation sphere. The ratios of g_{max}/g_{min} for the first solvation sphere of the bilayer and the waters indicate that the water-solute hydrogen bonding interactions are stronger than the interactions between water molecules. This is a key aspect of the behaviour of kosmotropes [10].

The RPDF of the B4 bilayer shows a tighter and more regular dispersion of solvent molecules surrounding the DOPC molecules. Unlike the B3 lipid bilayer, the peaks representing the probability of finding an oxygen atom (each of which stands for a water molecule) decrease evenly as the distance from the bilayer increases. Like the sphingomyelin bilayer, the ratio of g_{max}/g_{min} is slanted towards stronger solute-water interactions than water-water interactions; however, the values of g_{max}/g_{min} for solute-water interactions and g_{max}/g_{min} for water-water interactions are very close together – almost equivalent. Together, these two factors indicate that while the l_d bilayer also appears to be influencing the solvent in a kosmotropic way, its influence is not quite as strong as the l_o bilayer.

The simulations of the SM and the DOPC bilayers demonstrate fairly low numbers of hydrogen bonds in the bulk water. The SM bilayer has only 0.51 hydrogen bonds for every water molecule, while the DOPC bilayer has just 0.96. Water has, on average, approximately two hydrogen bonds per water molecule in the first solvation sphere. The average number of hydrogen bonds for several solvation spheres would likely be lower than the average for the first solvation sphere, since the number and accessibility of

hydrogen bond donors and acceptors decreases as the distance from the solute increases, but the solvation above the B3 and B4 bilayers have less than half as interconnected as bulk water. These values seem too low to be explained simply by geometry and the number of hydrogen bond donors and acceptors; instead, they are indicative of kosmotropic solutes which re-order waters nearest to them, disrupting the naturally present hydrogen bond network.

These low values could, however, be the result of using rigid water molecules during the simulations or the reaction field model for long-range electrostatics, to bring down the computational cost, or the use of the reaction field model for long-range. One way to test this possibility would be to change the electrostatics model, and/or remove the rigidity from the water molecules, and compare the frequency of hydrogen bonds.

Based on the unary bilayer models studied here, the l_o domains appear to be fairly kosmotropic near the bilayer, and to have a more dispersed and disordered bulk solvent. The l_d domains appear to be a bit more uniformly solvated but to also have a kosmotropic influence on the hydrogen bond network of the solvent. Overall, the simulations performed with these particular models indicate that there is a significant presence of ordered water near the surface of the myelin sheath. From these results it is not possible to determine if water structures contribute to axonal neurotransmission, but with evidence that they exist, the possibility also exists that they might.

CHAPTER 3 WATER AND SYNAPTIC NEUROTRANSMISSION

3.1 THE SYNAPTIC GAP

The focus of this thesis has, until now, been on the balance between two separate phases: a lipid bilayer and its solvent waters. The natural complement to lipid-water simulations of axonal neurotransmission is the exploration of solvated neurotransmitters, which are central to synaptic neurotransmission. It is likely that the motion of water plays some role in the movement of neurotransmitters through the synaptic gap, but the question remains as to what degree water influences synaptic neurotransmission. Is water as passive as is commonly believed, or can it be labelled a neuromodulator of synaptic neurotransmission? As before, the water-structure theory being investigated is the kosmotrope/chaotrope behaviour of the solutes, but in this case the systems of interest are monophasic, much smaller, and can be treated with a very different computational method. This chapter will focus on the anatomy and physiology of the synapse, on the theory and operation of CPMD, and on the simulations which were carried-out to investigate the behaviour of water in the synaptic gap.

3.1.1 Anatomy and Physiology of the Synaptic Gap

Synaptic neurotransmission is the essential process which allows thousands of neurons to network and orchestrate complicated tasks. A synapse consists of the presynaptic neuron, the postsynaptic neuron and the void between them, called the synaptic gap (see Figure 3.1) [47]. The presynaptic neuron is represented by the synaptic bulb, which is a slight bulge at the tip of an extension coming off of the neuron's axon (see Figures 2.1 and 3.1). In some cases the post synaptic neuron is represented by a cell body or even the axon of another neuron, but in most cases the presynaptic neuron synapses with the dendrite of another neuron [47]. Whichever combination of pre- and postsynaptic tissue forms the synapse, the two neurons communicate in one of two ways: electrically or chemically. Like most biological process the synapse is dominated by cause and effect; the presynaptic neuron only "communicates" with the postsynaptic neuron when an AP has

spread down the length of the axon to the synaptic bulb. In an electrical synapse, ions from the AP of one neuron flow directly into another neuron [47]. If sufficient ions flow across an electrical synapse the postsynaptic neuron may be stimulated to generate its own AP. The electrical synapse is most common in the developing embryo and in smooth and cardiac muscle tissue [47]. The vast majority of the nerves of the body are linked by chemical synapses.

A chemical synapse has a more complicated mechanism which utilizes voltage-gated calcium (Ca^{2+}) channels, synaptic vesicles, exocytosis, neurotransmitters and neurotransmitter receptors [47]. When an AP reaches the synaptic bulb the Ca^{2+} channels open, and an influx of Ca^{2+} causes synaptic vesicles to migrate towards the presynaptic membrane [47]. The neurotransmitters are released into the synaptic gap by exocytosis, and they drift through the 20 – 50 nm wide cleft until they diffuse out of the synaptic gap, are degraded by enzymes, are transported back into the presynaptic neuron, or bind to a receptor on the postsynaptic membrane [47]. The binding of the neurotransmitters to these ligand-gated receptors forces their open conformation, and allows for the influx of Na^{+} ions into the postsynaptic neuron [47]. This influx, just like those described in Chapter 2, may trigger an AP if the transmembrane potential threshold of -55 mV is reached. The anatomy and mechanisms of a chemical synapse are presented in Figure 3.1 below.

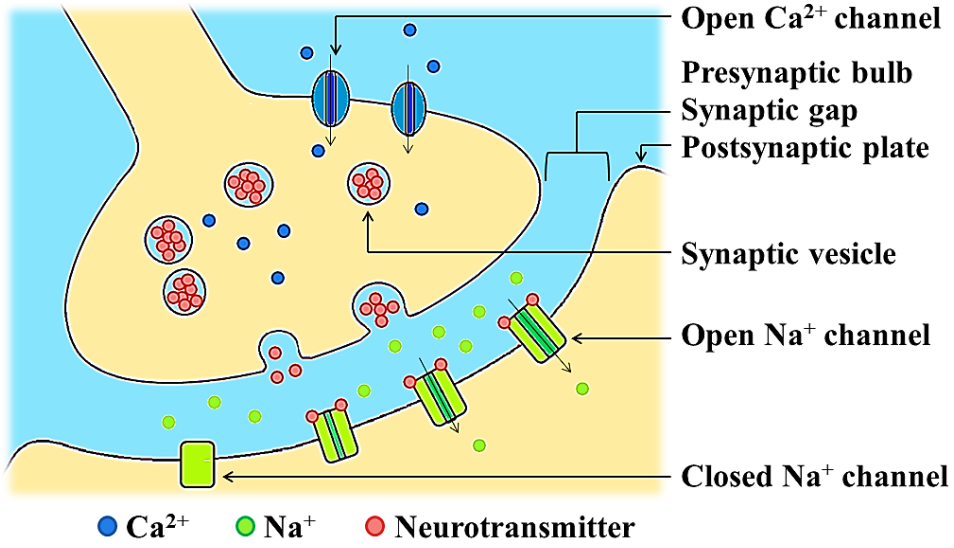

Figure 3.1: The main features of the chemical synapse [47].

The complicated action of triggering exocytosis and waiting for neurotransmitters to bind to receptors results in a 0.5 msec delay, not an insignificant amount of time when an AP travels at top speeds of 0.13 mm/msec [47]. The driving forces for moving neurotransmitters across the gap are understood to be the chemical gradients of neurotransmitters and Brownian motion. Brownian motion is a description of the random diffusion of particles through a liquid or a gas. While it is common to discuss such a process as random, in truth it is driven by thousands of interactions between solvent and solute molecules which together impart forces on solutes, driving them one way or another. The water which, for the most part, fills the synaptic gap, performs the same act of pushing and pulling on the neurotransmitters as it does the grains of pollen which lead to Brown's original investigation in 1828 [110]. Brownian motion is to a great extent a simple example of cause and effect - it turns up everywhere from tree rings to the stock market - but on a molecular level the causes are very high in number and even more difficult to observe [111]. Knowing that a more intimate relationship between water and its solutes is possible – via the kosmotrope/chaotrope effect – it is necessary to explore the relationship between this influence and the random diffusion of neurotransmitters through the synaptic gap.

Of the three possibilities for neurotransmitters – kosmotrope, chaotrope or nothing at all – it is difficult to predict which would improve the mobility of the neurotransmitter and decrease the transit time across the synaptic gap. Would a kosmotropic neurotransmitter be shuttled across the synaptic gap by the constraints it imposes on the surrounding solvent, or would the increased size of the cohesive unit slow down its diffusion? Would a chaotropic neurotransmitter travel faster because it has a freer path, or would its motion be more stagnant due to a type of insulation from interactions with the naturally flowing solvent? Investigation of the diffusion of neurotransmitters, and the possible role of water as a neuromodulator, must include various levels of solvation spheres to determine first, whether there is a kosmotrope/chaotrope effect and second, what this might mean for neurotransmission.

3.1.2 Molecules of Interest

There are approximately 100 molecules which "are either known or suspected neurotransmitters" [47]. While any of these could be studied in the manner presented here, it is good to start with some of the more well-known and more abundant neurotransmitters whose behaviour has greater consequence on biological function.

Acetylcholine (ACh) is the "best-studied" and one of the most important excitatory neurotransmitters [47]. It is degraded and removed from the synaptic gap by the enzyme acetylcholinesterase, meaning that ACh has a limited time to leave the presynaptic neuron and act upon the postsynaptic neuron. Water structures, if present, would be especially important in enabling ACh neurotransmission. Gamma aminobutyric acid (GABA) is the most important inhibitory neurotransmitter in the CNS [47]. Ionization of the GABA molecule depends on the pH, and so each of these structures should be evaluated. The four ionic states to be investigated are: neutral or GN (with the protonated carboxyl group, COOH and the neutral amino group, NH_2), anionic or GA (COO^- and NH_2), cationic or GC (COOH and NH_3^+) and zwitterionic or GZ (COO^- and NH_3^+). The structures of ACh and GABA are shown in Figure 3.2 below.

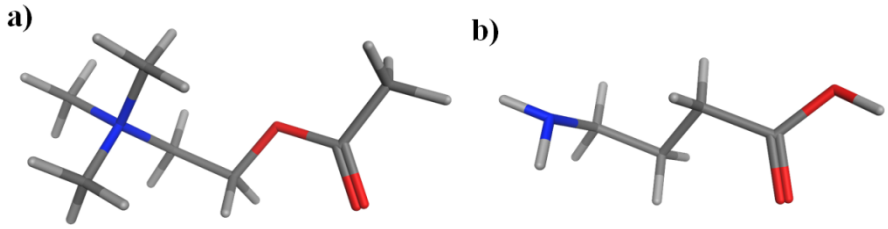

Figure 3.2: Structures of the neurotransmitters a) ACh and b) GABA.

Unlike the systems discussed in Chapter 2, solvated neurotransmitters can be examined using a higher level of theory and a more involved computational method. Small molecules such as these have routinely been explored for their stability, dynamics, and influence on neighbouring waters using the *ab initio* MD model, CPMD [112–115].

3.2 CAR-PARRINELLO MOLECULAR DYNAMICS

Modelling a system containing only one solute, and a handful of solvent waters is a simpler task than modelling fully solvated lipid bilayers. Having fewer atoms to describe essentially means one can create a more thorough description of each, and it can allow for the components of those atoms to be described more accurately. While MD focuses mainly on the motion of nuclei, in CPMD simulations the behaviour of both electrons and nuclei are described and explored simultaneously [74]. The advantage of doing this is much more and much richer information about the system of interest [116]. CPMD is a combination of classical mechanics, quantum mechanics and solid state physics, and as such "*ab initio* MD has a sufficient level of maturity to make it the method of choice for a very large class of problems" [117]. This section will focus on the theoretical basis of CPMD and the considerations involved in preparing and running a simulation.

3.2.1 From Schrödinger to Pseudopotenials

The central concept of quantum mechanics is wave-particle duality; a phenomenon that allows us to describe an electron or an entire molecule with a wavefunction. From the wavefunction, we can theoretically explore any of the observable properties of a chemical system, and even predict the behaviour of systems not yet tested or seen experimentally. We can apply the Hamiltonian operator to a wavefunction, according to the well-known Schrödinger equation, to obtain the energy of the state represented by the wavefunction. So, what do the wavefunction and the Hamiltonian look like? The Hamiltonian is a sum of each of the various classes of interactions in a given system. For example, in a system with N electrons and M nuclei the Hamiltonian is [118]:

$$\widehat{H} = -\sum_{i=1}^{N} \frac{1}{2}\nabla_i^2 - \sum_{I=1}^{M} \frac{1}{2M_I}\nabla_I^2 - \sum_{i=1}^{N}\sum_{I=1}^{M} \frac{Z_I}{r_{jI}} + \sum_{i=1}^{N-1}\sum_{j=i+1}^{N} \frac{1}{r_{ij}} + \sum_{I=1}^{M-1}\sum_{J=I+1}^{M} \frac{Z_I Z_J}{R_{IJ}} \quad \textbf{(3.1)}$$

This well-defined operator describes the electron kinetic energy, the nuclear kinetic energy, and Coulombic interactions between nuclei and electrons, between two nuclei and between two electrons [118]. In Born-Oppenheimer Molecular Dynamics the energy only depends on the kinetic energy of nuclei and electrons, which results in expensive

matrix diagonalizations at every step. In CPMD, fictitious dynamics are used to reduce the amount of time spent on calculations. The energy equation in CPMD is a sum of kinetic nuclear and electron energies, and the fictitious electron dynamics [117]:

$$E_{TOT}^{CPMD} = \sum_I \frac{1}{2} M_I \dot{\vec{R}}_I^2 + E\left[\{\dot{\psi}_i\}, \{\vec{R}_I\}\right] + \frac{1}{2}\sum_i \mu_i \langle \dot{\psi}_i | \dot{\psi}_i \rangle \qquad \textbf{(3.2)}$$

The main difference between the Born-Oppenheimer Hamiltonian and the CPMD Hamiltonian is the fictitious electron mass, μ, in the electron kinetic energy term. The fictitious electron mass is used to keep the frequency of electrons much higher than that of the nuclei, so that no net energy transfer occurs between them [74, 117]. A fictitious electron mass of between 400 Hartree atomic units (a.u.) to 800 a.u. works best for this, and for systems which contain water a value below 800 a.u. is recommended [117, 119]. Once the appropriate value is chosen and the energy equation is prepared, all one needs is a wavefunction.

Compared to the Hamiltonian, developing the wavefunction is a substantially more difficult task. For a many body system there is "no 'correct' solution" [74]. As a result there are a number of different methods used to approximate the form of the wavefunction. One of the most popular models employs Density Functional Theory (DFT), which operates on the premise that the all the properties of a system in the ground state are correlated to its density, and that the density of a chemical system can be explored through single particle wavefunctions [118, 120, 121]. Rather than creating a single expression for a many-body problem, Kohn and Sham built a wavefunction out of individual descriptions for molecular orbitals. This description, known as a basis set, is the most common way in which the wavefunction of a chemical system is modelled. In CPMD, these Kohn-Sham molecular orbitals are expanded into what are known as plane wave basis sets [117, 119].

Plane wave basis sets are popular in solid state physics, as well as in *ab initio* MD, because they are naturally suited to period systems, because they reduce the number of electrons which need to be modelled and because their force calculations are less demanding than standard basis sets [74, 118, 119]. Since plane wave basis sets are not

centered on atomic nuclei, and do move with them in time, there is no need to calculate the force this exerts on the electrons [118]. For the same reason, plane wave basis sets perform very well in the description of loosely bound and diffuse electrons [118]. Unfortunately, plane waves only behave well for smooth potentials, and cannot handle the cusps and nodes of core electrons near the nucleus [117, 122]. This is dealt with by differentiating the descriptions of valence electrons from core electrons.

The core electrons experience relativistic effects due to interaction with the nucleus, exchange-correlation with one another and with valence electrons, but they contribute very little to chemical reactivity or to a chemical model, other than increased calculation times. It is the behaviour of valence electrons that dictates the vast majority of chemical reactivity and the properties of a chemical system. To improve upon the deficient plane wave description of core electrons, and to reduce computational cost, core electrons are approximated by a pseudopotential. A pseudopotential is a function which gives the same shape as the plane wave basis set outside the core radius, r_c, but has no radial nodes inside it [74, 117, 118]. A pseudopotential has the general form:

$$V_{pp}(r,r') = \sum_{l=0}^{\infty}\sum_{m=-1}^{l} V^{l}(r)P^{lm}(\omega) \qquad \textbf{(3.3)}$$

in which r and r' are the radii between which the pseudopotential applies, and P^{lm} is the projection of angular momentum functions [119]. Just as with force field equations and basis sets, there are numerous options available and the choice depends on the system and property being studied; however every pseudopotential wavefunction, Ψ_{pseudo}, is designed so that it is continuous with the plane wave wavefunction, Ψ_v, at the core radius (see Figure 3.3) [117, 119].

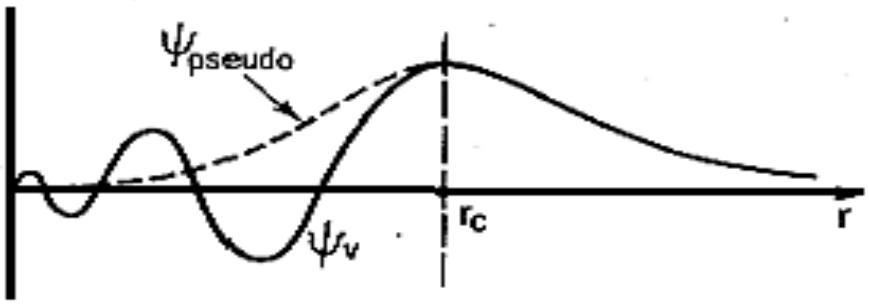

Figure 3.3: Overlap of a plane wave basis set and a pseudopotential [117].

One benefit of using pseudopotentials with plane waves is that any interactions between core electrons and valence electrons can be accounted for by using an angular momentum-dependent pseudopotential [119]. As well, the relativistic effects of core electrons can be readily incorporated into the pseudopotential [119]. The most common pseudopotential – for systems comprised of non-metals – is the improved norm-conserving functionals of Troullier and Martins [117, 123]. This pseudopotential works well for light main-group elements and it has built-in parameters to handle exchange and correlation (see Section 3.2.3) [117].

Choosing the appropriate pseudopotentials for the atoms – as there is a separate function for each atom type – also influences the required plane wave cut-off for the simulation. Because plane waves are delocalized, the user must decide at what distance, from the origin, a particle stops being described [119]. The user can therefore control how much information is included, by increasing or decreasing the space in which a particle is described. If the value for the cut-off is under-estimated there can be significant errors introduced into the calculations via the exclusion of pertinent data. On the other hand, if the cut-off is unnecessarily large the time to calculate the system is increased. The goal is to use a value in which the system converges, and the ideal cut-off varies between systems [119]. For all pseudopotentials the margin of error seems to plateau at a minimum near 50 Ry (Rydberg energy), and the typical cut-off used for the Martins-Troullier pseudopotentials is 70 Ry [117, 119].

The next step in setting-up a model for the wavefunction of a system in CPMD, is to select an approximation for the non-local part of the pseudopotential [119]. To allow for the proper description of orbital types above *s*, *p*, *d*, and *f*, the pseudopotential is split into a "local" and a "non-local" part. The local core describes the standard orbitals, while the non-local part describes areas most needed for excited and charged states [119]. The non-local pseudopotential can be described either by numerical integration (as in the Gauss-Hermit scheme) or by "projection on a local basis set" (as in the Kleinman-Bylander scheme) [117, 119]. The Gauss-Hermit scheme does not produce non-local "ghost"

states, but the Kleinman-Bylander scheme tends to be more popular because it requires minimal calculation, and shows good transferability and accuracy [119].

The plane-wave basis and the pseudopotential – with the proper cut-off and non-local descriptions – can provide the energy of the system, based on the probability density of the particles in the system. This algorithm is then subjected to the CPMD equations, which move the particles in the system through a trajectory, and create a dynamic simulation of the motion of the electrons and the nuclei.

3.2.2 Combining Classical and Quantum Mechanics

In classical MD, the overall simulation process starts with a calculation of the forces acting on each of the particles in their starting positions. Then, those forces are applied for the duration of the user-defined timestep, the atoms are moved to the new positions determined from the solution to Newton's Second Law of Motion, and the process is restarted from the beginning. In CPMD the general process is much the same, but the calculations at each step are quite different due to the inclusion of electrons, and the significant mathematical differences between force fields and basis sets. For every timestep the total energy of the system is calculated – from the density – as a sum of all kinetic energy, external local and non-local pseudopotential contributions, exchange-correlation energy and electrostatic energy [119, 124]. For classical systems the motion of nuclei (M) is given by [124]:

$$M_k \ddot{\mathbf{r}}_k = -\frac{\partial V(\mathbf{r})}{\partial \mathbf{r}_k} \tag{3.4}$$

in which is the $V(\mathbf{r})$ is the potential at any point in space, $\mathbf{r}$. The equations of motion in CPMD are comparable but motions of nuclei and electrons (μ) are calculated separately at each step in the simulation. The equations used to describe their motion are derived "from the extended Lagrangian for atoms and electrons" to give [119,124]:

$$M_k \ddot{\mathbf{R}}_k = -\frac{\partial \mathrm{E}_{KS}[\Phi,\mathbf{R}]}{\partial \mathbf{R}_k} \tag{3.5}$$

$$\mu \ddot{\Phi}_i = -\frac{\partial \mathrm{E}_{KS}[\Phi,\mathbf{R}]}{\partial \Phi_i} - \sum_j \Lambda_{ij} \Phi_j \tag{3.6}$$

in which E_{KS} is the energy of the Kohn-Sham equations, Φ is the density and **R** is the position in space.

Certain aspects of CPMD calculations match well to the classical MD method. For example CPMD also requires use of statistical ensembles to specify which macroscopic properties are constant and which are variable, and barostats and thermostats to control those which are selected to remain near a constant value. All of the same ensembles described for use in MD simulations are available to the CPMD user, though the NVT ensemble is the most popular. In this ensemble the target temperature is controlled by the Nosé-Hoover chain thermostat [119]. The Nosé-Hoover chain thermostat uses a type of iterative control in which the main thermostat is controlled by another thermostat, which itself is regulated [119]. This structure is necessary to ensure that the simulation does not revisit the original state, and restart the simulation from the beginning. Only a few layers of regulation are required to achieve this effect and it "is found to be much more efficient in imposing the desired temperature" than coupling to a heat bath [119]. If the pressure needs to be controlled, as in the isobaric-isothermal (NPT) ensemble, it is done by allowing for "fluctuations" in the size of the simulation cell, similar to in MD simulations [119]. Controlling the pressure in CPMD is mostly used to explore phase changes of solids, and will not be used here.

3.2.3 Other Considerations for the CPMD Method

A quantum mechanical model of electrons is complicated by the phenomenon of exchange. Exchange is the effect on the energy of a system when the positions of identical particles are switched, or their wavefunctions overlap. This is most commonly expressed in the Pauli Exclusion Principle, which states that no two identical particles may have the same value for all four of their quantum numbers (principal, angular momentum, magnetic and spin). In a classical model the movement of one electron will automatically affect the other, but when they are expressed in a quantum sense, as functions of electron density, this correlation does not appear to occur. The correlated motion of electrons is included in the DFT model using what are known as exchange-

correlation functionals. An exact model of exchange-correlation does not exist, and so it must be approximated [74]. One way to do this is to assume the electron distribution of the system is uniform, as in the local-spin-density approximation (LDA) [74]. Although false, this approximation does a good job of representing the exchange hole. In LDA the energy of exchange-correlation, E_{XC} is represented by the following integral [74]:

$$E_{XC}[\rho(\mathbf{r})] = \int \rho(\mathbf{r})\varepsilon_{\mathrm{XC}}\big(\rho(\mathbf{r})\big)d\mathbf{r} \quad \textbf{(3.7)}$$

The integration of the LDA depends on the density, ρ, and ε_{XC}, the exchange-correlation functional. This does provide a means to model exchange-correlation, but the underlying assumption that electron density is homogenous is known to be incorrect [74]. In truth, the electron density is quite inhomogenous and rises and falls between different points in space. The solution to this problem is to use non-local functions and to calculate "the gradient of the density at each point in space" in order to approximate the true electron density [74, 125, 126]. This scheme was first employed in the widely used BLYP (Becke-Lee-Yang-Parr) exchange-correlation functional, which uses separate descriptions for the exchange [74, 125–127]. The energy associated with the gradient-corrected exchange-correlation functional is represented by [119]:

$$E_{XC} = \int \rho(\mathbf{r})\varepsilon_{\mathrm{XC}}(n, \nabla n)d\mathbf{r} \quad \textbf{(3.8)}$$

in which n is the electron density. Gradient-corrected functionals are especially important for describing hydrogen bonding, and water.

Like in classical MD simulations, CPMD simulations of solvated systems usually involve the use of PBC. PBC are naturally defined in CPMD, and are employed simply by specifying the cell dimensions in the job file; however, when a simulation of an isolated system is preferred, the CPMD calculation is still done with a periodic cell [119]. This has the potential to introduce significant errors into the calculations, as molecules in the main simulation cell will invariably interact with those in neighbouring cells. The remedy for this is to apply a Poisson Solver to restrict long-range forces to within the simulation cell [119]. The standard Poisson Solver is the Hockney method, which is closely related to the electron density and the electrostatic potential [119]. The Hockney method provides an exact solution to Poisson's equation (by requiring an electron density of zero

at the edge of the simulation cell) and it is faster and more accurate than other methods [119]. There can be many other parameters to consider when running CPMD calculations, depending on what you are trying to simulate, but these considerations will not be discussed as they were not factors in this particular research.

3.3 Building and Simulating Solvated Neurotransmitter Systems

CPMD is a more demanding method of computational chemistry than MD, and as such it requires a higher level of computing power. The CPMD simulations in this study were completed using the ACEnet (Atlantic Computational Excellence Network) high performance computing resources [128]. Every calculation requires a submit script file and a job file (see Section 3.3.3), but the first step is to establish the atomic coordinates.

3.3.1 Preparing Chemical Systems for CPMD Simulations

The initial structure for a CPMD simulation is sometimes obtained from experiment, through a databank, but it can also be produced with any of the available molecular drawing programs; the starting molecules were created using GaussView 5.0.8 [129]. Regardless of how the initial coordinates are produced, it is best to pre-optimize the structure with an MM force field [117]. The starting ACh and GABA molecules were minimized in MOE 2010.10, using the MMFF94x force field, to obtain an optimal starting conformation. These energy-minimized molecules were then solvated with between one and nine layers of water, and were re-minimized. In total, 55 systems were created; one of each of the neurotransmitters was left in gas phase (for a total of five), one of each of the neurotransmitters was solvated for a simulation in a periodic cell, and 45 solvated systems were generated for non-periodic simulations. (A more complete description of the systems can be found in Section 3.3.4.) After minimization a short MD simulation was run on all 55 systems to remove hot spots, and the output geometry was minimized a third time. The atomic coordinates for each system were taken from this final minimization.

3.3.2 Building and Submitting the Job File

The CPMD job file is a simple list containing the atomic coordinates, and the chosen methods and parameters for the intended simulation. The file is composed of various categorical sections, each containing the pertinent keywords on one line, followed by the user-defined value on the next line. For example, to specify the pseudopotential cut-off the keyword is "CUTOFF" and the desired numerical value of the cut-off, in Ry, is written on the next line of the file. The main categories of the job file are the CPMD section for general control of the simulation, the DFT section for control of the exchange and correlation parameters, the SYSTEM section in which the cell size and related cut-offs and parameters are established, and the ATOMS section for the atomic coordinates and the desired pseudopotential files for each atom type [119].

The details of the parameters not already explained will be omitted from this discussion, with the exception of the parameters used to set-up periodic and isolated system. A periodic system is established with the keyword SYMMETRY and by using either a numerical identifier or a description, such as "SIMPLE CUBIC", on the following line [119]. An isolated system can be specified either with a symmetry value of zero or by writing "ISOLATED MOLECULE" [119]. After the periodicity the file must designate the size of the cell. For an isolated system the simulation cell size is determined by which Poisson Solver is used. For the Hockney method the system must be centered in the middle of the simulation cell, and the cell must be at least 3 Å away from outermost atom on all four sides [119]. This allows for the Hockney solver to properly taper the charge density to zero at the borders of the simulation cell. For all systems the cell size was found by finding the greatest distance between two atoms in a system, and adding 6 Å to find the minimum allowable dimensions. All systems, periodic and isolated, used a box-shaped cell with 90° angles and sides of equal length.

Every CPMD-simulated system requires a minimum of three CPMD jobs. The first job establishes an optimized wavefunction from the starting atomic coordinates, the second job uses the wavefunction in a short CPMD simulation – with no thermostat – to estimate

an appropriate value for the fictitious electron mass (called the electron kinetic energy, or EKINC), and the third job is the full CPMD simulation. An example of the wavefunction, EKINC and full CPMD job files can be found in Appendices A, B, and C, respectively. The job files were transferred to the ACEnet cluster using WinSCP 4.3.3 and the cluster was accessed with PuTTY 0.60 [128, 130, 131]. The jobs were submitted to the ACEnet queue using a standard submission script, which states the computing requirements of the job, and the identifying and organizational information for input and output data; see Appendix D for an example of a job submission script.

3.3.3 The Solvated Neurotransmitter Systems

The two neurotransmitters, ACh and GABA, were simulated in gas and solution phase, and with both isolated and periodic systems. Comparing the gas phase to the solution phase allows for some discussion as to the energy differences in mobility between solvated and unsolvated molecules, and the relative stability of the solvation. Simulating the solvated neurotransmitters in a periodic system is representative of a bulk solution situation, and is the general approach to solvated systems. On the other hand, simulating a series of isolated, solvated systems may be useful for studying the behaviour of the solvation sphere, and not the bulk behaviour. The GABA molecule was studied in its four ionic states (neutral, anionic, cationic and zwitterionic), to establish a more complete picture of the kosmotrope/chaotrope behaviour of the molecule. In total there were 11 ACh systems, and 44 GABA systems (11 for each of the four ionic states). The systems which were successfully simulated are summarized in Table 3.1 below.

Table 3.1: The neurotransmitter systems created for CPMD simulations.

Solute	H_2O in isolated systems	H_2O in periodic system
ACh	0, 4, 9, 29, 55	33
GN	0, 4, 10, 25	32
GA	0, 3, 7, 19, 37	34
GC	0, 2, 10, 28, 44	35
GZ	0, 2, 11, 20, 44	31

Once the systems failed to run due to memory limitations the larger systems were not simulated. For future reference all systems will be referred to by the neurotransmitter and number of waters. For example, "GA19" is the anionic form of GABA, with 19 water molecules. Of the 165 jobs (3 jobs for each of the 55 systems) which were set-up to be performed, only 105 were small enough to be done on the ACEnet cluster [128]. Of these 105 jobs, 96 were successfully completed. Numerous equipment outages and long wait times in the job submission queue on the cluster prevented a few of the smaller jobs from being completed, but the completed jobs were transferred back from the cluster using WinSCP 4.3.3 [130].

3.4 Results from the Solvated Neurotransmitter Study

Of the eleven systems created for the ACh molecule, four of these were fully simulated via the CPMD method. The systems with only one or two layers of solvation – the A4 and A9 systems – were completed, but the trajectory files used for analysis were not printed due to problems with the computing cluster. The systems with greater than four layers of solvation – such as the A78 system – had too many waters to be computationally affordable with the current resources, and were not completed. The unsolvated ACh molecule, A0, and the solvated A33 system with PBC were successfully completed.

Of the 44 systems created for the GABA molecule, in its various ionic states, 16 of these were fully simulated via the CPMD method. Like the ACh systems, the GABA systems with less than two layers of solvation did not produce meaningful results and the systems with greater than four layers of solvation (in this case those with greater than 44 waters) were not able to be completed due their high memory demands. The unsolvated GN0, GA0, GC0 and GZ0 systems were completed, as well as the solvated GN25, GN43, GA19, GA37, GC10, GC28, GC44, GZ20 and GZ44 isolated systems and the solvated GN32, GA34, GC35 and GZ31 systems with PBC.

Analysis of the solvated neurotransmitter systems was done using the VMD 1.9 software, and consists of the study of the RMSD, RPDF, g_{max}/g_{min} ratios of the first solvation peak, and the number of hydrogen bonds per frame of the CPMD simulation trajectory [108]. For the most part, the same protocols for analysis were used for the neurotransmitters as were used for the lipid bilayer systems (see Section 2.4 for a discussion of the theory and parameters used for set-up and data analysis). The main exception is that, as there is no phosphorous in the neurotransmitters being studied, the RPDF was only calculated for carbon and nitrogen. As with the lipid bilayers, the g_{max}/g_{min} ratio was calculated using the maximum of the second peak for the g_{max} (because the first peak in these systems corresponds to the carboxyl group) and the smallest value at the base of this peak for the g_{min}. The results of the successful simulations will be presented here, followed by a discussion of these results and their implications.

3.4.1 The Root-mean-square Deviation Analyses of the Neurotransmitter Simulations

Due to the number of Ach and GABA systems studied the individual graphs of the RMSD values will not be shown. The average values for RMSD of each atom type in the A33 system are shown in Table 3.2 below.

Table 3.2: The averages of the calculated RMSD values, by atom type for the CPMD simulations of the ACh systems.

System	C	H	O	N	C, H, O and N
A0	0.280	0.494	0.283	0.162	0.423
A33	*0.413*	*0.934*	*0.655*	*0.319*	*0.841*

From the values in Table 3.2 it appears that the isolated ACh in the gas phase is slightly less mobile than the solvated molecule with periodic boundary conditions (italicized). This makes sense given that *in vacuo* there are fewer molecules moving. For all systems the oxygen and the hydrogen are the most mobile, and the carbon and nitrogen are more stable. In the case of hydrogen, the increased mobility in the gas phase simulation comes from being at the end of the molecule, where there is a greater degree of freedom. For the solvated system the observed motion of hydrogen is a combination of location on the

solute, and its presence in the water molecules. In the case of oxygen, the higher mobility comes mainly from its presence in the water molecules. The carbon is slightly more mobile than the nitrogen because it is also present at the ends of the molecule where motion is less restrained. The only slightly odd value in this comparison is that – contrary to all the other atoms types – the RMSD for nitrogen in the A33 system is lower for the gas phase system than for the solvated system. While it is not a great deal lower (only 21% lower than the solvated system), it does disagree with the trends observed for the other atoms. This reduced mobility may be because without water present there are fewer forces interacting with the nitrogen group and displacing the molecule. The RMSD values for the GABA systems are shown in Table 3.3 below.

Table 3.3: The averages of the calculated RMSD values, by atom type, for the CPMD simulations of the GABA systems.

System	C	H	O	N	C, H, O and N
GN0	0.294	0.951	0.353	0.457	0.751
GN25	0.508	0.813	0.598	0.534	0.743
GN32	*0.404*	*0.918*	*0.689*	*0.629*	*0.842*
GN43	0.499	0.787	0.616	0.612	0.732
GA0	0.260	0.655	0.499	0.303	0.539
GA19	0.434	0.991	0.842	0.581	0.926
GA34	*0.236*	*0.833*	*0.625*	*0.418*	*0.762*
GA37	0.478	0.857	0.757	0.339	0.815
GC0	0.258	0.520	0.469	0.427	0.463
GC28	0.562	0.917	0.746	0.539	0.856
GC35	*0.327*	*0.873*	*0.627*	*0.430*	*0.793*
GC44	0.598	0.921	0.603	0.539	0.801
GZ0	0.589	1.018	0.855	0.251	0.881
GZ20	0.433	0.919	0.728	0.411	0.845
GZ31	*0.395*	*0.950*	*0.719*	*0.508*	*0.870*
GZ44	0.210	0.627	0.562	0.265	0.598

The trends of the average RMSD values for the GABA systems are similar to the trends observed for the ACh systems. In general, the hydrogen and the oxygen tend to be more mobile than the carbon and the nitrogen. Also like the ACh systems, RMSD values tend to be higher for the solvated systems than for the unsolvated systems. For the neutral, anionic and cationic systems, the carbon and the nitrogen are more mobile when solvated than when unsolvated. It is important to note that the periodic systems (indicated in Table 3.3 with italicized letters) behave similarly to the isolated systems. This provides some indication that the two methods perform equally well, and produce similar results.

3.4.2 The Radial Pair Distribution Analyses of the Solvated Neurotransmitter Systems

The RPDF is a graph which can provide unique insights into the behaviour of water in a solvated system. As such, the RPDF results of all of the solvated systems will be shown on separate graphs. The calculated RPDF values for the A33 system are shown in Figure 3.4 below.

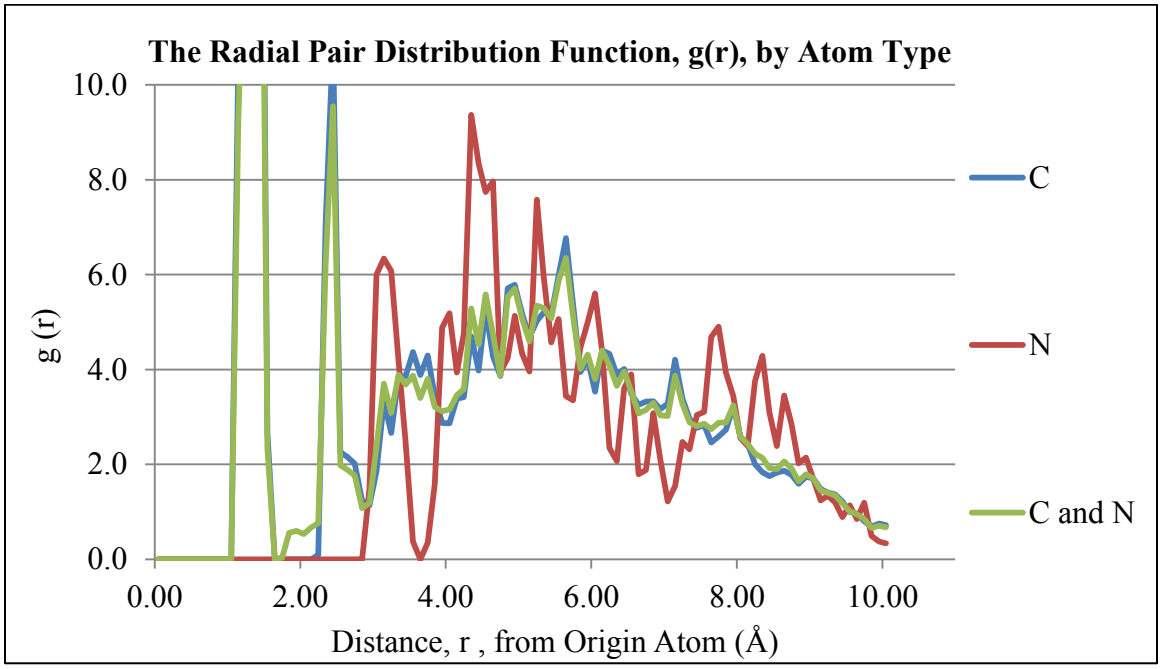

Figure 3.4: The calculated RPDF values for the A33 system.

The graph of the RPDF values indicates that the amine moiety has substantially different solvation than the carbon. This is evident because the trend for solvation surrounding the

carbon and nitrogen together is much more like the trend for carbon alone, than for the trend of nitrogen solvation. The RPDF produced here is a normalized curve for all of a certain atom type in a system, the carbon dominates the shape of the curve for carbon and nitrogen combined because there is more carbon than nitrogen in the system. Also, the nitrogen is surrounded by methyl groups and is less accessible to the solvent waters, compared to the oxygen in the ester moiety. The irregularity of the peaks in the graph of the RPDF also suggests that the solvation was not cleanly organized into solvation spheres, that it was more disorganized. This may indicate that the simulation needed to run for longer to generate a smoother probability of oxygen distribution, or it may indicate that the outer solvation spheres are much less ordered than the first solvation sphere, indicative of a kosmotropic solute.

The systems containing a neutral GABA solute (GN25, GN32 and GN47) show the same trend as the A33 system. The trends of their RPDFs are shown in Figures 3.5, 3.6, and 3.7 (respectively) below.

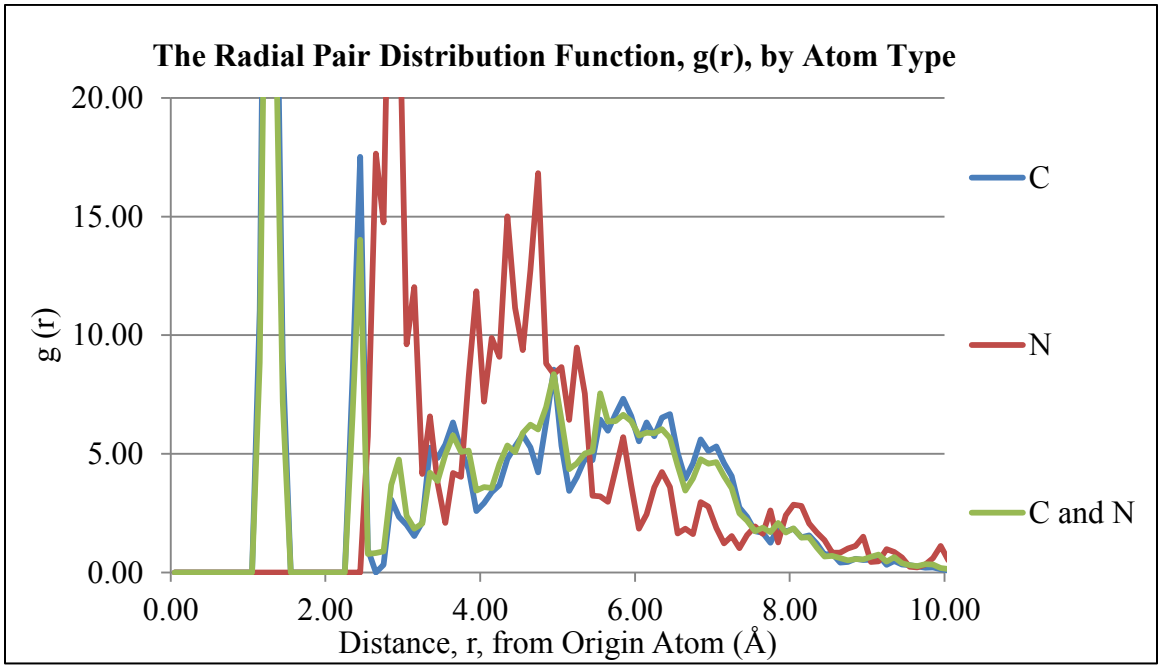

Figure 3.5: The calculated RPDF values for the GN25 system.

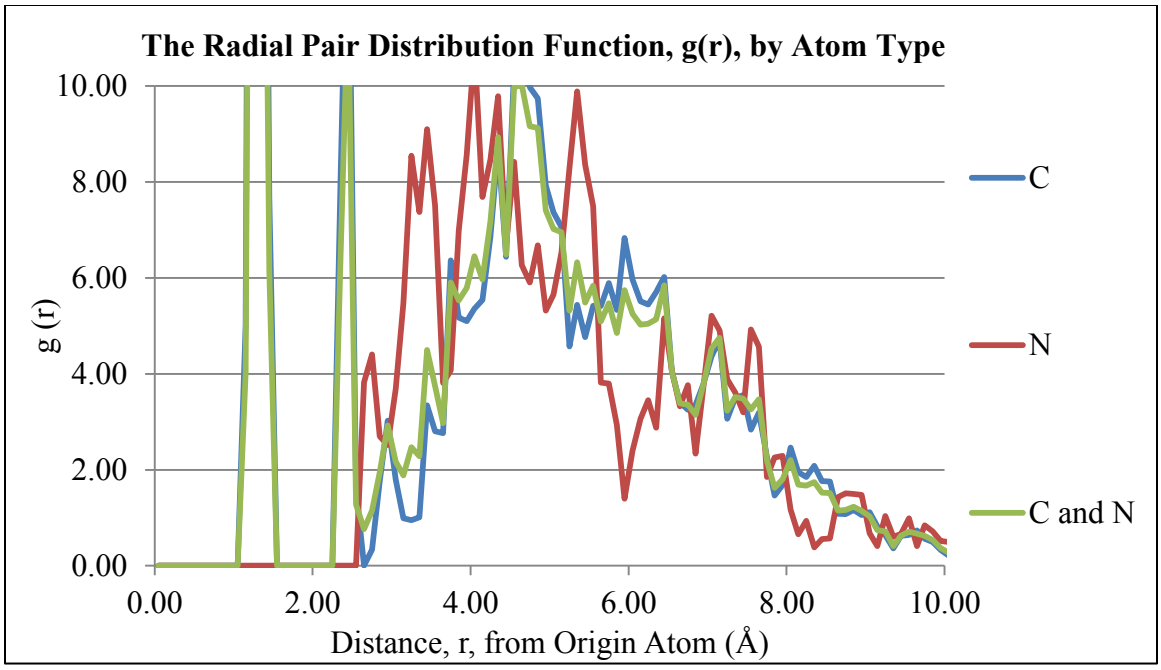

Figure 3.6: The calculated RPDF values for the GN32 system.

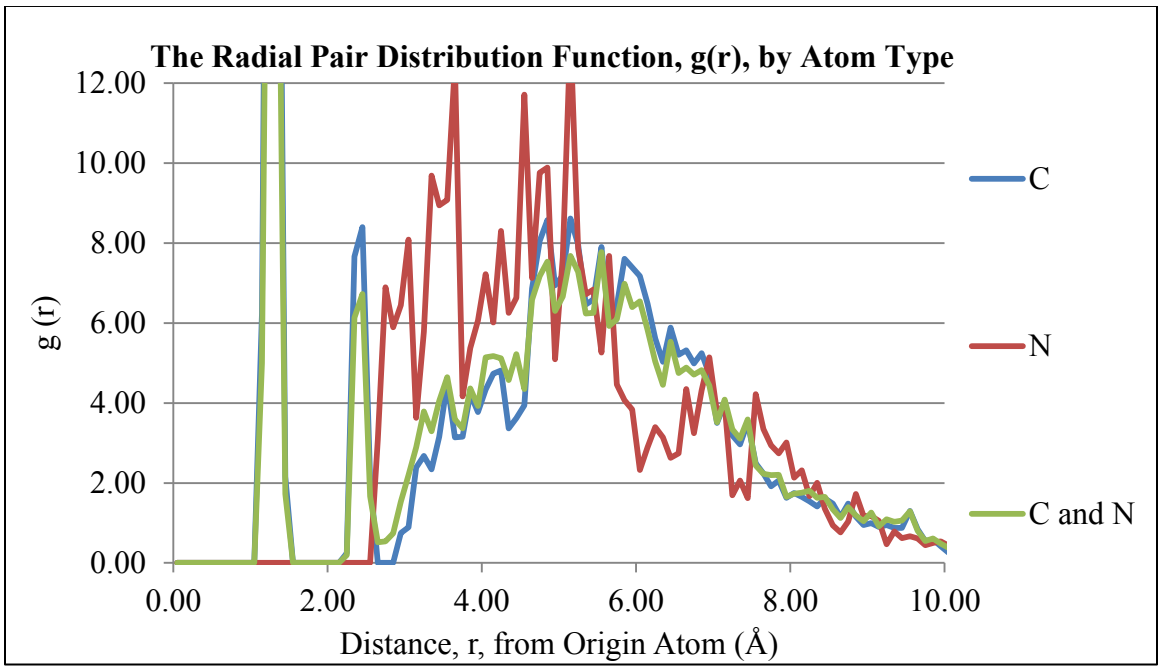

Figure 3.7: The calculated RPDF values for the GN43 system.

The neutral GABA systems indicate that the first solvation peak for carbon occurs at approximately 2.5 Å, and that beyond this there is an irregular solvation sphere spread out between 3.0 Å and 10.00 Å. The first solvation peak around nitrogen does not occur until around 2.8 Å, nearing the outside of the normal range for hydrogen bonding. While this does not mean hydrogen bonding to the lone pairs on nitrogen did not occur, it does mean that the solvent was less attracted to the N-terminus of the molecule than the C-terminus in the first solvation sphere. The three trends for RPDF surrounding nitrogen also show a spread out solvation sphere following the first peak area, also indicating a level of disorder in the outer solvent. The second sphere for nitrogen also tends to be closer to the N-terminus than to the C-terminus. The combination of these facts seems to indicate that the C-terminus interacts well with water, but that it slightly disperses the outer solvation spheres, and that while the N-terminus is slightly less interactive with its inner solvation sphere, its outer solvation spheres remain closer than to the C-terminus. In both cases the relative disorder of the outer solvation spheres, compared to the distinct inner solvation sphere, indicates that neutral GABA may be kosmotropic. The RPDF trends for the GA19, GA34 and GA37 systems are in Figures 3.8, 3.9 and 3.10 (respectively) below.

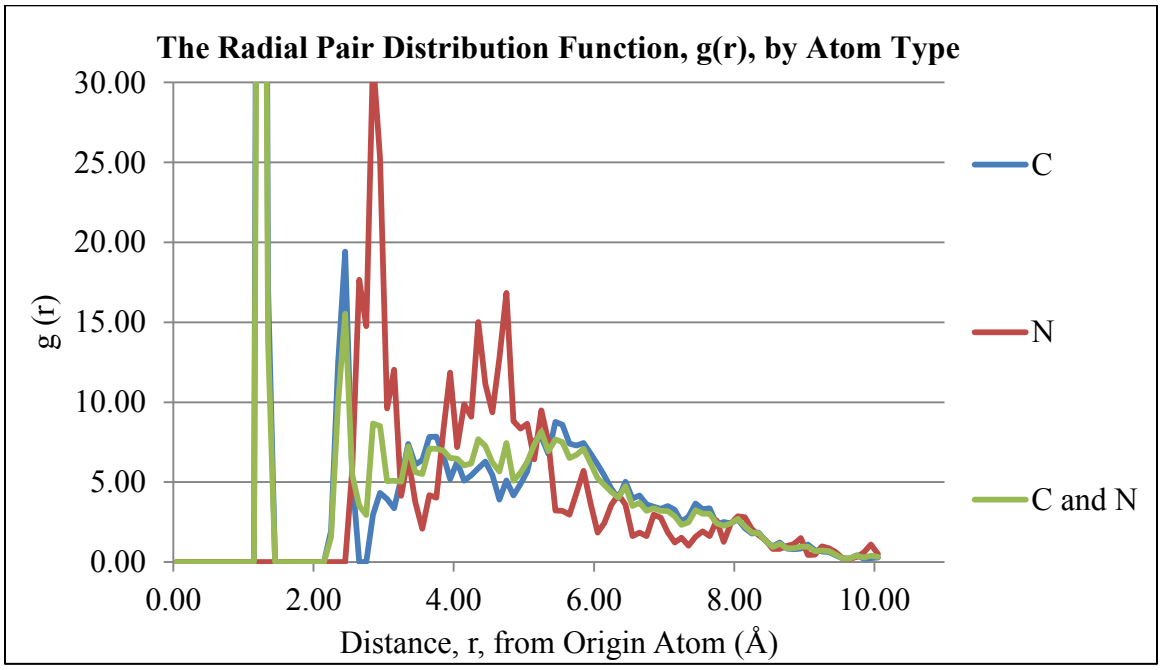

Figure 3.8: The calculated RPDF values for the GA19 system.

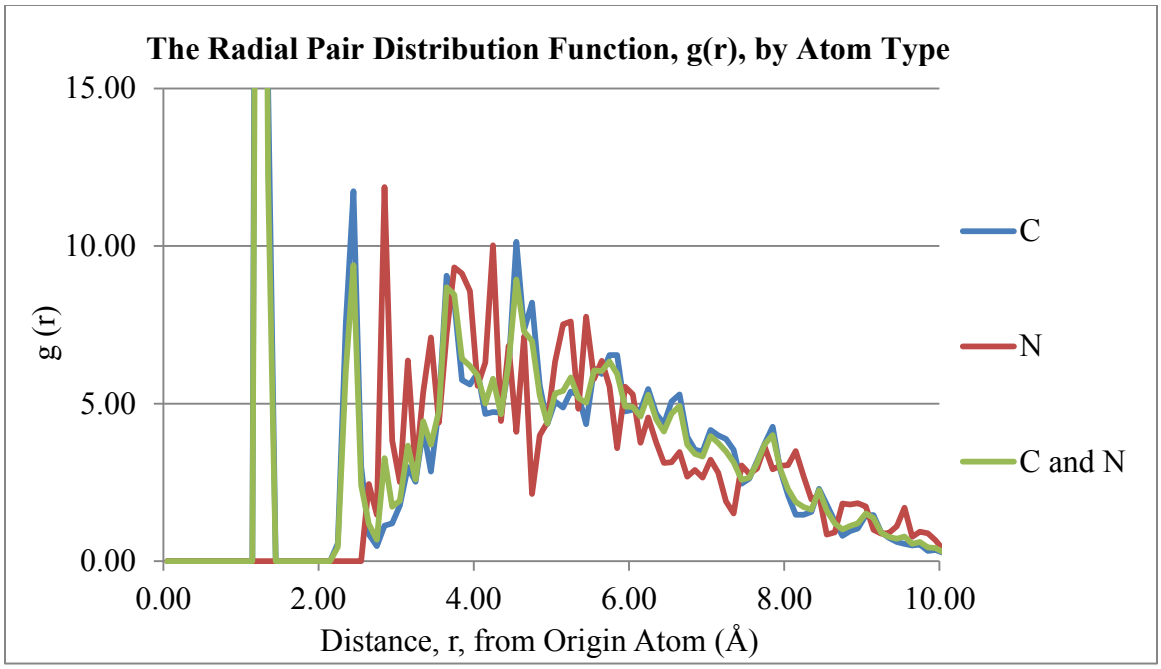

Figure 3.9: The calculated RPDF values for the GA34 system.

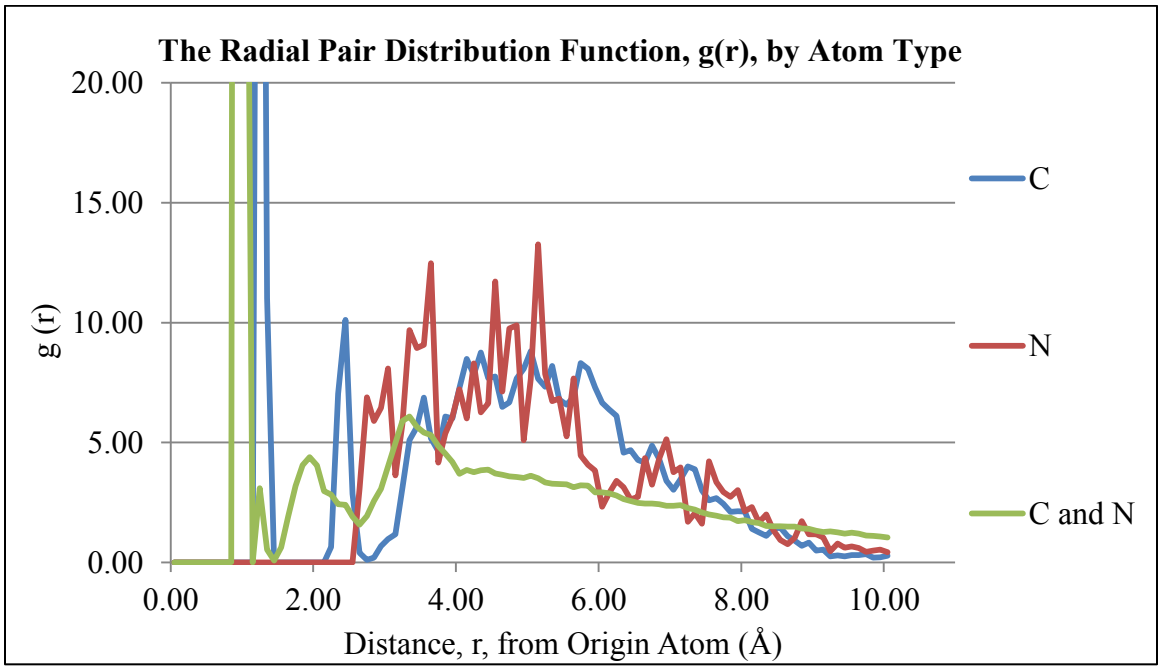

Figure 3.10: The calculated RPDF values for the GA37 system.

The RPDF for the GA19, GA34 and GA37 systems present many traits common to the graphs already discussed. The first large peak is for the carboxyl group, the following

peaks represent the various layers of solvation, and the jagged curves indicate irregular solvation and relative disorder of the outer water molecules. Like the RPDF curves for the neutral GABA systems, the nitrogen curves for GA19, GA34 and GA37 have broader second solvation sphere which appears fairly irregular and disordered. Some features, however, are unique to these systems. The RPDFs for GA19, GA34 and GA37 show slightly more regular peak decay in the curve for carbon indicating that the solvation of the anionic GABA molecule is not as disruptive as the neutral molecule. In the RPDF for GA37, the normalized trend for carbon and nitrogen together shows two distinct and smooth solvation spheres which do not appear in either of the curves for the individual atom types. This is the first system in which the carbon solvation does not dominate the normalized RPDF of the complete molecule, and in which the solvation effects of the two atom types combine to create an entirely different trend from their own. It appears that under basic conditions the N-terminus and the C-terminus have a more balanced effect on their solvation spheres, than when the acidic proton is still attached to the carboxyl group.

The RPDF trends for the GC28, GC35 and GC44 systems are in Figures 3.11, 3.12, and 3.13 (respectively) below.

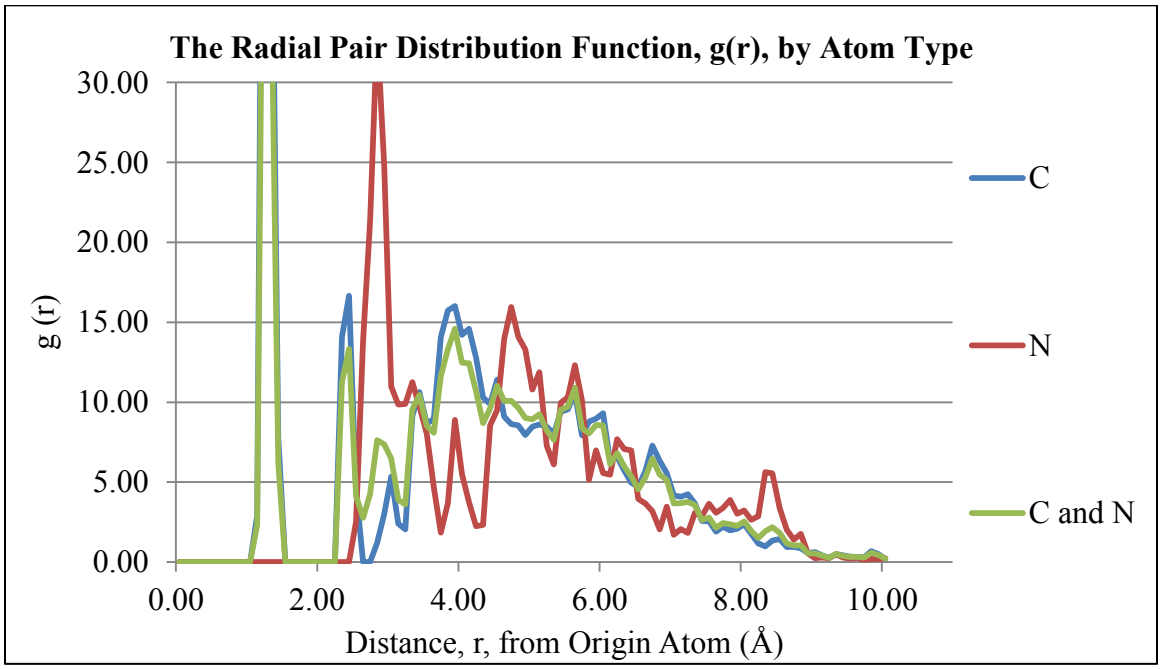

Figure 3.11: The calculated RPDF values for the GC28 system.

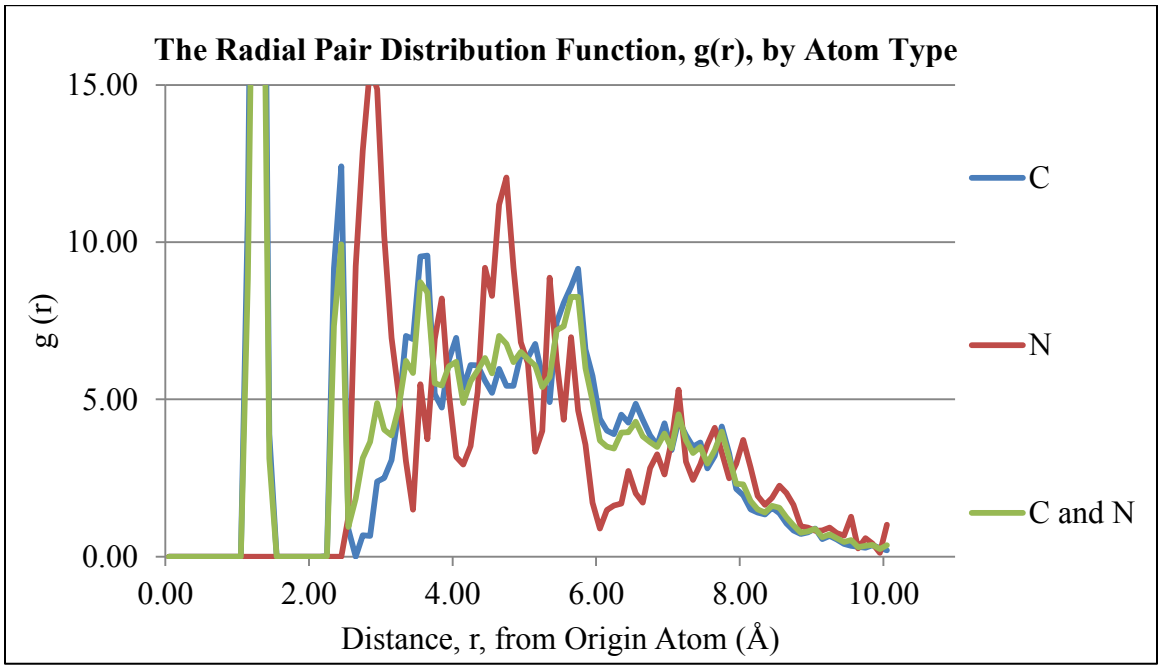

Figure 3.12: The calculated RPDF values for the GC35 system.

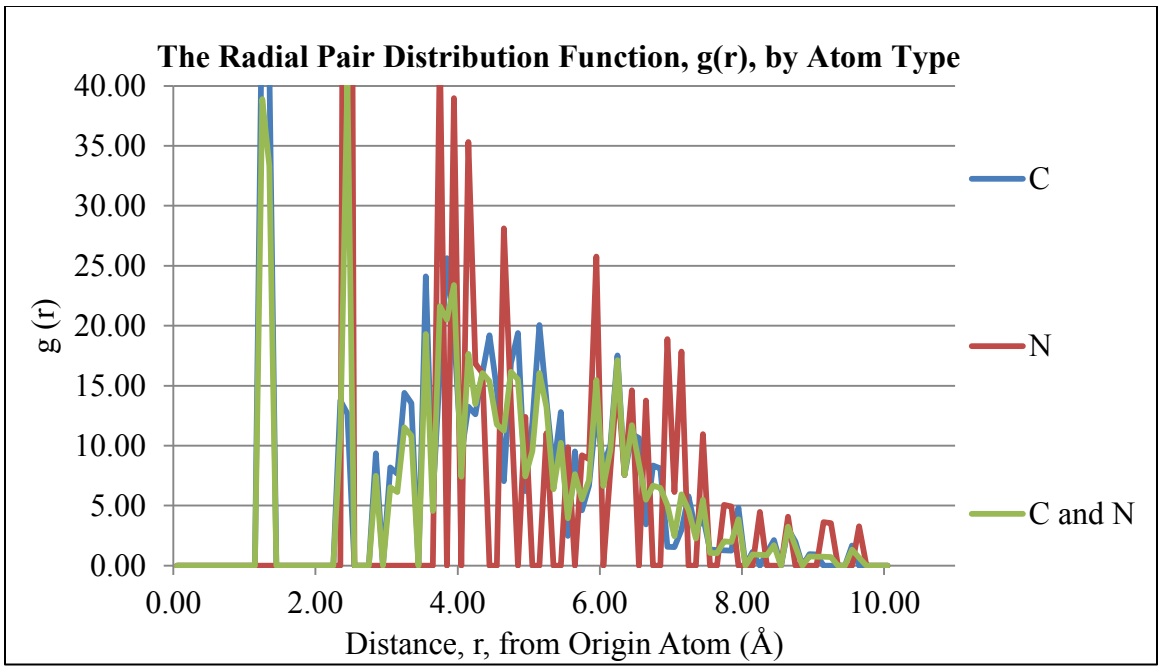

Figure 3.13: The calculated RPDF values for the GC44 system.

The RPDF for the GC systems trends have the same general shape as the anionic systems discussed previously: sharp peaks for the carboxyl groups, a distinct first solvation peak for carbon and nitrogen, followed by broader (and jagged) solvation spheres for both carbon and nitrogen, and the water surrounding the nitrogen is slightly further away than the carbon solvation. Unlike the GA systems, the solvation of carbon on GC dominates the combined RPDF for nitrogen and carbon together. This supports the idea that a protonated carboxyl group has a larger effect on solvation than a charged carboxyl group. The GC44 system, while it is more jagged than the GC28 and GC35 RPDF, does show some signs of the expected peak decay. Despite this, the overall shape of the RPDF and the stark contrast between the first solvation sphere and the outer solvation spheres, indicate that the cationic solute – the most likely form which exists in the synaptic gap, given that the pH in that region is known to be acidic – likely exerts a kosmotropic effect on the solvent [36].

The last class of GABA systems are those which contain the zwitterionic form of the molecule; the RPDF trends for the GZ20, GZ31 and GZ44 are in Figures 3.14, 3.15 and 3.16 (respectively) below.

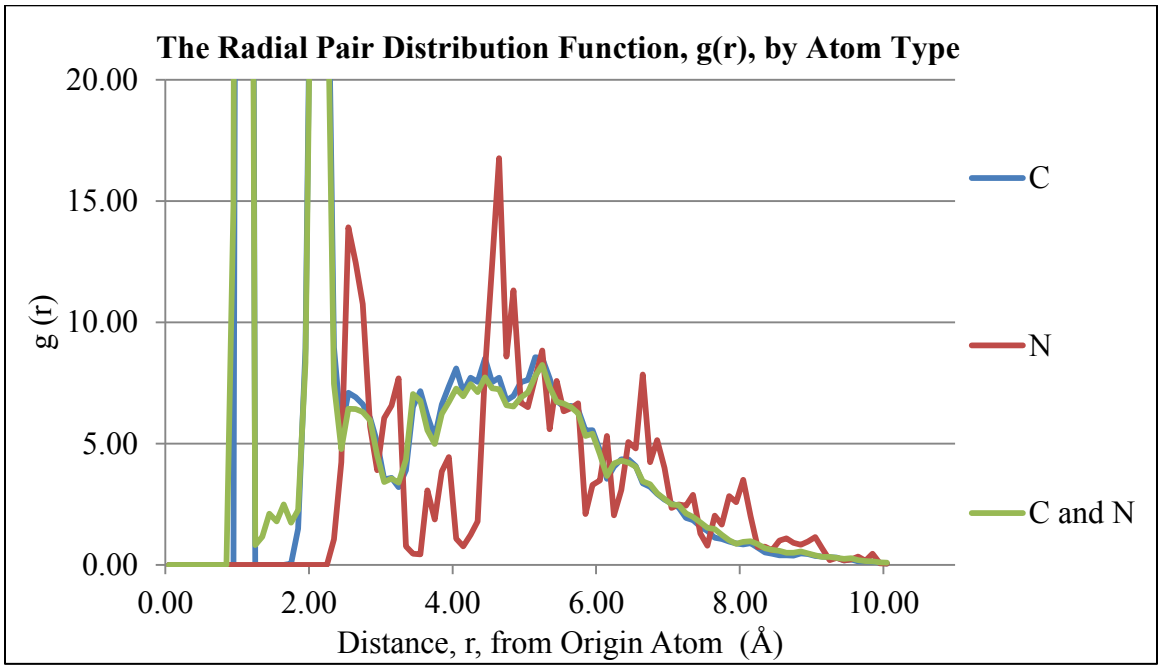

Figure 3.14: The calculated RPDF values for the GZ20 system.

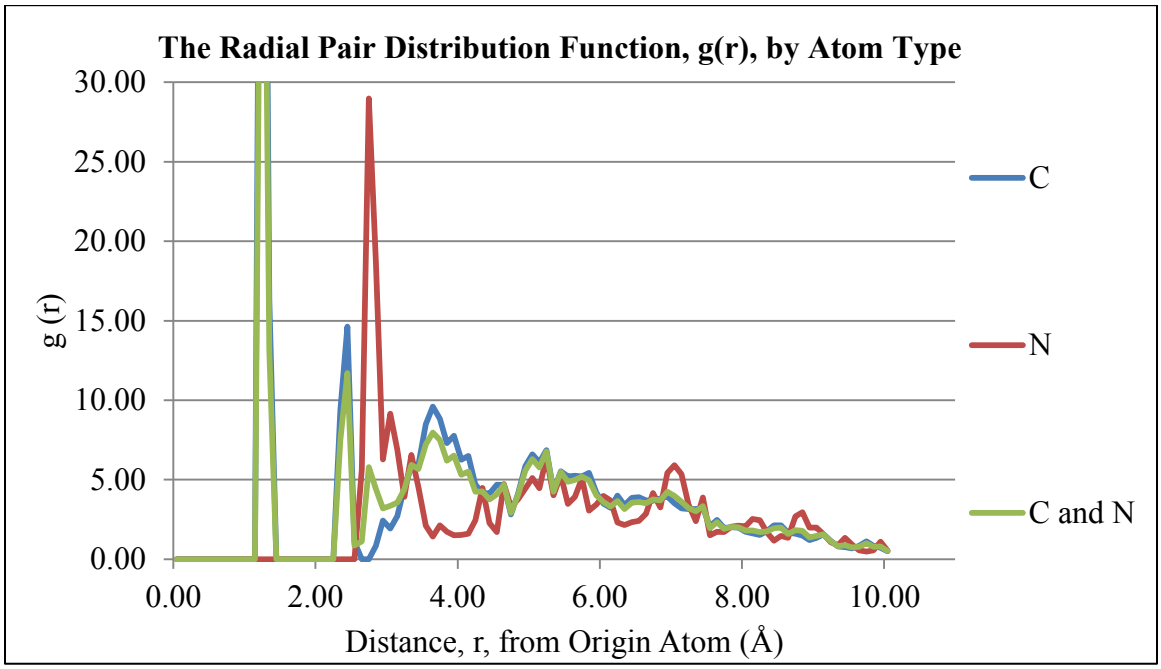

Figure 3.15: The calculated RPDF values for the GZ31 system.

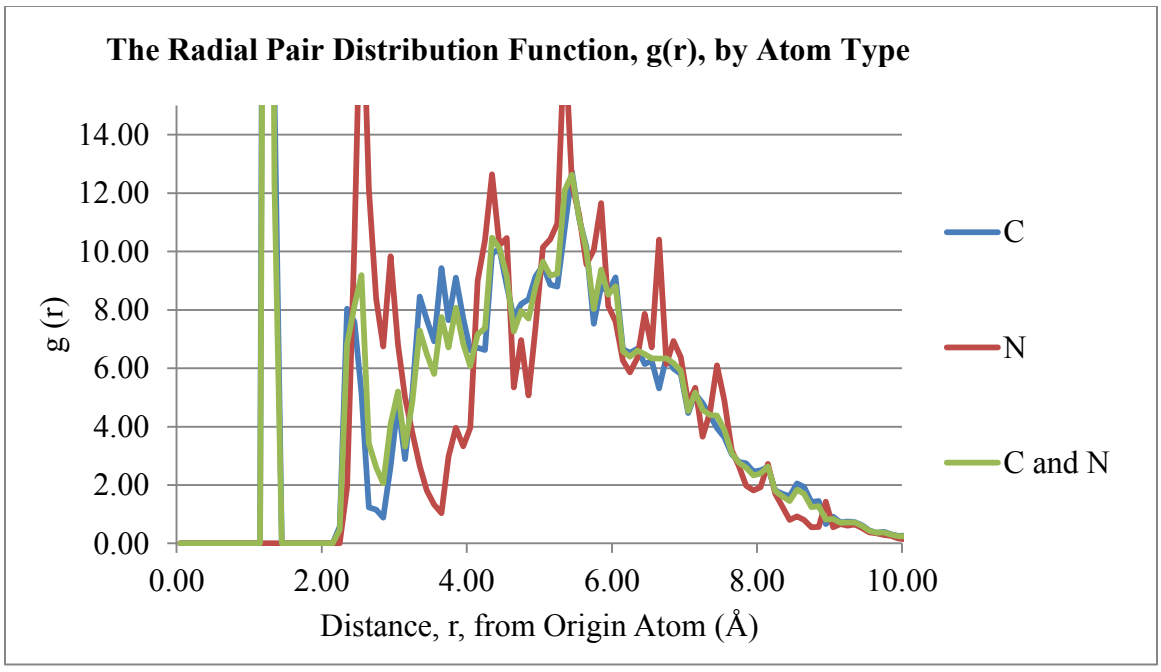

Figure 3.16: The calculated RPDF values for the GZ44 system.

The RPDF for the systems containing zwitterionic GABA have very distinct trends for each of the atom types. For all three systems, the solvation of the aliphatic chain and the carboxyl moiety shows one sharp solvation peak just outside 2.0 Å, and a broader second solvation sphere starting at around 3.0 Å. The second solvation sphere for carbon in the smaller, isolated GZ20 system is broad and diffuse, indicating little order, whereas the periodic GZ32 systems has a distinct third solvation sphere which begins just under 5.0 Å away from the origin atoms. The largest system, GZ44, has a very disordered and jagged second solvation sphere. Also, The RPDF curves for the solvation of nitrogen is not consistent between the three GZ systems. The difference between these systems may indicate that and effect that zwitterionic GABA has on the order or disorder of solvation depends on the amount of solvation present. The most solvated system would be the periodic system, for which a somewhat greater degree of order is observed. This may be a result of competitive interactions with the charged regions on either end of the molecule, or how those charges are described during the simulation. Overall, the differences between the first and outer solvation spheres indicate that the GZ solute also exerts a kosmotropic effect on its solvent.

The insights from the RPDF trends can help develop a qualitative picture of the solvation of a given molecule, but to establish the intermolecular strength of that solvation network it is necessary to evaluate the ratio between the highest and lowest values for the first solvation peak. The g_{max}/g_{min} ratios for the all of the ACh and GABA systems are presented in Table 3.4 below (on the following page). All of the neurotransmitters have a higher value of g_{max}/g_{min} for solute-water interactions than for water-water interactions in the first solvation sphere. These values agree with the trends seen in the graphs of the RPDFs showing greater order in the first solvation sphere, than in the surrounding solvation spheres. The difference between the solute-water and water-water interactions is the most obvious when periodic boundary conditions are imposed and the water experiences the forces it normally would in a bulk solution. These trends also indicate that the solutes are acting as kosmotropes.

Table 3.4: The g_{max}/g_{min} ratios for water-water and water-solute interactions in the solvated neurotransmitter systems.

System	Water-water g_{max}/g_{min}	Water-solute g_{max}/g_{min}	Difference
A33	5.434	8.861	3.427
GN25	6.847	17.265	10.418
GN32	3.746	15.426	11.680
GN43	4.605	13.004	8.399
Average GN	5.066	15.232	**10.166**
GA19	4.438	5.264	0.826
GA34	4.154	8.003	3.849
GA37	4.145	5.858	1.713
Average GA	4.292	5.561	**2.129**
GC28	3.404	4.816	1.412
GC35	3.790	10.469	6.679
GC44	4.652	5.413	0.761
Average GC	3.949	6.899	**2.950**
GZ20	2.469	9.334	6.865
GZ31	3.173	13.522	10.349
GZ44	3.435	4.466	1.231
Average GZ	3.026	9.107	**6.081**

From the average differences between the g_{max}/g_{min} ratio for the water-solute and water-water interactions a comparison can be made between the solvation of the various ionic states of GABA. The GN and the GZ molecule show the largest differences between water-solute and water-water interactions, while the ratios for the GA and GC systems are much closer together. Given that the kosmotrope/chaotrope effect is driven in part by charge, one might expect the trend to be polarized between the least and most charged forms of the molecule (the neutral and the zwitterionic forms, respectively). Instead, it is evident that how these molecules interact with water (compared to how water self-

interacts) is very similar. The molecules with a net charge of zero have a greater disparity between water-water and water-solute hydrogen bonds, than those with a non-zero net charge. There are (at least) two possibilities leading to this pattern. If the water-solute bonds always have the same degree of strength, then molecules with no net charge are the most kosmotropic. On the other hand, if the water-water bonds are always the same, then molecules with no net charge have the strongest bonds to the first solvation sphere. From this value it is hard to tell which scenario is more representative of the real situation, and the hydrogen bonds themselves must be examined more closely.

3.4.3 The Hydrogen Bond Analyses of the Solvated Neurotransmitter Systems

The hydrogen bonds, per frame of each simulation trajectory, will be presented according to the class of solute in the system (i.e., all the GC trajectories will be presented together). The number of hydrogen bonds, having up to a maximum length of 3.0 Å and a maximum angle of 20°, for the ACh, GN, GA, GC and GZ systems are shown in Figures 3.17 – 3.21 below.

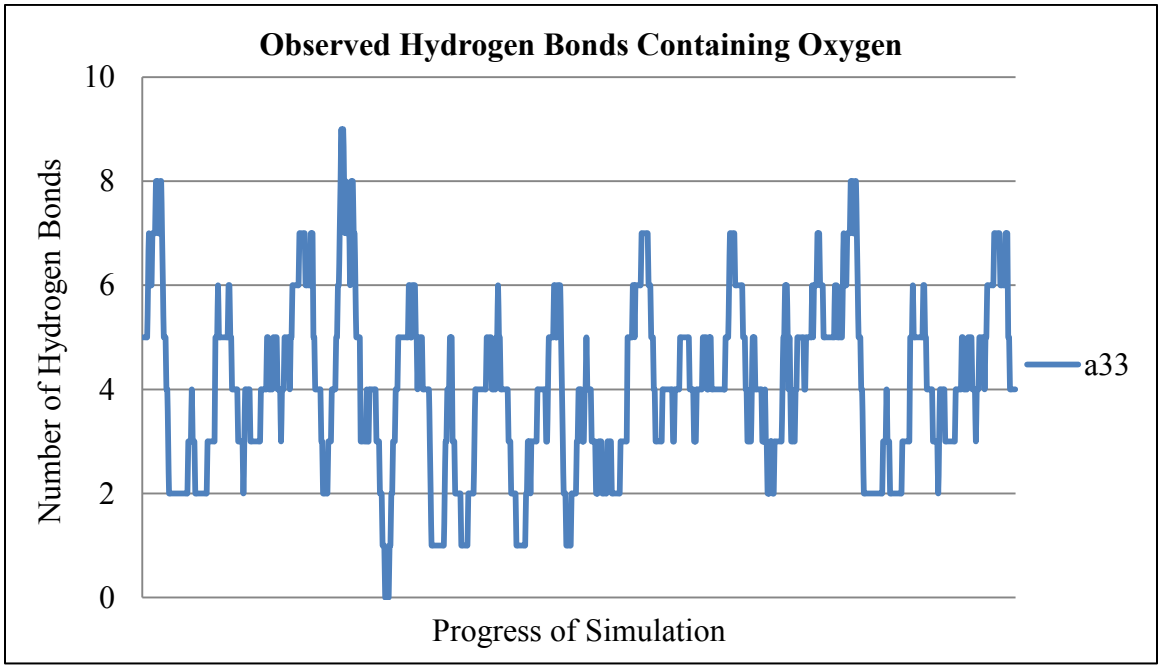

Figure 3.17: The number of hydrogen bonds observed during the CPMD simulations of the A33 system.

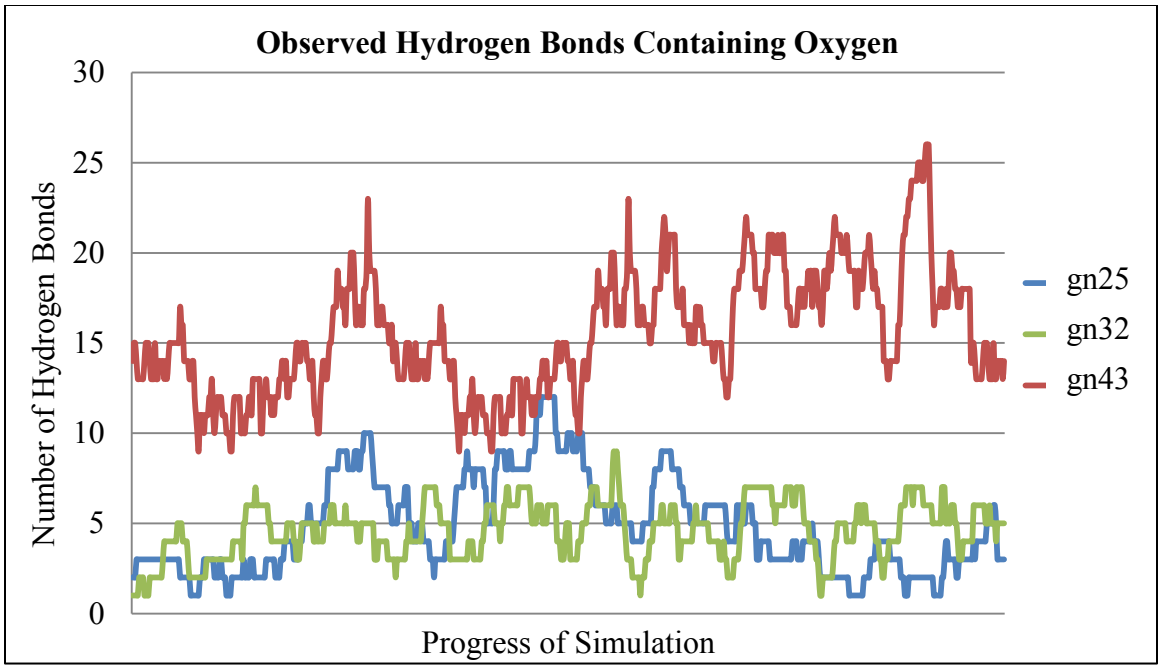

Figure 3.18: The number of hydrogen bonds observed during the CPMD simulations of the GN systems.

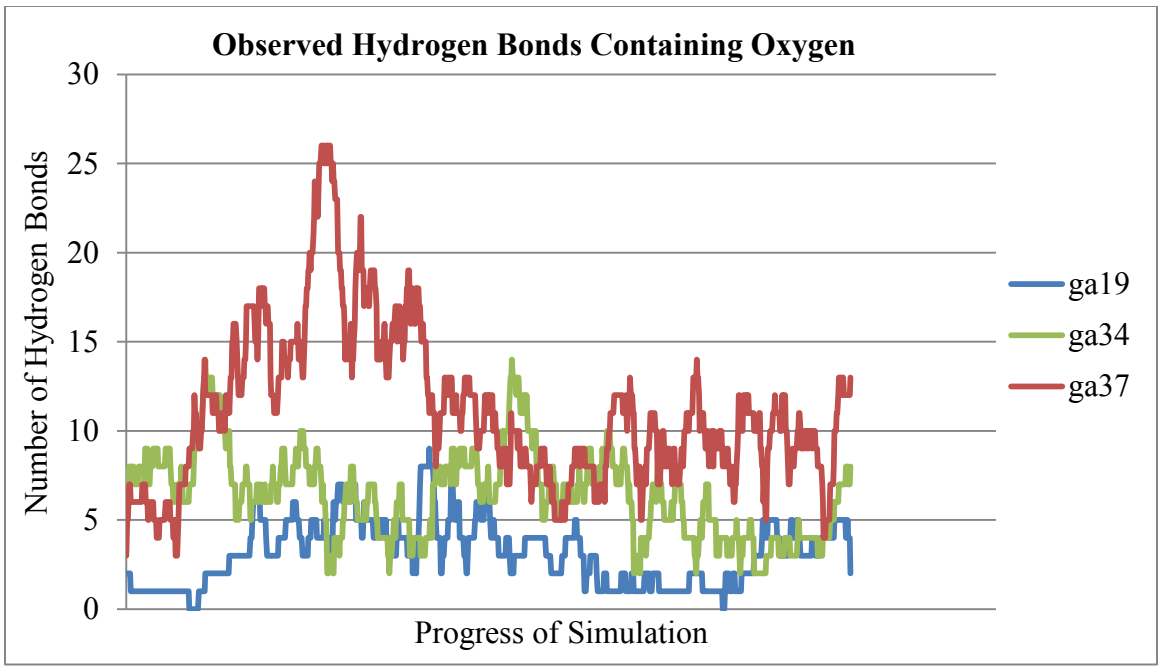

Figure 3.19: The number of hydrogen bonds observed during the CPMD simulations of the GA systems.

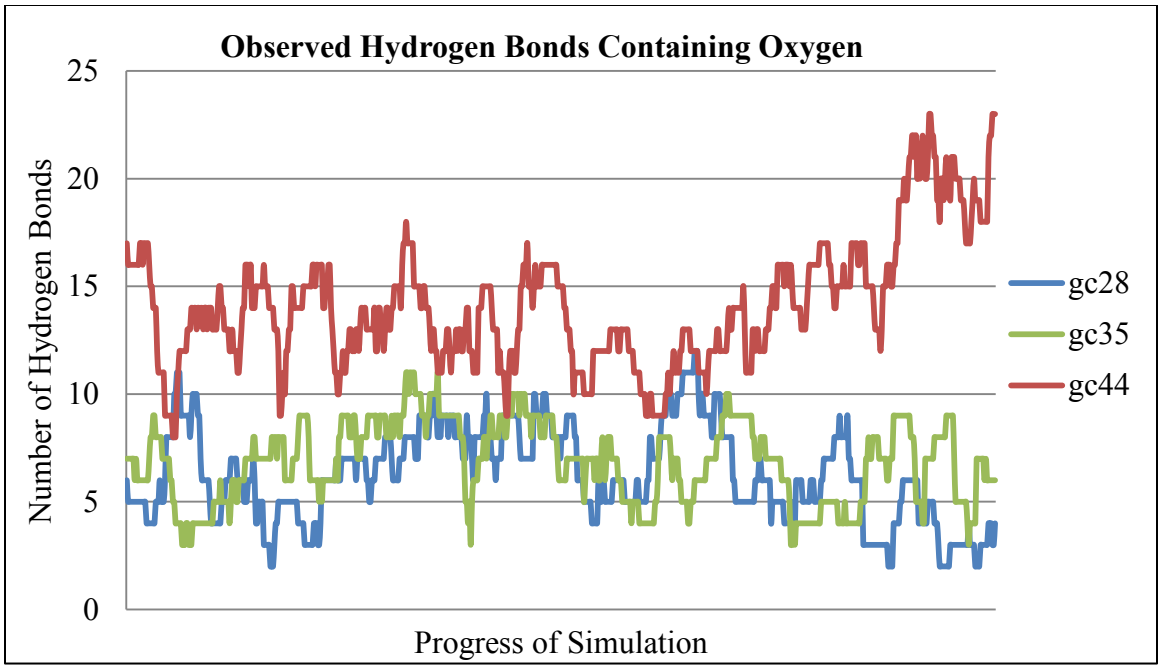

Figure 3.20: The number of hydrogen bonds observed during the CPMD simulations of the GC systems.

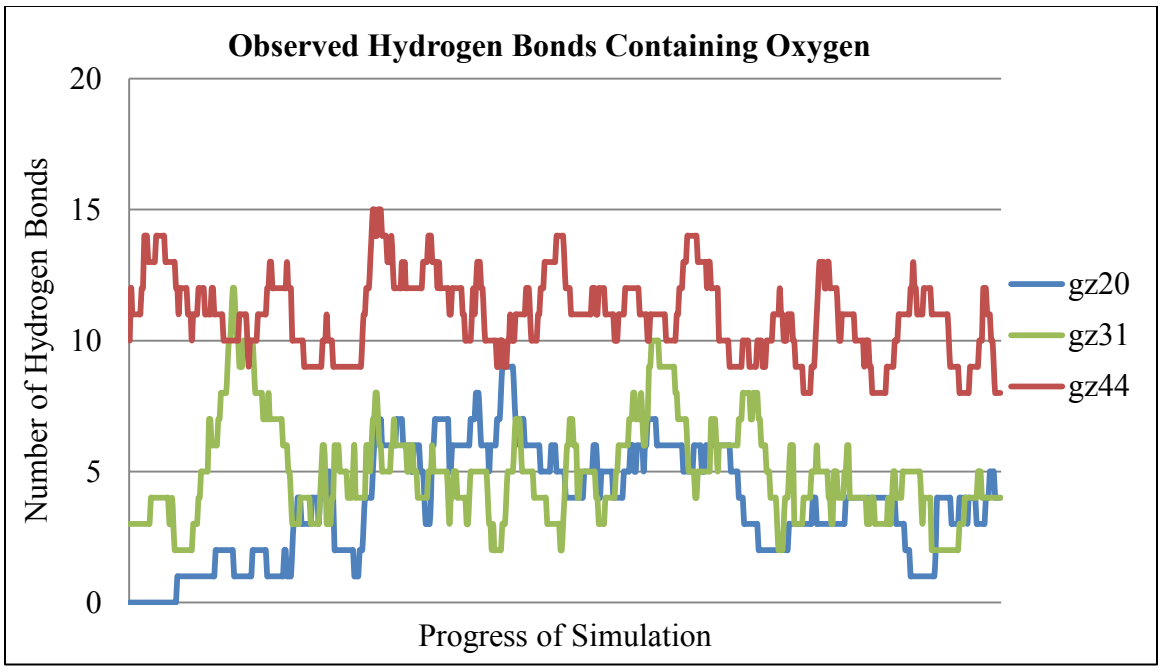

Figure 3.21: The number of hydrogen bonds observed during the CPMD simulations of the GZ systems.

As expected, the number of hydrogen bonds in each of the neurotransmitter simulations fluctuates as it did during the lipid bilayer simulations. For all of the classes of solutes, the periodic system fluctuates in the same range as the isolated system with a similar degree of solvation. The trends for the periodic systems do not perfectly match the isolated systems, but there is no reason that they should, given that the systems have very different starting geometries and do not have the same number of water molecules present. Nonetheless, this is further confirmation that the isolated systems perform very similarly to the periodic systems.

The systems with a higher degree of solvation fluctuate about a higher number, simply due to a greater number of hydrogen bond acceptors and donors in the system. They do, however, demonstrate less regular or periodic fluctuation than the systems with less solvation. The GA37 system shows a steady increase to a maximum about half way through the simulation and then a decrease towards the number of hydrogen bonds at the beginning of the simulation. The number of hydrogen bonds in the GC44 system fluctuates steadily for most of the simulation, but near the end it increases rapidly and finishes at a maximum value for the trajectory. The systems with less solvation, or with periodic boundaries, appear to be more stable than isolated systems with large solvation spheres. This may also reflect the fact that in a larger bulk solution the hydrogen bond network is simply more dynamic and less consistent. If the computational resources were available it would be interesting to compare these results with a higher level of solvation.

Even without investigation of larger solvation spheres, the numbers of hydrogen bonds in these systems can provide a great deal of information about the general ability of these water molecules to form hydrogen bonds with one another when surrounding the various solutes. The average number of hydrogen bonds for each simulation is presented in Table 3.5 below for comparison.

Table 3.5: The average number of hydrogen bonds observed during the simulations of the solvated neurotransmitter systems.

System	Hydrogen bonds	Ratio of hydrogen bonds to H_2O
A33	*4.0*	*0.13*
GN25	4.8	0.19
GN32	*4.6*	*0.14*
GN43	15.5	0.36
GA19	3.5	0.18
GA34	*8.2*	*0.24*
GA37	12.0	0.32
GC28	6.3	0.23
GC35	*6.9*	*0.20*
GC44	15.2	0.35
GZ20	3.8	0.19
GZ31	*5.0*	*0.16*
GZ44	11.0	0.25

The expected value for the number of hydrogen bonds is just below two per water molecule [10]. The chief observation from this set of data is that all of the neurotransmitters have far below this number – none of them have greater than an average of 0.5 hydrogen bonds per water molecule. Thus, both neurotransmitters appear to be acting as kosmotropes, regardless of their ionic state, in agreement with the information provided by the RPDFs and the g_{max}/g_{min} ratios discussed previously.

Again we see that the values produced when using periodic boundary conditions (italicized) are fairly consistent with the isolated systems of similar solvation. The ratio of hydrogen bonds to waters present does indicate that the periodic systems contain slightly less hydrogen bonding than the isolated systems. This effect is very subtle, but it can be explained by the lack of forces from the periodic simulation cells influencing the motion and interaction of molecules inside the simulation cell. In general, isolated systems may

slightly over-estimate the frequency and strength of hydrogen bonding. Nevertheless, the values are quite close and their results can be combined to analyze the general performance of each class of solute. The average ratios for the hydrogen bonding in the ACh and GABA systems are shown in Figure 3.22 below.

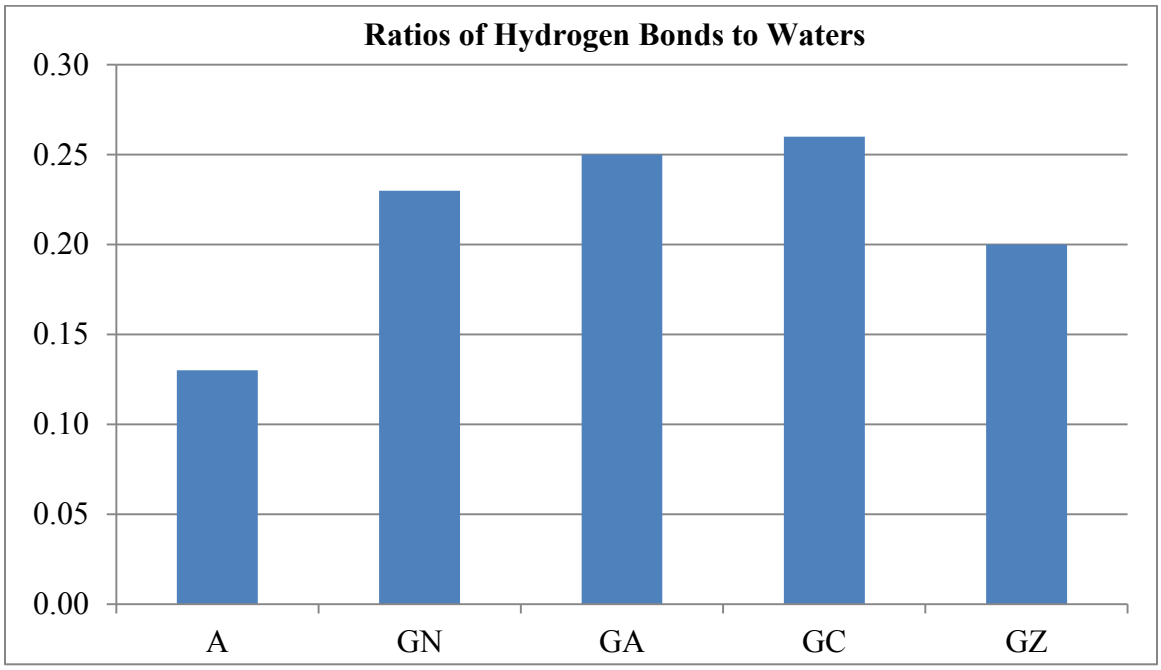

Figure 3.22: The average number of hydrogen bonds per water molecule, for each class of solute.

Two important trends are visible from the graph in Figure 3.22. Firstly, The GABA molecules have a fairly consistent rate of hydrogen bonding, despite the differences in their ionic states. The slight differences do indicate that changes in pH would affect the stability in the solvation of this molecule. It appears that deprotonation of the carboxyl group under basic conditions would tend to decrease the hydrogen bonding, or protonation of the amine group under acidic conditions would increase it. The hydrogen bonding under a more neutral pH depends on the form – neutral of zwitterionic – in which the molecule exists. Since the zwitterionic molecule is the most likely form under neutral conditions, the net charge of zero would cause the least amount of hydrogen bonding in the solvent of this molecule. While both molecules are kosmotropic, the excitatory ACh neurotransmitter is a stronger kosmotrope, than the inhibitory GABA neurotransmitter.

3.5 DISCUSSION OF THE RESULTS FROM THE NEUROTRANSMITTER STUDY

The RMSD values for ACh and GABA, like those calculated for the B3 and B4 bilayers, confirm a higher mobility for solvent atom types than for the carbon and nitrogen in the solutes. They generally demonstrate a lower degree of mobility for the unsolvated molecules, than for those which are affected by the high mobility of small water molecules, as well as slight differences between periodic systems and isolated systems. Overall, however, the RMSD values are fairly consistent and indicate that the simulations performed well and produced comparable results.

The RPDF, g_{max}/g_{min} and hydrogen bonding results of the neurotransmitter study provide unique insight into the solvation of ACh and GABA. The solvation of these molecules was generally less regular than the solvation of the lipid bilayers; the jagged peaks in the RPDF trends, and the frequent lack of the anticipated decaying peaks, both point towards dispersion of the outer water molecules around ACh and GABA, compared to the first solvation sphere. The solvation of carbon tends to dominate the RPDF for carbon and nitrogen combined. This is due in part to the nitrogen being outnumbered by carbon, but in the case of ACh it is also because the nitrogen is buried behind a trio of methyl groups and the end of the alkyl chain. Under basic conditions, when the carboxyl group of GABA becomes deprotonated, the solvation of the amine group and the carbons are more balanced. In general, the first solvation sphere of carbon is closer to the origin atom of the RPDF than it is for nitrogen, while the opposite is true for the higher solvation sphere. The first solvation sphere tends to be sharp and distinct, while the higher solvation spheres are broad and jagged. Certain trends within the GABA systems allow for a discussion of how the pH affects kosmotropic behaviour. It was found that the anionic GA and the cationic GC form are more disruptive than the neutral GN molecule. It also appears that for the zwitterionic molecule the level of kosmotropic behaviour depends on the degree of solvation present.

The kosmotropic trends were confirmed by the g_{max}/g_{min} ratio for water-solute interactions being stronger than water-water interactions, across the board, and the

biggest differences were seen when periodic boundary conditions were used and the forces of a bulk solution were implied. The kosmotropic classification was also confirmed by the very low number of hydrogen bonds observed in the bulk solution, compared to the number of water molecules present. In all cases the ratio of hydrogen bonds to water molecules was well below the value of two seen in normal bulk water.

So what do these results mean for neurotransmission? Neurotransmission is all about speed, and one of the defining characteristics of a neurotransmitter is whether it is fast-acting of slow-acting. A fast-acting neurotransmitter is one whose effect is felt very quickly, and whose effect is short in duration [132]. Conversely, a slow-acting neurotransmitter takes a bit more time to act, but acts for a longer period of time [132]. From these definitions one might suppose that excitatory neurotransmitters tend to be fast-acting – leading to better reaction times – and that inhibitory neurotransmitters are necessarily slower-acting; in fact, this is not the case. It may sound counter-intuitive but the inhibitory neurotransmitter GABA is classified as fast-acting and the excitatory ACh is considered slow-acting [132]. The main reason is that these classifications do not specifically refer to their transit time through the synaptic gap. Instead, they describe the activity which occurs after a given neurotransmitter has bound to a post-synaptic receptor [132]. This does not preclude solvation from either playing a role in the speed of each neurotransmitter's action, or from being related to it. Considering the differences observed between the solvation of ACh and of GABA, several statements can be made about the possible relationship between a neurotransmitters mode of action and its effect on solvation.

The first possibility is the non-case, where there is no relationship between the strength and/or order of solvation, and the relative speed of a neurotransmitters activity. This case is presented for the sake of completeness, but knowing that the molecules need to diffuse through water in order to act and that this process influences the overall time of neurotransmission, it does not seem likely that water is either passive or irrelevant. It is more likely, from the results, that water is playing an active role in the behaviour of these molecules. It may be that a less kosmotropic molecule moves faster through a bulk

solution than a more chaotropic molecule, perhaps the reduced interactions with the solvent sphere lead to less drag through the bulk solution. In this situation the GABA molecule would diffuse more rapidly across the synapse than the ACh, contributing to its faster mechanism of action. The other possibility is that fast excitatory neurotransmission is preferred, and that the strongly kosmotropic nature of slow-acting ACh compensates for some of the time spent on the post-synaptic processes. Perhaps the more kosmotropic a neurotransmitter is, the more quickly it can diffuse across the synapse due to the weakened intermolecular forces in the path of the neurotransmitter and the reduced resistance to its flow. In either case the water is playing an active role in the overall speed of neurotransmission, and is altering the mode of action of both classes of neurotransmitters.

CHAPTER 4 CONCLUSION

4.1 SOLVATED LIPID MEMBRANES

4.1.1 Water Structures and the Myelin Sheath

From the results of the MD simulations completed here it appears that both lipid types are somewhat kosmotropic. The organized water structures do not definitively indicate that water structures play a role in axonal neurotransmission. In reality the myelin sheath is much more complicated – riddled with membrane proteins, surrounded by electrolytes and acidic protons, and constantly shifting due to endocytosis and exocytosis – than the models presented here. Including more of these types of features in the model would drastically increase the computational cost of the simulations, but it would be a more effective means of examining the behaviour of axonal solvation.

4.1.2 Proposed Future Research of Axonal Neurotransmission

If this particular project were pursued further, the best approach would be to include a better mix of the lipids known to form the l_o and l_d domains of the cellular membrane. A tertiary membrane, or higher, with ample pre-simulation time to prepare the system for the final production simulation, would be a good place to start.

It would also be useful to use fully flexible water molecules and to include a number of the sodium ions, potassium ions, chloride ions and acidic protons expected to exist within the brain and known to play a role in neurotransmission; perhaps the counterions and the lipid bilayer work together to order the axonal solvent molecules. This would most likely require a different force field, and use of the more computationally demanding PME description of long-range electrostatics. If the computational resources are available, the length of the simulation should also be increased to allow for any periodic interactions to be observed. The scale of this particular system, however, may simply be too large and complex for most computational simulations, and experimental methods may be more effective. There have been many instances in which lipid-only bilayers were made and

supported on a substrate for the examination of domain formation. Could these thin films be tested for their conductivity, using "pure" water, or even a weakly saline solution? Whichever route is taken, further investigation of the solvation of the myelin sheath in relationship to the processes which govern axonal neurotransmission is not only warranted, but is recommended.

4.2 SOLVATED NEUROTRANSMITTERS

4.2.1 Water Organization in the Synaptic Gap

From the results of the CPMD simulations completed it can be said that both of the ACh and GABA neurotransmitters are kosmotropic. The real question is whether this property plays a role in the mechanism of action of these neurotransmitters. To this end, a greater variety of neurotransmitters should be studied, but even without this information the behaviour of these molecules can be compared and a new hypothesis created. Based on the fact that these molecules do in fact influence the water structures which surround them it can be said that the water also influences these molecules, because the solvation process is driven by the properties of water and of solutes working in coordination.

The slow-acting excitatory ACh kosmotrope demonstrates a stronger influence on its solvent than the fast-acting inhibitory GABA kosmotrope, but it is unclear whether this makes the diffusion of ACh or of GABA faster. Again, a broader investigation of the solvation of neurotransmitters should be completed to help answer this question.

4.2.2 Proposed Future Research of Synaptic Neurotransmission

The work completed in this project indicates that the role of water in synaptic neurotransmission can begin to be investigated by CPMD simulations. The first step in expanding this project would be to increase the length of the simulations and the diversity of the molecules being examined. A variety of other neurotransmitters could be investigated using the methods outlined in this thesis. It would be useful to explore neurotransmitters with a range of structural and functional diversity, so that a more

complete picture of the role of the kosmotrope/chaotrope effect within the synapse can be developed, especially for comparison between fast- and slow-acting neurotransmitters.

Due to the complications and limitations experienced with the available computational resources, any future work should concentrate first on using smaller solvation spheres. It was found that isolated systems perform as well as periodic systems, and so either method could be used. In addition to regular solvation, it would be useful to examine the water behaviour around neurotransmitters when there are counterions present, such as sodium, potassium and chloride. The use of counterions would require a different force field for pre-simulation minimization, and a more thorough bench-marking procedure to establish the appropriate value for the plane-wave cut-off. It would also be important to include acidic protons in the simulations, seeing as they often play a role in water structures, and the synapse is known to be acidic.

4.3 FINAL SUMMARY

This thesis has presented several questions concerning the neurotransmission process, the investigation undertaken to address those questions, the results and their implications. The central goal was to develop and test models of neurological systems in order to assess the possibility that water can be considered a neuromodulator; an active player in the neurotransmission process. Several models of myelin sheath in the CNS were developed, and several algorithms for their simulation attempted, before a stable model and algorithm were established. Fewer attempts were required to create models of the solvated neurotransmitters, but many of the systems built were too large and required too much memory to simulate. In the end, the simulations which were successfully completed indicate that water structures may indeed exist at the surface of the myelin sheath, structures which could be involved in axonal neurotransmission, and that there is a strong probability of water playing a role in the activity of synaptic neurotransmitters. This research provides the first pieces of evidence that water is a neuromodulator.

BIBLIOGRAPHY

1. Estrin, D.A., Paglieri, L., Corongiu, G. & Clementi, E. (1996). Small clusters of water molecules using Density Functional Theory. *J. Phys. Chem.*, 100: 8701–8711.
2. Tuckerman, M.E., Laasonen, K., Sprik, M., & Parrinello, M. (1995). *Ab initio* molecular dynamics simulation of the solvation and transport of H_3O^+ and OH^- ions in water. *J. Phys. Chem.,* 99: 5749–5752.
3. Chen, H. & Voth, G.A. (2010). Kinetics of proton migration in liquid water. *J. Phys. Chem. B,* 114: 333–339.
4. Mei, H.S., Tuckerman, M.E., Sagnella, D.E., & Klein, M.L. (1998). Quantum nuclear *ab initio* molecular dynamics study of water wires. *J. Phys. Chem. B,* 102: 10446–10458.
5. Izvekov, S. & Voth, G.A. (2002). Car-Parrinello molecular dynamics simulations of liquid water: New results. *J. Chem. Phys.,* 116: 10372–10376.
6. Vuilleumier, R. & Borgis, D. (1998). Quantum dynamics of an excess proton in water using an extended empirical valence-bond hamiltonian. *J. Phys. Chem. B*, 102: 4261–4264.
7. Westhof, E. (1993). *Water and Biological Macromolecules: Topics in molecular and structural biology.* Boca Raton, FL: CRC Press Incorporated.
8. Goodisman, J. & Blades, R. (2000). Conductivity of pure irradiated water. *J. Phys. Chem. A*, 104: 12029–12044.
9. Hay, C.E., Marken, F. & Blanchard, G.J. (2010). Solvent-dependent changes in molecular reorientation dynamics: The role of solvent-solvent interactions. *J. Phys. Chem. A*, 114: 4957–4962.
10. Hribar, B., Southall, N., Vlachy, V. & Dill, K.A. (2002). How ions affect the structure of water. *J. Am. Chem. Soc.*, 124: 12302–12311.
11. Furmanchuk, A., Isayev, O., Shishkin, O.V., Gorb, L. & Leszcynski, J. (2010). Hydration of nucleic acid bases: A Car-Parrinello Molecular Dynamics approach. *Phys. Chem. Chem. Phys.,* 12: 3363–3375.
12. Lee, H.S. & Tuckerman, M.E. (2006). Structure of liquid water at ambient temperature from *ab initio* molecular dynamics performed in the complete basis set limit. *J. Chem. Phys.*, 125: 154507–154514.
13. Lee, H.S. & Tuckerman, M.E. (2007). Dynamical properties of liquid water from *ab initio* molecular dynamics performed in the complete basis set limit. *J. Chem. Phys.*, 126: 164501–164515.
14. Eigen, M. (1964). Proton Transfer, acid-base catalysis and enzymatic hydrolysis. *Angew. Chem. Int. Edn Engl.*, 3: 1–19.

15. Schuster, P., Zundel, G. & Sandorfy, C. (1976). *The Hydrogen Bond: Recent Developments in Theory and Experiments. Structure and Spectroscopy, Volume 2.* Amsterdam, Holland: North-Holland Publishing Co.
16. Barrer, R.M. & Stuart, W.I. (1957). Non-stoichiometric clathrate compounds of water. *Proc. Roy. Soc. A-Math. Phys.*, 243: 172–189.
17. Marx, D., Tuckerman, M.E., Hutter, J. & Parrinello, M. (1999). The nature of the hydrated excess proton in water. *Nature*, 397: 601–604.
18. Kirchner, B. (2007). Eigen or Zundel ion: News from calculated and experimental photoelectron spectroscopy. *Chem. Phys. Chem.,* 8: 41–43.
19. Buffett, B. & Archer, D. (2004). Global inventory of methane clathrate: Sensitivity to changes in the deep ocean. *Earth Planet. Sc. Lett.,* 227: 185–199.
20. Environment Canada. (2009). *Canada's 2007 Greenhouse Gas Inventory: A Summary of Trends* [PDF file]. Retrieved from: http://www.ec.gc.ca/Publications/F62F0CF4-5254-45F2-9365-B01BE0576174%5CCanadas2007GreenhouseGasInventoryASummaryOfTrends.pdf
21. Mann, D.J. & Halls, M.D. (2003). Water alignment and proton conduction inside carbon nanotubes. *Phys. Rev. Lett*., 90: 195503–4.
22. Gu, W. & Helms, V. (2009). Tightly connected water wires facilitate fast proton uptake at the proton entrance of proton pumping proteins. *J. Am. Chem. Soc.*, 131: 2080–2081.
23. Reddy, G., Straub, J.E. & Thirumalai, D. (2010). Dry amyloid fibril assembly in a yeast prion is mediated by long-lived structures containing water wires. *Proc. Natl. Acad. Sci*., 14: 21459–21464.
24. Raghavender, U.S., Kantharaju, Aravinda, S., Shamala, N. & Balaram, P. (2010). Hydrophobic peptide channels and encapsulated water wires. *J. Am. Chem. Soc.*, 132: 1075–1086.
25. Venable, R.M. & Pastor, R.W. (2002). Molecular dynamics simulations of water wires in a lipid bilayer and water/octane model systems. *J. Chem. Phys.*, 116: 2663–2664.
26. Moelbert, S., Normad, B. & De Los Rios, P. (2004). Kosmotropes and chaotropes: Modelling preferential exclusion, binding and aggregate stability. *Biophys. Chem.,* 112: 45–57.
27. Collins, K.D. (1995). Sticky ions in biological systems. *Proc. Natl. Acad. Sci*., 92: 5553–5557.
28. Suhr, J.A., Hall, J., Patterson, S.M. & Niinistö, R.T. (2004). The relation of hydration statues to cognitive performance in healthy older adults. *Int. J Psychophysiol.,* 53: 121–125.

29. Wilson, M.-M.G. & Morley, J.E. (2003). Impaired cognitive function and mental performance in mild dehydration. *Eur. J. Clin. Nutr.,* 57: S24–S29.
30. Kalinowska, A., Losy, J. (2006). PECAM-1, a key player in neuroinflammation. *Eur. J. Neurol.,* 13: 1284–1290.
31. Rosi, S., Ramirez-Amaya, V., Vazdarjanova, A., Esparza, E.E., Larkin, P.B., Fike, J.R., et al. (2009). Accuracy of hippocampal network activity is disrupted by neuroinflammation: Rescue by memantine. *Brain*, 132: 2464–2477.
32. Tait, M.J., Saadoun, S., Bell, B.A. & Papadopoulos, M.C. (2008). Water movements in the Brain: Role of aquaporins. *Trends Neurosci.,* 31: 37–43.
33. Macaulay, N., Hamann, S. & Zeuthen, T. (2004). Water transport in the brain: Role of cotransporters. *Neurosci.,* 129: 1031–1044.
34. Kobayashi, H., Yanagita, T., Yokoo, H. & Wada, A. (2004). Molecular mechanisms and drug development in aquaporin water channel diseases: Aquaporins in the brain. *J. Pharm. Sci.,* 96: 264–270.
35. Yamashita, T. & Voth, G.A. (2010). Properties of hydrated excess protons near phospholipid bilayers. *J. Phys. Chem. B,* 114: 592–603.
36. Cooke, S.F. & Lilley, S. (2002). Acidity at the synapse: pH influences plasticity and memory. *Trends Neurosci.,* 25(9): 446–447.
37. Magistretti. J.P., Pellerin, L., Rothman, D.L. & Shulman, R.G. (1999). Energy on demand. *Science,* 283: 496–497.
38. Hertz, L. & Robinson, S.R. (1999). Energy for neurotransmission. *Science,* 285: 639a.
39. Griffin, J.L. (199) Energy for neurotransmission. *Science,* 285: 639–640.
40. Neuromodulator. (n.d.). In *The Free Dictionary*. Retrieved from http://medical-dictionary.thefreedictionary.com/neuromodulator
41. Neuromodulator (n.d.). In *Merriam-Webster's Medical Dictionary*. Retrieved from: http://www.merriam-webster.com/medical/neuromodulator?show=0&t=1299782873
42. Shneker, B.F. & McAuley, J.W. (2005). Pregabalin: A new neuromodulator with broad therapeutic indications. *Ann. Pharmacother.,* 39: 2029–2037.
43. Boison, B. (2008). Adenosine as a neuromodulator in neurological diseases. *Curr. Opin. Pharmacol.,* 8: 2–7.
44. Abe, K. & Kimura, H. (1996). The possible role of hydrogen sulfide as an endogenous neuromodulator. *J. Neurosci.,* 16(3): 1066–1071.
45. Rosenstein, F.J. & Chappell, R.L. (2003). Endogenous zinc as a retinal neuromodulator: Evidence from the skate (*Raja erinacea*). *Neurosci. Lett.,* 345: 81–84.
46. Scheler, G. (2004). Regulation of neuromodulator receptor efficacy–implications for whole-neuron and synaptic plasticity. *Prog. Neurobiol.,* 72: 339–415.

47. Tortora, G.J. & Derrickson, B. (2006). *Principles of Anatomy and Physiology* (11th ed). Hoboken, NJ, USA: John Wiley & Sons, Inc.
48. Paulev, P.E. & Zubieta-Calleja, G. (2004). *New Human Physiology, Textbook in Medical Physiology And Pathophysiology: Essentials and Clinical Problems* (2nd ed). Copenhagen, Denmark: University of Copenhagen. Retrieved from: http://www.zuniv.net/physiology/book/chapter1.html
49. Kandel, E.R., Schwarts, J.H. & Jessel, T.M. (1991). *Principles of Neural Science* (3rd ed). New York, NY: Elsevier Science Publishing Co., Inc.
50. Nave, R. (2011). Gauss's Law. Retrieved from: http://hyperphysics.phy-astr.gsu.edu/hbase/electric/gaulaw.html
51. Nave, R. (2011). Gauss's Law, Integral Form. Retrieved from: http://hyperphysics.phy-astr.gsu.edu/hbase/electric/gaulaw.html#c2
52. Simons, K. & Toomre, D. (2000). Lipid rafts and signal transduction. *Nat. Rev. Mol. Cell Bio*., 1: 31–41.
53. Simons, K. & Ikonen, E. (1997). Functional rafts in cell membranes. *Nature*, 387: 569–572.
54. Samsonov, A.V., Mihalyov, I. & Cohen, F.S. (2001). Characterization of cholesterol-sphingomyelin domains and their dynamics in bilayer membranes. *Biophys. J.*, 81: 1486–1500.
55. Ayuyan, A.G. & Cohen, F.S. (2008). Raft composition at physiological temperature and pH in the absence of detergents. *Biophys. J.*, 94: 2654–2666.
56. Bunge, A., Müller, P., Stöckl, M., Herrmann, A. & Huster, D. (2008). Characterization of the ternary mixture of sphingomyelin, POPC, and cholesterol: Support for an inhomogenous lipid distribution at high temperatures. *Biophys. J.,* 94: 2680–2690.
57. Crane, J.M. & Tamm, L.K. (2004). Role of cholesterol in the formation and nature of lipid rafts in planar and spherical model membranes. *Biophys. J.*, 86: 2965–2979.
58. De Almeida, R.F.M., Fedorov, A. & Prieto, M. (2003). Sphingomyelin/phosphatidylcholine/cholesterol phase diagram: Boundaries and composition of lipid rafts. *Biophy. J.*, 85: 2406–2416.
59. Frazier, M.L., Wright, J.R., Pokorny, A. & Almeida, P.F.F. (2007). Investigation of domain formation in sphingomyelin/cholesterol/POPC mixtures by fluorescence resonance energy transfer and Monte Carlo simulations. *Biophys. J.*, 92: 2422–2433.
60. Gandhavadi, M., Allende, D., Vidal, A., Simon, S.A. & McIntosh, T.J. (2002). Structure, composition, and peptide binding properties of detergent soluble bilayers and detergent resistant rafts. *Biophys. J.*, 82: 1469–1482.

61. Gao, W.-Y., Quinn, P. & Yu, Z.-W. (2008). The role of sterol rings and side chain on the structure and phase behaviour of sphingomyelin bilayers. *Mol. Membr. Biol.*, 25: 485–497
62. Pandit, S.A., Jakobsson, E. & Scott, H.L. (2004). Simulation of the early stages of nano-domain formation in mixed bilayers of sphingomyelin, cholesterol and dioleylphosphatidylcholine. *Biophys. J.*, 87: 3312–3322.
63. Quinn, P.J. & Wolf, C. (2009). The liquid-ordered phase in membranes. *Biochim. Biophys. Acta*, 1788: 33–46.
64. Van Meer, G., Voelker, D.R. & Feigenson, G.W. (2008). Membrane lipids: Where they are and how they behave. *Nature*, 9: 112–124.
65. Wang, T.-Y. & Silvius, J.R. (2003). Sphingolipid partitioning into ordered domains in cholesterol-free and cholesterol-containing lipid bilayers. *Biophys. J.*, 84: 367–378.
66. Róg, T & Pasenkiewicz-Gierula, M. (2001). Cholesterol effects on the phosphatidylcholine bilayer nonpolar region: A molecular simulation study. *Biophy. J.*, 81: 2190–2202.
67. Jahn, O., Tenzer, S. & Werner, H.B. (2009). Myelin proteomics: molecular anatomy of an insulating sheath. *Mol. Neurobiol.*, 40: 55–72.
68. Andersen, S.S.L., Jackson, A.D. & Heimburg, T. (2009). Towards a thermodynamics theory of nerve pulse propagation. *Prog. Neurobiol.*, 88: 104–113.
69. Heimburg, T. & Jackson, D. (2005). On soliton propagation in biomembranes and nerves. *Proc. Natl. Acad. Sci*., 102: 9790–9795.
70. Nag, K. (2008). *Structure and Dynamics of Membranous Interfaces.* Hoboken, NJ: John Wiley & Sons, Inc.
71. Pedersen, U.R., Peters, G.H., Schrøder, T.B. & Dyre, J.C. (2010). Correlated volume-energy fluctuations of phospholipid membranes: A simulation study. *J. Phys. Chem. B*, 114: 2124–2130.
72. Almeida, J.A.S., Morán, M.C., Infante, M.R. & Paid, A.A.C.C. (2010). Interaction of arginine-based cationic surfactants with lipid membranes: An experimental and molecular simulation study. *Archive for Org. Chem.*, 5: 34–50.
73. Patra, M. & Karttunen, M. (2004). Lipid bilayers driven to a wrong lane in molecular dynamics simulations by subtle changes in long-range electrostatic interactions. *J. Phys. Chem. B*, 108: 4485–4494.
74. Leach, A.R. (2001). *Molecular Modelling: Principles and Applications.* Essex, UK: Pearson Prentice Hall.
75. Devireddy, R.V. (2010). Statistical thermodynamics of biomembranes. *Cryobiology*, 60: 80–90.

76. MacKerell Jr., A.D., Wiórkiewicz-Kuczera, J. & Karplus, M. (1995). An all-atom empirical energy function for the simulation of nucleic acids. *J. Am. Chem. Soc.*, 117: 11946–11975.
77. MacKerell Jr., A.D., Banavali, N. & Foloppe, N. (2001). Development and current status of the CHARMM force field for nucleic acids. *Biopolymers*, 56: 257–265.
78. Halgren, T.A. (1996a). Merck Molecular Force Field. I. Basis, form, scope, parameterization, and performance of MMFF94. *J. Comput. Chem.*, 17: 490–519.
79. Halgren, T.A. (1996b). Merck Molecular Force Field. II. MMFF94 van der Waals and electrostatic parameters for intermolecular interactions. *J. Comput. Chem.*, 17: 520–552.
80. Halgren, T.A. (1996c). Merck Molecular Force Field. III. Molecular geometries and vibrational frequencies. *J. Comput. Chem.*, 17: 453–586.
81. Halgren, T.A. (1996d). Merck Molecular Force Field. IV. Conformational energies and geometries for MMFF94. *J. Comput. Chem.*, 17: 587–615.
82. Halgren, T.A. (1996e). Merck Molecular Force Field. V. Extension of MMFF94 using experimental data, additional computational data and empirical rules. *J. Comput. Chem.*, 17: 616–641.
83. Halgren, T.A. (1999a). Merck Molecular Force Field VI. MMFF94s option for energy minimization studies. *J. Comput. Chem.*, 20: 720–729.
84. Halgren, T.A. (1999b). Merck Molecular Force Field VII. Characterization of MMFF94, MMFF94s, and other widely available force fields for conformational energies and for intermolecular-interaction energies and geometries. *J. Comput. Chem.*, 20: 730–748.
85. Izvekov, S. & Parrinello, M. (2004). Effective force fields for condensed phase systems from *ab initio* molecular dynamics simulation: A new method for force-matching. *J. Chem. Phys.*, 120: 10896–10913.
86. Halgren, T.A. (1995). Potential energy functions. *Curr. Opin. Struc. Biol.*, 5: 205-210.
87. Halgren, T.A. & Damm, W. (2001). Polarizable force fields. *Curr. Opin. Struc. Biol.*, 11: 236–242.
88. Gontrani, L., Ramondo, F. & Caminiti, R. (2006). Energy dispersive X-ray diffraction and molecular dynamics meet: The structure of liquid pyrrole. *Chem. Phys. Lett.*, 417: 200–205.
89. Singh, D., Marla, S.S. & Verma, D. (2007). Analysis of MMFF94x and AMBER99 force fields using aspartic, serine metallo-proteases and sugar-binding protein data sets. *Online J. Bioinformatics*, 8: 45–55.
90. Gill, P., Murray, W., Wright, M. (1981). *Practical Optimization*. London, England: Academic Press.

91. Molecular Operating Environment (MOE) (version 2009.10) [Computer software]. Montréal, Canada: Chemical Computing Group, Inc.
92. Molecular Operating Environment (MOE) (version 2010.10) [Computer software]. Montréal, Canada: Chemical Computing Group, Inc.
93. Hinchliffe, A. (2000). *Modelling Molecular Structures* (2nd ed.). West Sussex, England: John Wiley & Sons, Ltd.
94. Ruhle, V. (2007). Berendsen and Nosé-Hoover thermostats. [PDF document]. Retrieved from: http://www.mpip-mainz.mpg.de/~andrienk/journal_club/thermostats.pdf
95. Hunenberger, P.H. (2005). Thermostat algorithms for molecular dynamics. *Adv. Polym. Sci*., 173: 105–149.
96. Bond, S.D., Leimkuhler, B.J. & Laird, B.B. (1999). The Nosé-Poincaré method for constant temperature molecular dynamics. *J. Comp. Phys.*, 151: 114–134.
97. Cordomi, A. & Perez, J.J. (2007). Molecular dynamics simulations of rhodopsin in different one-component lipid bilayers. *J. Phys. Chem.*, 111: 7052–7063.
98. Krepkiy, D., Mihailsecu, M., Freites, J.A., Schow, E.V., Worcester, D.L., Gawrisch, K., et al. (2009). Structure and hydration of membranes embedded with voltage-sensing domains. *Nature*, 462: 473–482.
99. Rivail, L., Chipot, C., Maigret, B., Bestel, I., Sicsic, S. & Tarek, M. (2007). Large-scale molecular dynamics of a G protein-coupled receptor, the human 5-HT_4 serotonin receptor, in a lipid bilayer. *J. Mol. Struct.*, 817: 19–26.
100. Jang, H., Ma, B. & Nussinov, R. (2007). Conformational study of the pretegrin-I (PG-I) dimer interaction with lipid bilayers and its effect. *BMC Struct. Biol.,* 7: 21–35.
101. Niemelä, P.S., Ollila, S., Hyvönen, M.T., Karttunen, M. & Vattulainen I. (2007). Assesing the nature of lipid raft membranes. *PLoS Comput. Biol*., 3: 0304–0312.
102. SYBYL (version 7.2) [Computer software]. St. Louis, Missouri: Tripos, L.P.
103. Tieleman, P. (2010). PLPC128.pdb [Data file]. Retrieved from: http://moose.bio.ucalgary.ca/files/plpc128.pdb
104. Tieleman, P. (2010). DPPC64.pdb [Data file]. Retrieved from: http://moose.bio.ucalgary.ca/files/dppc64.pdb
105. Clark, M., Cramer III, R.D. & Van Opdenbosch, N. (1989). Validation of the general purpose Tripos 5.2 force field. *J. Comp. Chem.,* 10(8): 982–1012.
106. SYBYL (version X) [Computer software]. St. Louis, Missouri: Tripos, L.P.
107. Open Babel [Computer software]. Available from: http://openbabel.org/wiki/Main_Page
108. Visual Molecular Dynamics (VMD) (version 1.9) [Computer software]. Available from: http://www.ks.uiuc.edu/Research/vmd/

109. Li, J.-J. (2007). Radial distribution function. Retrieved from: http://www.iams.sinica.edu.tw/lab/jlli/thesis_andy/node14.html
110. Brown, R. (1828). A brief account of microscopical observations made in the months of June, July and August, 1827, on the particles contained in the pollen of plants; and on the general existence of active molecules in organic and inorganic bodies. *Phil. Mag*., 4: 161–173.
111. Biagini, F., Hu, Y., Øksendal, B. & Zhang, T. (2008). *Stochastic Calculus for Fractional Brownian Motion and Applications*. London, England: Springer-Verlag, Ltd.
112. Zahn, D. (2004). Car-Parrinello molecular dynamics simulation of base-catalyzed amide hydrolysis in aqueous solution. *Chem. Phys. Lett.,* 383: 134–137.
113. Van Erp, T.S. & Meijer, E.J (2003). *Ab initio* molecular dynamics study of aqueous solvation of ethanol and ethylene. *J. Chem. Phys*., 118: 8831–8840.
114. Jungwirth, P., Curtis, J.E. & Tobias, D.J. (2003). Polarizability and aqueous solvation of the sulphate dianion. *Chem. Phys. Lett.*, 357: 704–710.
115. Murugan, N.A. & Hugosson, H.W. (2008). Investigations into conformational transitions and solvation structure of a 7-piperidino-5,9-methanobenzo[8]annulene in water. *Phys. Chem. Chem. Phys.*, 10: 6135–6143.
116. Carloni, P., Rothlinsberger, U. & Parrinello, M. (2002). The role and perspective of *ab initio* molecular dynamics in the study of biological systems. *Acc. Chem. Res.*, 35: 455–464.
117. Gervasio, F.L. (2004). *(A short) CPMD tutorial* [PowerPoint slides]. Retrieved from: http://ccp2006.postech.edu/content/mater/CPMD_tutorial.ppt
118. Santiso, E.E. & Gubbins, K.E. (2004). Multi-scale molecular modelling of chemical reactivity. *Mol. Simulat.*, 30: 699–748.
119. The CPMD Consortium (2008). *Car-Parrinello molecular dynamics: An ab initio electronic structure and molecular dynamics program (for CPMD v. 3.13.2)*. Zurich, Switzerland and Stuttgart, Germany.
120. Hohenberg, P. & Kohn, W. (1964). Inhomogenous electron gas. *Phys. Rev.*, 136: B864–B871.
121. Kohn, W. & Sham, L.J. (1965). Self-consistent equations including exchange and correlation effects. *Phys. Rev.*, 140: A1133–A1138
122. Schlegel, H.B. & Millam, J.M. (2001). *Ab initio* molecular dynamics: Propagating the density matrix with Gaussian orbitals. *J. Chem. Phys.*, 114: 9758–9763.
123. Troullier, N. & Martins J.L. (1991). Efficient pseudopotentials for plane-wave calculations. *Phys. Rev. B*, 43(3): 1993–2006.
124. Hutter, J. (2002). *Lecture Notes: Introduction to ab initio molecular dynamics*. [PDF document]. Retrieved from: http://metodos.fam.cie.uva.es/~doctorado/carlos/Intro-abinit-mol-din.pdf

125. Becke, A.D. (1988). Density-functional exchange-energy approximation with correct asymptotic correction. *Phys. Rev.*, A38: 3098–3100.
126. Becke, A.D. (1992). Density Functional Thermochemistry. I. The effect of the exchange-only gradient correction. *J. Chem. Phys.*, 96: 2155–2160.
127. Lee, C., Yang, W. & Parr, R.G. (1988). Development of the Colle-Salvetti correlation energy formula into a functional of the electron density. *Phys. Rev.*, B37: 785–789.
128. Atlantic Computational Excellence Network (ACEnet) [High-performance computing resources]. St. John's, Newfoundland: http://www.ace-net.ca/wiki/ACEnet
129. GaussView (version 5.0.8) [Computer software]. Wallingford, Connecticut: Gaussian, Inc.
130. WinSCP (version 4.3.3) [Computer software]. Available from: http://winscp.net/eng/index.php
131. PuTTY (version 0.60) [Computer software]. Available from: http://www.chiark.greenend.org.uk/~sgtatham/putty/download.html
132. McCormick, D.A. (1992). Neurotransmitter actions in the thalamus and cerebral cortex. *J. Clin. Neurophysiol*., 9: 212–223.

APPENDIX A Sample CPMD File Input for Wavefunction Optimization

```
&CPMD
LSD
OPTIMIZE WAVEFUNCTION
CONVERGENCE ORBITALS
 1.0d-6
CENTER MOLECULE ON
PRINT FORCES ON
&END
&SYSTEM
SYMMETRY
 0
ANGSTROM
CELL
 18.0 1.0 1.0  0.0  0.0  0.0
CUTOFF
 90.0
CHARGE
 1
MULTIPLICITY
 1
&END
&DFT
FUNCTIONAL BLYP
GC-CUTOFF
 5.0d-6
&END
&ATOMS
... ... ...[insert xzy coordinates of system with atom
type, number, MAXL and .psp specified]... ... ...
&END
```

APPENDIX B Sample CPMD File Input for short MD simulation (with no Thermostat) for Estimation of the Fictitious Electron Mass

```
&CPMD
LSD
MOLECULAR DYNAMICS CP
 RESTART LATEST COORDINATES WAVEFUNCTION
TRAJECTORY XYZ
TEMPERATURE
 310.0D0
MAXSTEP
 500
EMASS
 600.0
TIMESTEP
 5.0
CENTER MOLECULE ON
PRINT FORCES ON
&END
&SYSTEM
SYMMETRY
 0
POISSON SOLVER HOCKNEY
ANGSTROM
CELL
 30.0 1.0 1.0  0.0  0.0  0.0
CUTOFF
 90.0
CHARGE
 1
MULTIPLICITY
 1
&END
&DFT
FUNCTIONAL BLYP
GC-CUTOFF
 5.0d-6
&END
&ATOMS
... ... ...
&END
```

APPENDIX C Sample CPMD File Input for full MD Simulation (with Thermostat)

```
&CPMD
LSD
MOLECULAR DYNAMICS CP
 RESTART LATEST COORDINATES WAVEFUNCTION
TRAJECTORY XYZ SAMPLE
 5
TEMPERATURE
 310.0D0
NOSE IONS
 310 4000
NOSE ELECTRONS
 0.009 15000
MAXSTEP
 5000
EMASS
 600.0
TIMESTEP
 5.0
CENTER MOLECULE ON
PRINT FORCES ON
&END
&SYSTEM
SYMMETRY
 0
POISSON SOLVER HOCKNEY
ANGSTROM
CELL
 30.0 1.0 1.0  0.0  0.0  0.0
CUTOFF
 90.0
CHARGE
 1
MULTIPLICITY
 1
&END
&DFT
FUNCTIONAL BLYP
GC-CUTOFF
 5.0d-6
&END
&ATOMS
... ... ...
&END
```

APPENDIX D Sample CPMD Job Submission Script

```
#$ -S /bin/csh
#$ -cwd
#$ -l h_rt=48:00:00
#$ -l h_vmem=8G
#$ -pe ompi* 16
#$ -R yes
#$ -j n
#$ -N a
#$ -o a.out
#$ -e error.out
mpirun /usr/local/CPMD/cpmd-3-13 a.inp
/home/emartin/pseudo/pseudo_extlib/ > a.out
```